



Norwegian University of
Science and Technology

Effect of Porosity on the Hydrothermal Stability of CuSAPO-34 for the deNO_x Process

Guro Sørli

Master of Science

Submission date: May 2016

Supervisor: Karina Mathisen, IKJ

Co-supervisor: Karsten Kirste, IKJ

Norwegian University of Science and Technology
Department of Chemistry

Guro Sørli

MASTER THESIS

Effect of Porosity on the Hydrothermal Stability of CuSAPO-34 for the deNO_x Process

Supervisor: Associate professor Karina Mathisen

Acknowledgement

Firstly, I would like to thank Dr. Karina Mathisen for accepting me onto this journey. I am eternally grateful for her support and guidance throughout this adventure. She has always been a source of inspiration with an effect of me wanting to stretch even further in any situation. She has believed in me throughout this adventure, and for this, I am forever thankful. I would also like to thank the staff at the Swiss-Norwegian Beam Line (SNBL) at the European Synchrotron Radiation Facility (ESRF) for their assistance during my stay in Grenoble.

Furthermore, I could not have done this without Ph.D. candidate Karsten Kirste, post.doc Tina Kristiansen and Ph.D. candidate Stian Forselv. You have given me answers, early in the morning and late in the night. You have given me technical, lifesaving guidance and training. Lastly, you have always given me support and making this a joyful experience, especially in the laboratory. This also goes for the rest of the research group. I cannot count how many times you guys made me laugh by telling a joke or putting on a crazy song in the lab when I especially needed it. You have brought me sunshine, no matter how much rain that poured down.

I also want to thank all of my friends and family for giving me the amount of support I could not have dreamt of. Thank you, Øyvind and Jon-Abraham, for all the joy you have given me and making late nights at the university a game of laughs. Thank you, Kine and the rest of the stable crew, for giving me so much support and putting up with me when my head was always stuck at the university. Thank you, mom and dad, for beings rocks I always can rely on. Last, but not least, thank you Knut André for your patience, your support and your kindness.

Abstract

Hierarchical SAPO-34 with incorporated copper was tried synthesised both through a dry gel conversion and a hydrothermal method. Crystalline copper incorporated hierarchical SAPO-34 was not obtained through these directions. However, the hydrothermal method provided crystalline SAPO-34 and the degree of uniformity concerning mesoporosity was determined by N₂- physisorption (BET).

The crystalline SAPO-34 was ion exchanged with copper(II)nitrate and copper(II)tetraamine in order to determine activity for NO conversion in HC-SCR. For comparison, a conventional microporous SAPO-34 and mesoporous SBA-15 was ion exchanged as well in order to compare the effect of porosity.

XRD was used in order to confirm crystallinity, ICP-MS analyses were performed to determine copper uptake in ion exchanges. Furthermore, the activity of NO conversion was measured by a microreactor coupled to a GC-MS. Here, the conventional Cu-SAPO-34 was found to be more active than the hierarchical Cu-SAPO-34, whereas the hierarchical Cu-SAPO-34 had similar conversion as the mesoporous SBA-15. Ex Situ XAS spectroscopy was performed in order to tell differences of the local environment for copper before and after HC-SCR for the hierarchical Cu-SAPO-34. In addition, the conventional SAPO-34 and the mesoporous SBA-15 were also analysed Ex Situ pre reaction. Here, it was found that copper migrate at high temperatures and formed copper(II)oxide for the hierarchical SAPO-34.

Sammendrag

Formålet med denne masteroppgaven er å syntetisere hierarkisk SAPO-34 med inkorporert kobber i gitterverket. Dette er interessant og samfunnsviktig forskning da dette materialet er påtenkt som en ny type dieselmotorkatalysator for NO_x -gasser. Per i dag eksisterer ikke gode nok løsninger for fjerning av NO_x fra dieselmotorens eksos, noe også Volkswagen-skandalen viste siste år. Stadig blir nye krav satt av myndighetene, men produsentene sliter med å nå målet da dagens løsninger rett og slett ikke er gode nok. Tapene blir forbrukerne og miljøet på grunn av økt forurensing.

I denne masteroppgaven er det prøvd to ulike innfallsvinkler for å nå målet, den ene via en tørr-gel konversjon og en annen hydrotermisk metode. Ingen av disse ga ønsket produkt, men den hydrotermiske metoden ga krystallinsk SAPO-34. Hvorvidt denne var hierarkisk ble bestemt av N_2 fysisorpsjon (BET). Her ble det funnet ut at materialet inneholdt mesoporor, men disse var ikke uniforme som ønsket. Likevel var materialet bimodalt og man kan dermed si at det var hierarkisk.

Den krystallinske, hierarkiske SAPO-34 ble ionebyttet med både kobber(II)nitrat og kobber(II)tetraamin for å kunne måle hvor aktivt katalysatoren var for ønsket reaksjon, altså NO konversjon. I tillegg ble konvensjonell SAPO-34 samt mesoporøs SBA-15 også ionebyttet med samme løsninger og det ble også kjørt reaksjon på disse. Dette for å avgjøre hvorvidt aktiviteten er avhengig av porøsiteten.

Røntgendiffraksjon (XRD) ble brukt til å bestemme krystallinitet og ICP-MS avgjorde kobberopptak i katalysatormaterialene. Videre, ble det benyttet en mikroreaktor koblet til en GC-MS for bestemmelse av NO konversjon. Den konvensjonelle CuSAPO-34 var den mest aktive for dette formålet, mens den hierarkiske SAPO-34 og den mesoporøse SBA-15 hadde liknende konversjon. For å avgjøre om det skjedde en endring i kobberets lokale miljø, ble hierarkisk CuSAPO-34 undersøkt via Ex Situ røntgen absorpsjon spektroskopi (XAS) ved ESRF i Grenoble før og etter reaksjon i mikroreaktor. Konvensjonell SAPO-34 og mesoporøs SBA-15 ble også analysert Ex Situ, dog før reaksjon i mikroreaktor. Resultatene her indikerer at kobberet i hierarkisk SAPO-34 migrerer til kobber(II)oksid ved høye temperaturer.

Table of Content

Acknowledgement	I
Abstract.....	II
Sammendrag	III
List of abbreviations	VII
1.0 Introduction.....	1
2.0 Theory.....	3
2.1 Chemistry behind NO _x formation and its development	3
2.2 Reduction of NO _x in passenger cars.....	4
2.3 Copper containing catalysts for NO _x reduction.....	6
2.4 Catalyst materials.....	8
2.4.1 Conventional SAPO-34.....	8
2.4.2 Hierarchical SAPO-34	11
2.4.3 Mesoporous SBA-15.....	13
2.4.4 Copper on support material.....	14
2.5 X-Ray Diffraction (XRD).....	16
2.6 BET Theory	17
2.7 Scanning electron microscope	18
2.8 Inductively coupled plasma- mass spectrometry	19
2.9 X-ray absorption spectroscopy (XAS).....	20
3.0 Experimental.....	23
3.1 Synthesis	23
3.1.1 Hierarchical SAPO-34	23
3.1.2 SBA-15	27
3.1.3 Ion exchange	30
3.2 Characterization	31
3.2.1 X-ray Diffraction (XRD)	31
3.2.2 BET	31
3.2.3 Scanning Electron Microscopy (SEM)	31
3.2.4 Inductively Coupled Plasma- Mass Spectroscopy (ICP-MS)	31
3.3 Experimental HC-SCR.....	33
3.4 X-ray Absorption Spectroscopy (XAS).....	35
4.0 Results.....	37
4.1 Characterization	37

4.1.1 X-ray Diffraction (XRD)	37
4.1.2 BET	45
4.1.3 Scanning Electron Microscopy (SEM)	51
4.1.3 Inductively Coupled Plasma-MS (ICP-MS)	52
4.2 HC-SCR	55
4.3 X-ray Absorption Spectroscopy (XAS)	59
4.3.1 XANES	60
4.3.2 EXAFS	64
5.0 Discussion	71
5.1 Synthesis	71
5.2 Effect of porosity	73
6.0 Conclusion	76
7.0 Further work.....	77
8.0 References.....	78
9.0 Appendices.....	A
Appendix A: Risk evaluation.....	C
Appendix B: Additional BET	O
Appendix C: Additional SEM.....	Q
Appendix D: Additional HC-SCR results	S
Appendix E: Additional XANES.....	U
Appendix F: Additional EXAFS.....	W

List of abbreviations

AFAC	Amplitude reduction factor
Al	Aluminium
Al ₂ O ₃	Alumina catalyst support material
BaO	Barium oxide
BaCO ₃	Barium carbonate
Ba(NO ₃) ₂	Barium nitrate
BET	Brunauer-Emmet-Teller
BJH	Barrett-Joyner-Halenda
CHA	Zeolite framework type code (Chabazite)
CTAB	Cetrimonium bromide
CTAOH	Cetrimonium hydroxide
Cu	Copper
DEA	Diethylamine
DOC	Diesel oxidation catalyst
DPF	Diesel particulate filter
EGR	Exhaust Gas Resirculation
ESRF	European Synchrotron Radiation Facility
e.g.	for example et al. and others (citing several authors)
eV	electron volts
EXAFS	Extended X-ray absorption fine structure
FT	Fourier transformed
g	gram
GC-MS	Gas chromatography with mass spectrometer
HC	Hydrocarbon
HNO ₃	Nitric acid
ICP-MS	Inductively coupled plasma mass spectrometry
i.e.	that is/meaning that
in-situ analysis	simultaneous to reaction
IUPAC	International union of pure and applied chemistry
K	Kelvin
L	Liter

LNT Lean NO_x Trap
M Molar
MFC Mass flow controller
mg milligram
min minutes
mL milliliter
MS Mass spectrometer
MTO Methanol-to-Olefins
NH₃ Ammonia
nm nanometers
NO Nitric oxide
NO₂ Nitric dioxide
N₂ Nitrogen
O₂ Oxygen
P Phosphorous
PEG Poly(ethylene) glycol
PEO Poly(ethylene) oxide
PO Propylene oxide
Pd Palladium
Pt Platina
P-XRD Powder X-ray diffraction
Rh Rhodium
P123 Pluronic 123 (poly(ethylene glycol)-poly(propylene glycol)-poly(ethylene glycol))
SAPO Silicoaluminophosphate
SBA-15 silica gel type
SCR Selective catalytic reduction
SEM Scanning Electron Microscopy
Si Silicon
SNBL Swiss-Norwegian beamlines
SO₂ Sulphur dioxide
SSZ-13 Zeolite of chabazite structure
TEAOH Tetraethylammonium hydroxide

TEM Transmission Electron Microscopy

TEOS Tetraethyl ortosilicate

TMOS Tetramethoxysilane

TSE Tensile strength effect

VESTA Visualization for Electronic and Structural Analysis

wt% Weight percent

XANES X-ray absorption near-edge structure

XAS X-ray Absorption Spectroscopy

XRD X-ray diffraction

ZSM-5 Zeolite type

Å Ångström (10⁻¹⁰ m)

1.0 Introduction

In every high temperature combustion in presence of air, formation of nitrogen monoxide (NO) and nitrogen dioxide (NO₂) is a fact. These oxides are known as NO_x. There are of course different known sources of these gases, although the predominant ones are power plants, oil- and gas production, industries, and traffic. Figure 1.1 shows an overview of NO_x air emission with associated sources from Norwegian territory in the time period from 1990 to 2014. Here it is obvious to see a decrease during the time period, although emissions associated to oil and gas extraction have increased.¹

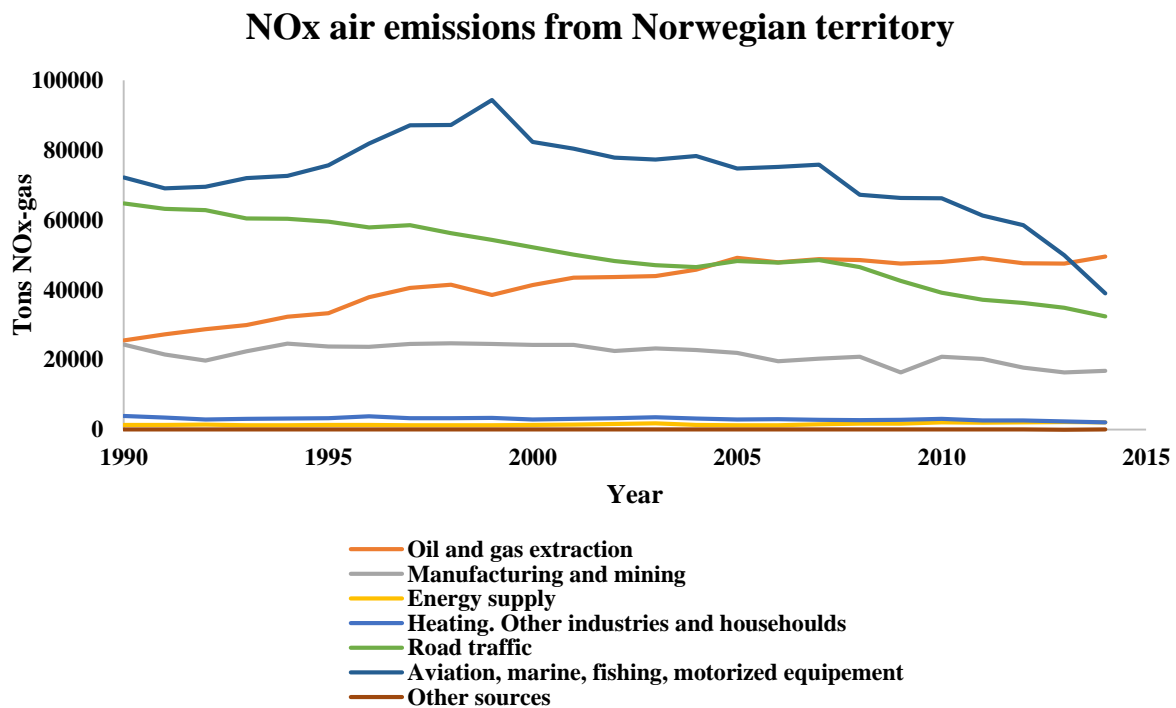


Figure 1.1: NO_x air emissions from Norwegian territory, 1990-2014.¹

As seen in figure 1.1, there are four distinct sources for NO_x and this project addresses emissions from transport and especially passenger cars. Emissions associated to transport have decreased significantly the last two decades due to stricter regulations. As an example, the newest Euro 6 standard imposes a further NO_x reduction to 0,08 g_{nox}/km^{2.3}. During the last year, different news and cases has shown that this is not fulfilled yet and still some work has to be done before these regulations can be reached. This addresses especially diesel vehicles, but also some gasoline cars. One of the most important news last year was the so-called

Volkswagen-scandal where it was shown that almost 11 million cars have less NO_x-emissions in a test situation compared to everyday driving.⁴

Unfortunately, NO_x are highly reactive with unfortunate consequences. NO alone attaches to the hemoglobin and reduces oxygen transport efficiency. The more toxic NO₂ can cause inflammation of lung tissue and in more severe cases it can cause a fatal condition called *bronchiolitis fibrosa obliterans*.^{1,5} In reaction with hydrocarbons at daytime, NO_x will form photochemical smog. Smog may be harmful for human health, including toxic smog-produced ozone, damage different materials, be toxic to plants, and may affect the atmosphere in a negative direction. Furthermore, NO_x are a known source for acid rain. Acidity of water and land may cause significant loss of fish and/or vegetation.^{1,5,6}

Luckily, in terms with stronger regulations from the governments, more research is addressed this problematic situation concerning vehicles. This thesis is a part of that research, where new types of catalyst materials concerning NO_x is under the radar.

2.0 Theory

During this chapter, the theory behind and associated to the work addressed to the project will be elaborated. Firstly, the chemical background will be explained before an elaboration of catalyst material and characterization methods are explained.

2.1 Chemistry behind NO_x formation and its development

The chemistry behind NO_x formation relates to formation of oxygen and nitrogen atoms at very high combustion temperatures by following reactions⁵:



Where M is a third body highly energized by heat that imparts enough energy to break the chemical bonds. Once formed, they promote a chain reaction forming nitric oxide:



The net reaction is therefore as follows:



Although NO is the primary form of NO_x released into the atmosphere, it is highly reactive and conversion to NO₂ is relatively rapid in the troposphere. Hence, the principal reactive nitrogen oxides species in the troposphere are NO, NO₂ and HNO₃. Conversion between these occur through cycles among each other and this phenomenon is shown in figure 2.1 below.⁷

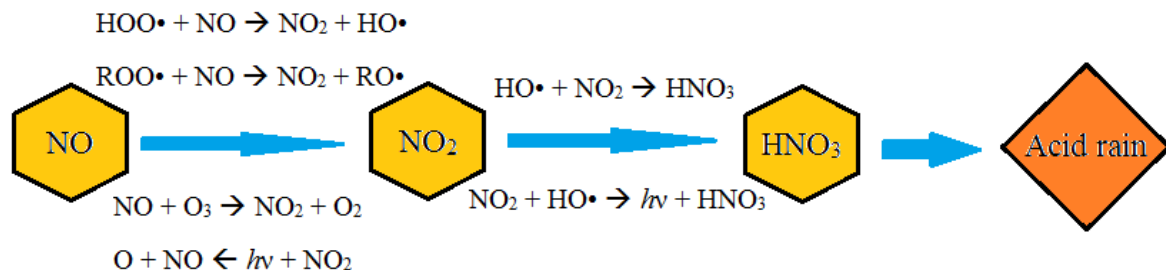


Figure 2.1: Atmospheric reactions between NO, NO₂ and HNO₃⁷

2.2 Reduction of NO_x in passenger cars

Regular fuel-based passenger cars either run on gasoline or diesel, and due to high temperature combustion they produce exhaust containing different gases. Amongst other, they both produce NO_x, but differ in quantity.

The stoichiometric air-to-fuel ratio inside the gasoline engine is ideally set to be 14.7 and as a consequence the reducing and oxidizing species in the exhaust is balanced.⁸ Most gasoline vehicles are equipped with a three-way catalyst and the reduction of exhaust gases from gasoline engines is therefore quite effective. This catalyst consists of Pt, Pd and Rh dispersed on a Al₂O₃ support.⁹ Three different reactions happen simultaneously catalysed by different combinations of metals, thereby the name of catalyst. These reactions are listed below in table 2.1.

Table 2.1: Overview of catalytic reactions and preferred catalyst⁹

Reaction		Catalyst
$\text{CO} + \text{O}_2 \rightarrow \text{CO}_2$	Oxidation	Pt, Pd
$\text{C}_x\text{H}_y + \text{O}_2 \rightarrow \text{CO}_2$	Reduction	Pt, Pd
$\text{NO} + \text{CO} \rightarrow \text{N}_2 + \text{CO}_2$	Reduction	Rh, Pd

Due to a leaner air-to-fuel ratio in diesel engines (depending on injection systems, but usually around 17-23) the environment is oxidizing and the exhaust contains more NO_x compared to the gasoline engine.^{4,8,9,10} The three-way catalyst as described above, cannot reduce NO_x emissions from diesel exhaust due to unbalanced ratio between the oxidizing and reducing species in the exhaust. The excess HC and CO are usually controlled by a diesel oxidation catalyst (DOC) instead, and this does not decrease emissions of NO_x. There are, however, four different ways to reduce NO_x emissions in diesel engines. Usually, a combination of one or more is most common together with a diesel particulate filter (DPF) and DOC, mounted in a specific order to decrease emissions.

The first option is to regulate the diesel injection. Here, modern nozzles and injection systems may reduce maximum temperature in the engine through a common rail system and less NO_x is produced during the combustion. The consequences however, are increased diesel consumption and worse performance of the car.¹¹

Another way is to recirculate parts of the exhaust back to the intake through an Exhaust Gas Recirculation (EGR) system. By doing this, the amount of oxygen decreases producing a richer environment in the engine. Due to increased amounts of inert gas, this will also decrease combustion temperature, leading to reduced NO_x emissions. Here it is also possible to cool the exhaust further and reduce NO_x emissions further. Even so, clogging of the EGR system is not rare and may cause (expensive) reparations.¹²

A lean NO_x trap (LNT) is a third possible way of reducing emissions of NO_x.^{13,14,15} LNT typically uses a blend of rhodium (Rh) and/or platinum (Pt) that catalyses the reduction/oxidation process and also a basic adsorbent consisting of either barium oxide (BaO) or barium carbonate (BaCO₃). The oxidation catalyst promotes formation of NO₂ which will adsorb to the basic adsorbent, forming Ba(NO₃)₂. Periodic regeneration, as in extra fuel injection, promotes a rich cycle in the catalyst and excess hydrocarbon (HC), carbon monoxide (CO) and hydrogen (H₂) react with the catalyst as the nitrate is released and reacts into nitrogen (N₂), hydrogen (H₂) and carbon dioxide (CO₂).

The last option for reduction of exhaust gases from diesel engines is selective catalytic reduction of NO_x (SCR). Often refers SCR to reduction of NO_x by ammonia (NH₃) or urea, where NH₃ or urea is added to the exhaust feed in order to act a reductant of NO. An equivalent amount of reductant and NO is required and as a consequence, an additional tank of NH₃ or urea is necessary.^{16,17,18} Hence, NH₃-SCR is not very suited for passenger cars due to frequent refills of NH₃ or urea and the responsibility of refills relies on the driver's concern of the environment. Additionally, there is a risk of NH₃ slip into the atmosphere. This type of technology is useful for stationary NO_x sources and is widely applied in treatment of NO_x emissions from heavy duty diesel vehicles where the responsibility of refills often relies on a company and not individuals.

2.3 Copper containing catalysts for NO_x reduction

Another promising technology of reducing NO_x emissions is selective catalytic reduction with hydrocarbons (HC-SCR) where excess hydrocarbon from the exhaust function as a reductant of NO. This process was first reported by Iwamoto et al in the early 90's, and was considered an epoch-changing discovery.¹⁹ HC-SCR is enhanced by presence of oxygen and proceeds even in presence of H₂O and SO₂, if the catalyst material can withstand such conditions. Copper containing silicoaluminophosphates were early seen as a viable possibility for this process²⁰. Copper is both cheap and have favourable availability compared to the more expensive, noble metals as Pt, Pd and Rh used in the three-way catalyst. Copper can be oxidized as well as reduced, which is a necessity for HC-SCR, shown in the proposed mechanism below.

Copper containing zeolites are active in several reactions concerning NO_x, amongst other in NO decomposition, NH₃-SCR, photocatalytic NO and N₂O reduction and HC-SCR.¹⁹ Consequently, there is not any doubt that copper may function excellent as active sites together with a support material that can withstand the conditions given by diesel vehicles.

In the exhaust feed from lean-burn engines there is approximately 0,05% NO_x, 5-10% O₂, 10 % H₂O and 0,05-0,1 % HC's and considering this, all NO_x could theoretically be converted to N₂²¹. In addition, there is a wide range of temperature the catalyst should be active in, usually around 100-200 °C during idling and more than 500 °C during full throttle.²² Hence, the catalyst should have a good selectivity to N₂, withstand big temperature differences, water vapour and other poisoning gases such as SO₂.²¹

In experiments, propene (C₃H₆) represents excess hydrocarbons (HC) in exhaust gas. The proposed mechanism is as follows²³:



Here, propene is the reductant for NO_x and copper is needed for activation of propene:



As an example has Cu-ZSM-5 showed high catalytic activity, but suffers of low (hydro)thermal stability and a more stable material is needed. Cu-ZSM-5 severely reduces its activity at high temperatures and has decomposed after exposure to water vapour. Lately, copper containing support materials from the chabazite family, SSZ-13 and SAPO-34 have been studied and hierarchical materials shows far better catalytic activity and hydrothermal stability than microporous materials.^{21,24,25} In earlier studies copper has shown efficiency for selective reduction of NO_x with propene, amongst other as ion exchanged in ZSM-5 and SAPO-34, where CuSAPO-34 has shown greater activity and better stability.^{21,25}

However, it is not yet decided how to exploit copper's properties and functionality together with a support material as a catalyst the best possible way concerning HC-SCR. Due to the fact that catalysis is a surface reaction, it is desired that as much copper as possible is available for catalysis. Therefore, it may be suited for the HC-SCR process that copper is supported onto a hydrothermal stable material with high specific surface. Another important aspect is that a catalyst material must withstand mechanical and hydrothermal stress due to the high pressures and temperatures. The catalyst must also have high conversion to desired product, and byproducts cannot be poisoning to the catalyst.

2.4 Catalyst materials

This subchapter concerns firstly the support material used in this thesis and afterwards it will be explained how copper may be introduced into/onto the support material.

2.4.1 Conventional SAPO-34

SAPO-34 is a zeotype where the framework consists of Si, Al and P as tetrahedral atoms with oxygen-bridges between them. This is a crystalline, microporous zeotype that shares topology to the mineral chabazite (CHA), where micropores are defined as smaller than 2 nm. SAPO-34 is three-dimensional and deemed as a small-pore zeotype. Due to the micropores this material has a high specific surface area, usually as much as 550 m²/g. The framework is composed by distorted hexagonal prisms that are linked together by four-member rings. This results in large, oval cavities called cages, whereas each cage is connected to 6 other cages through 8-member oxygens rings.^{26,27} Each cage is 0.75 nm in diameter and 0.82 nm high²⁸. The pore diameter is composed by the 8-member oxygen rings and the size is 0.38 nm * 0.43 nm²⁹.

Figure 2.2 shows the cage described above, and figure 4 shows the structure of SAPO-34 when looking directly at y-axis (a-direction) and z-axis (c-direction), collected from VESTA (Visualization for Electronic and STructural Analysis)³⁰. The blue dots represents the different T-atoms and the red dots represents oxygen.

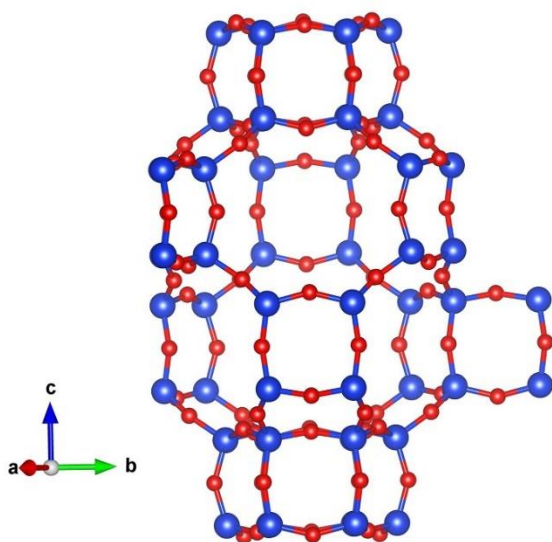


Figure 2.2: Visualization of the SAPO-34 cage that function as the structural building block. Here it is possible to see how the cage is bound by two distorted hexagonal prisms.

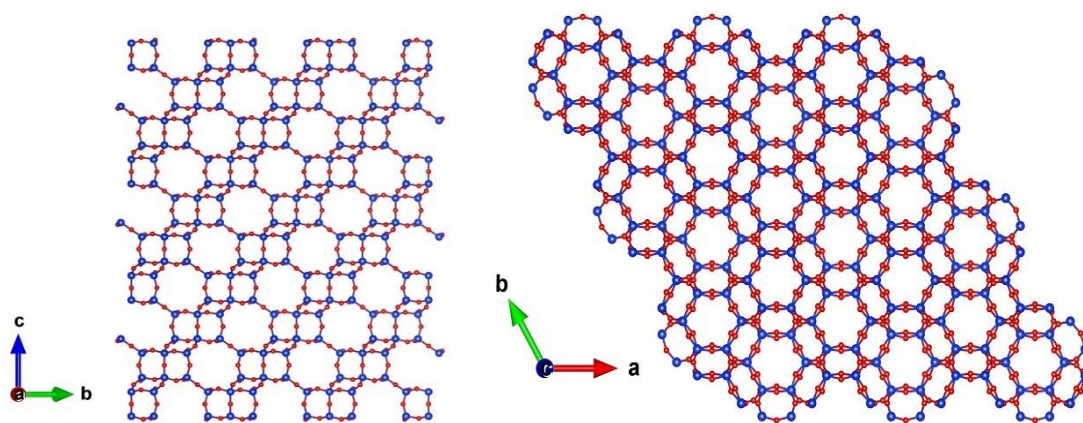


Figure 2.3: Structure of SAPO-34 as seen from two different directions. The left shows the structure from y-direction and it is possible to see the ordered 8-member rings. On the right the figure visualizes the structure from z-direction, and the arrangements of the 6-member rings is observable.

From figure 2.2 and 2.3 it is clear that the pores of SAPO-34 are created by the 4-member rings, 6-member-rings and the 8-member rings due to their ordered composition. Zeolites and zeotypes are known for their ability to function as molecular sieves. These selectivities lies in the pore system of the different materials. There are three different selectivities and the first can be described as reactant selectivity, where only molecules below size of the diameter of the pore can enter the pore. Hence, inside the pores or cages, only certain intermediates can form and only certain products can exit, all depending on the size of the pores.³¹

SAPO-34 is well-understood as it is often studied, mostly with respect to the methanol-to olefin (MTO) catalytic reaction^{28,29}. Here it has shown to be an excellent catalyst for the conversion, especially to lighter olefins due to its selectivity. Larger molecules are excluded due to the pores being smaller than the larger cages so the molecules cannot exit³². This type of selectivity also introduces another concern. As molecules are not permitted to exit the cages, these will clog after a certain time and hence deactivate the catalyst.

2.4.1.1 Diffusion Limitations

As mentioned above, deactivation of catalyst through clogging (coke) is a well-known issue concerning microporous materials. Another issue is diffusion limitations and this phenomenon is also partly the cause of clogging. Transport of reactant and product is determined by diffusion in and out of pores. Diffusion limitation is also a problem for the small-pore zeotype SAPO-34. To improve this material as catalyst it is necessary to develop a factor that may decrease diffusion limitations.

As for SAPO-34, the catalytic activity is of a reasonably high degree. Hence, the mass transfer of reactants and products will be the limiting factor. Diffusion is the main mechanism of mass transfer and as the overall reaction rate is as fast as the slowest step, it is vital to take concern of diffusion in catalysis. Molecular diffusion in intracrystalline pores is slow and therefore only the outer regions of the catalyst particles will participate in the conversion. The Thiele modulus, Φ , explains the main factors of porous diffusion in particles. If the Thiele modulus is high, larger parts of the particle is not used in the catalytic reaction. However, if the Thiele modulus is close to zero, the entire particle is utilized in the catalytic reaction.^{33,34} The Thiele modulus is determined by the following equation:

$$\Phi = \frac{r_{intrinsic}}{r_{diffusion}} = L * \sqrt{\frac{k_v}{D_{eff}}} \quad (11)$$

Here, L is the diffusion length, k_v is the intrinsic rate coefficient and D_{eff} is the effective diffusivity. In order to decrease the value of Φ , there are two different options that could be done. Either, decrease the diffusion length or increase the degree of diffusivity. In order to decrease the diffusion length, it is possible to decrease the particle size or apply a thin layer of microporous material onto a mesoporous or macroporous support. In order to increase the degree of diffusivity, the most common option is to modify the pore system of the catalyst.³⁵

Hence, one possibility is to add ordered mesopores into an ordered microporous structure. The mesopores will then function as super-highways for reactants and products to and from the active sites of the catalyst. Then the accessibility of the active sites will improve and decrease diffusion limitations.

2.4.2 Hierarchical SAPO-34

Hierarchical materials are materials that contains both micropores and mesopores, where mesopores have magnitude up to 50 nm. The connectivity between these can be illustrated in figure 2.4 below. Figure 2.4 (b) illustrates an interconnected hierarchical system where the voids between the microporous crystals functions as mesopores. Both figure (c) and (d) are intraconnected hierarchical systems, where (c) shows a system where micropores are intersected by mesopores that are accessible from the external surface. (d) illustrates mesopores as enclosed mesovoids.

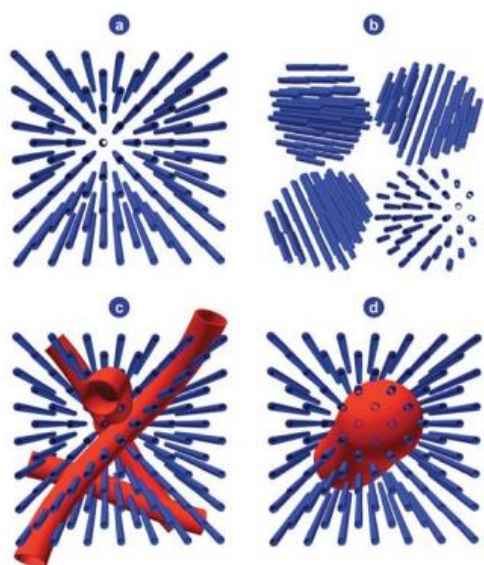


Figure 2.4: Illustration of connectivity in hierarchical materials. (a) illustrates a purely microporous material and (b) illustrates an interconnected hierarchical system. (c) and (d) illustrates two different intraconnected hierarchical systems. Reproduced from ref 36 with permission of The Royal Society of Chemistry.

Of the hierarchical systems illustrated in figure 2.4, (b) and (c) will increase the diffusivity, but (d) will not increase the transport efficiency due to the fact that the mesopores are enclosed by a network of micropores. Consequently, the reactants must diffuse through the micropores first and the mesopores here may be seen as unnecessary.

The hierarchical SAPO-34 is a zeotype quite similar to the conventional SAPO-34. The structural difference lies in the pore system, whereas the conventional is a crystalline microporous system, the hierarchical is an ordered micro- and mesoporous system. Ideally, the structure of the hierarchical SAPO-34 will be identical compared to the conventional one around ordered mesopores and may be visualized as figure 2.4 (c). This is tried illustrated in

figure 5 below where a possible mesopore formation within the structure of SAPO-34 is shown. This is illustrated in the z-direction of the SAPO-34 structure.

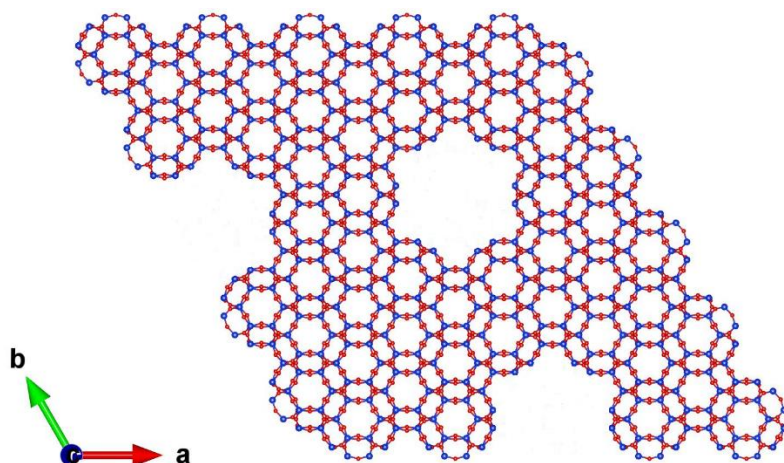


Figure 2.5: Illustration of possible mesopores within the SAPO-34 structure. Hence, the structure has both micropores and mesopores in the z-direction of SAPO-34 structure. The mesopores are not connected to the micropores in this direction, but they are connected to micropores in the other two directions.

Concerning synthesis of hierarchical materials, this can be done in two main directions. Either as an additional step during the initial synthesis, or as a post treatment of a finished product. As an additional step during the initial synthesis the clue lies in the choice of template which is added during the synthesis. Mesoporous templates can be large bulky molecules like surfactants or as an example, they can be carbon nanotubes or saccharides.^{36,37,38} Templates, also known as organic structure directing agents, force the different T-atoms to form the inorganic framework in certain directions and will be combusted off the solid during calcination. As a result, only the inorganic framework remains.

Post treatments of a finished product, involves manipulation and changing the original structure into a hierarchical structure. One way of doing this can be done through dry gel conversion where micropores are introduced into a mesoporous SAPO-34 monolith.³⁹

2.4.3 Mesoporous SBA-15

This project addresses the effect of porosity on hierarchical Cu-SAPO-34 for the deNO_x process. In order to compare conversion on the hierarchical Cu-SAPO-34 it was decided to compare conversion with the mesoporous silica SBA-15 in addition to conventional SAPO-34.

SBA-15 is a mesoporous silica where the pores are hexagonally ordered, with a large surface area, up to 900 m²/g. SBA-15 has thick pore walls, big pore diameter and has been applied, amongst other, in heterogeneous catalysis as catalyst support. The thick walls are up to 6,4 nm and this provides high hydrothermal and mechanical stability of the material. Consequently, SBA-15 is thought of as a good comparison to the SAPO-34.⁴⁰

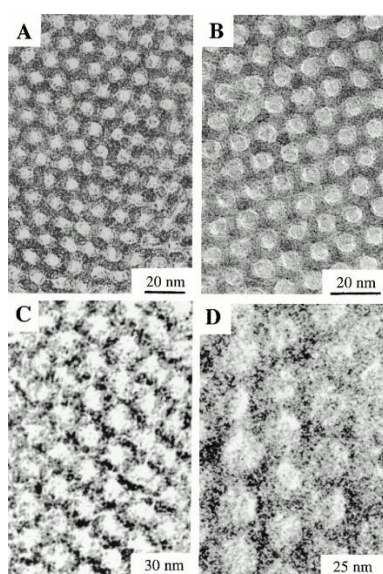


Figure 2.6: TEM images of SBA-15 of different pore sizes. The picture is reproduced from the work of Zhao et al with permission from AAAS⁴⁰.

2.4.4 Copper on support material

There are several ways of introducing copper into a zeotype or zeolite and these can be described as incorporation, impregnation and ion exchange. Impregnation is not relevant for this thesis and will therefore not be covered. Incorporation of metal cations into the framework of a zeotype can be made possible by adding desired amounts of a metal solution into the synthesis mixture⁴¹. By doing this, the metal cation can take place of a tetrahedral atom in the zeotype framework. Substitution of an aluminium atom will enhance acidity in the framework. This is illustrated in figure 2.7 below, where the blue dots represent the ordinary T-atoms in a SAPO-34, the red represents the oxygen bonds and the yellow illustrates copper atoms in the SAPO-34 structure.

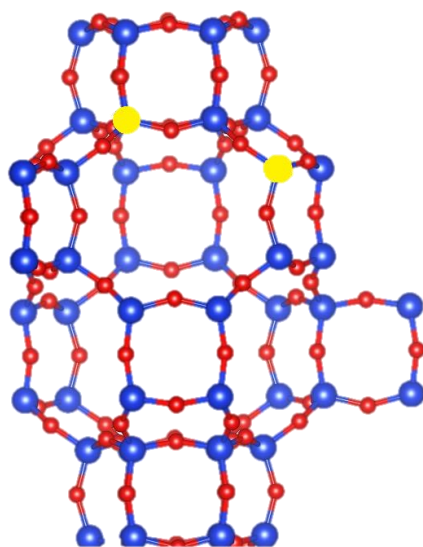


Figure 2.7: Illustration of incorporation of copper(II)ions into the framework of a SAPO-34. The yellow dots represent the copper atoms.

The T-atoms of a SAPO-34 are, as mentioned, Si, Al and P. Due to charge imbalance between these, formation of Brönsted acidic sites (H^+) are promoted. If a zeotype or zeolite is ion exchanged, these Brönsted acidic sites are replaced with a metal cation. This can be done with copper(II)ions by stirring a SAPO-34 in a copper(II) solution for 24 hours⁴². Often, ion exchange is performed in a basic solution to gain uptake of the metal cation. The exchanged cation is most likely to be find inside the characteristic cavity of the SAPO-34. Inside the cavity there are four different possible sites for the copper ion, as shown in figure 2.8 below.

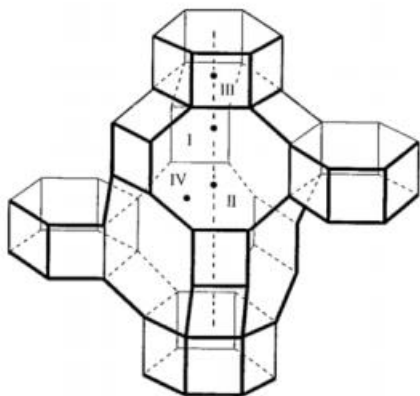


Figure 2.8: Cation sites in SAPO-34²⁶

Site I is supplanted from the 6-ring into the cavity, site II is found near the centre of the cavity, site III is located in the centre of the hexagonal prism and the last site is found close to the 8-ring.²⁶

Unfortunately, some SAPO-34 undergoes irreversible hydrolysis during ion exchange, as reported by Gao et al⁴³. They report that Si content within the samples and framework stress are the key factors that affect the hydrolysis of acidic Si-O-Al bond. The concrete hydrolysis degree depends on the Brønsted acid concentration and the crystal size of SAPO-34.^{43,44} In particular, SAPO-34 samples with high Al-O-Si bond density and framework stress experience more irreversible hydrolysis.

2.5 X-Ray Diffraction (XRD)

X-ray diffraction (XRD) is a non-destructive technique useful for determination of crystalline phase.⁴⁵ Meaning, the technique provides finger-print information about the crystallographic structure and the chemical composition of the sample. XRD is also useful for crystallites, then called powder x-ray diffraction (PXRD). Here a sample is radiated with monochromatic x-rays and depending on the crystallographic structure, these x-rays will scatter, as shown in figure 2.9.⁴⁵

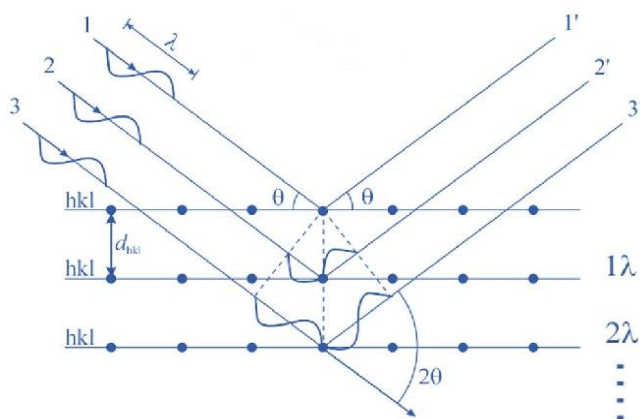


Figure 2.9: Radiation of sample

When the scattered, monochromatic x-rays are in phase, a peak can be seen in a diffractogram, as figure 2.10 below. This technique is therefore useful determining whether or not a sample is phase pure and crystalline. Each crystalline material has its own diffractogram. A phase pure SAPO-34 will have the diffractogram of the zeolite chabazite due to similar structure and chemical composition. The same applies for the hierarchical SAPO-34, so these cannot be distinguished by PXRD. The diffractogram of the chabazite structure is shown in figure 2.10, as calculated from the Atlas of Zeolite framework types.²⁸

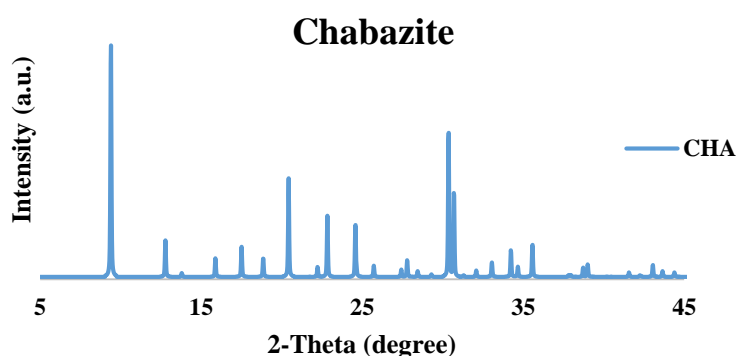


Figure 2.10: Diffractogram of chabazite

The same applies for incorporated or ion exchanged SAPO-34. As long as the copper has not precipitated out within the structure it will not give impurities in the diffractogram. If impurities occur, possible explanations have to be retrieved and development of synthesis must be considered in order to obtain desired product. The goal is therefore to obtain a diffractogram similar as possible to the one in figure 2.10.

2.6 BET Theory

The BET isotherm is named after Brunauer, Emmet and Teller and this is a physisorption isotherm that provides information about the specific surface area of solid materials. Here, an inert gas, often N_2 , is physisorbed on the surface and the quantity of gas molecules to form a monolayer on the surface determines the specific surface area. Simultaneously, the pressure is measured and this has to be performed at the liquefaction temperature of N_2 at 77 K. The relative pressure (P/P_0) is an important term here. P_0 is the equilibrium pressure for the condensed gas and when the relative pressure is approaching 1, the total coverage of adsorbed gas is approaching infinity. This means that the adsorbate condenses into multilayers on the surface of the material.⁴⁶

When the amount of gas adsorbed and desorbed is plotted against the relative pressure a BET isotherm is observed. IUPAC divide the BET adsorption isotherms in six different categories dependant on their shape. These six isotherms give specific information based on their shape. One of these shapes have a so-called hysteresis loop, where the gas is desorbed at lower pressure than the adsorption points. The hysteresis loops are divided into four different subcategories as well, dependant on the material. These isotherms are shown in figure 2.11.³⁴

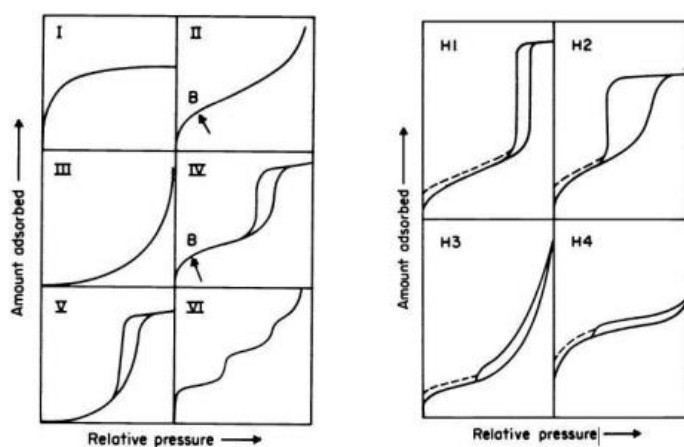


Figure 2.11: The six different adsorption isotherms are shown on the left, and on the right the four different hystereses are shown.

As seen in figure 10, there are 6 different adsorption isotherms, although only three of these are the most frequent. These are isotherm type I, II and IV. Type I isotherm is most commonly associated to microporous catalyst such as activated carbon or zeolites and may not be suited for values of specific surface area. However, type II or IV is well-suited for this process, where the type IV isotherm gives information about mesoporosity depending on the hysteresis loop. H1 hysteresis loop is usually associated to a narrow pore distribution of relatively uniform mesopores. H2 describes a more complex pore structure in which network effects are important. However, the H3 and H4 types do not possess well-defined mesopore structures and as a consequence it is not recommended to derive neither the pore size distribution nor the total pore volume. These hysteresis loops usually describe plate-like materials such as clays or similar material.³⁴

Pore size distribution may as well be interesting dealing with different catalyst materials and a known physisorption model created by Barret, Joyner and Halanda (BJH) may be applied. Condensed gas within the mesopores of a material will have a meniscus. This meniscus has a curvature directly related to the pore width, if Kelvin equation is applied. A hemispherical meniscus is connected to spherical pores and hemicylindrical meniscus arises from slit-shaped pores. The derivative of BJH adsorption will give answer to the most predominant pore width. Nevertheless, a well-known misconception concerning pore size distribution is the tensile strength effect (TSE). This appears as a peak at 3.8 nm in the pore size distribution, most commonly in the desorption branch due to forced closure of hysteresis loop.

2.7 Scanning electron microscope

Scanning electron microscope (SEM) is a versatile technique applied for mapping microstructure morphology and chemical composition of different samples and specimen. The sample is probed by a beam of electrons, usually from a tungsten gun, scanned across the surface of the sample. Interactions caused by the electronic beam makes it possible to form an image of the sample. This may then be used as comparison and conformation of known literature and give further information of samples.⁴⁷

An important factor when applying SEM is to have electrically conductive samples. If the sample itself is nonconductive, such as metal oxides, the sample has to be coated with an ultrathin layer of electrically conductive material, deposited either by low-vacuum sputtering or high-vacuum evaporation. This is due to build-up of negative charge. The coating material is usually gold, carbon and other heavy metals. However, gold is the preferred coating material

due to the electronic interactions between the beam and the sample. Further, if the coating is too thick it may obscure the small features of the surface.⁴⁷

When a sample is bombarded with negatively charged particles it may cause damages in different ways. If the sample is relatively nonconductive, negative charge may accumulate in the bulk material and may damage the image effect. Here, particles will appear extra bright in the image and this may decrease the quality of the image. Radiation damage is another, where the sample's surface is ruptured by the electron beam. This does not give a fulfilled image of the surface and decreases the quality of the image.⁴⁷

2.8 Inductively coupled plasma- mass spectrometry

Inductively coupled plasma-mass spectrometry (ICP-MS) is a technique relatively rapid, precise and accurate trace-element analysis for both solid and liquid sampled. Analysis using ICP-MS provides both qualitative and quantitative information of species in a sample. Here, plasma provides ionization of the atomic elements in the sample and a detector may then provide qualitative and quantitative (after calibration) information of the sample. The detector determines a signal based on the mass-to-charge ratio (m/z) of each element analysed. Almost every element may be detected due to the specificity of atom weight, even after ionization. However, isotopes and their abundancy must be considered during analysis as well as other interferences.⁴⁸

In this thesis, ICP-MS is especially useful for determination of copper content and the relationship between the different T-atoms in the catalyst material.

2.9 X-ray absorption spectroscopy (XAS)

X-ray absorptions spectroscopy (XAS) can be used to probe the chemical environment of transition metals in, amongst other, zeotypes. This technique is hence applicable for determining the chemical environment of copper(II)ions in a SAPO-34, and determining oxidation state and coordination number of the certain transition metal.

A synchrotron provides non-thermal electromagnetic radiation, generated by charged particles in a magnetic field.⁴⁹ Radiations are generated in a particle accelerator and storage rings, and can be used for different characterization methods. For the synchrotron, the charged particles in the storage rings are electrons. When accelerating these to almost relativistic speeds and subjecting them to magnetic fields, the polarizing radiation is obtained. The frequencies of the polarizing radiation can range from infrared to hard X-rays. Illustration of the synchrotron utilised in this thesis is shown in figure 2.12 below, collected from the ESRF homepage.

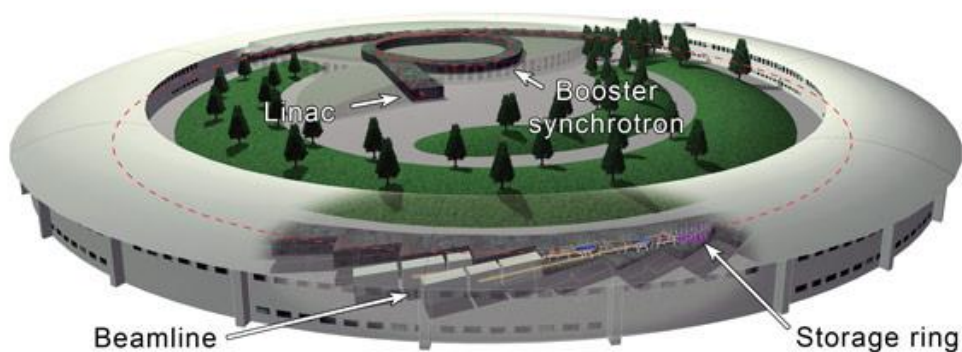


Figure 2.12: Illustration of a synchrotron, where the linear accelerator, booster synchrotron, storage ring and beamlines are marked.⁴⁹

When analysing a sample by XAS, X-rays from a synchrotron storage rings bombards a sample and the resulting transmitted or fluorescent intensity is measured. In other words, the X-ray absorption coefficient μ is measured as a function of photon energy E above an absorption edge.

For a transmittance experiment the linear absorption coefficient μ is calculated by following equation:

$$\mu x = \ln \frac{I_0}{I} \quad (12)$$

where x is the thickness of the sample, I_0 is the intensity of the incident beam and I is the intensity of the transmitted beam.⁵⁰

The XAS spectre is divided into two regions, XANES and EXAFS, this is shown in figure 2.13 below. This figure shows a plot of the absorption coefficient vs. the electron energy (in electron Volts (eV)). A discontinuity can be seen as the energy of the incident photons equal the binding energy of electrons in the 1s orbital of the element analysed. Half way up the discontinuity is referred to as the element's K-edge.

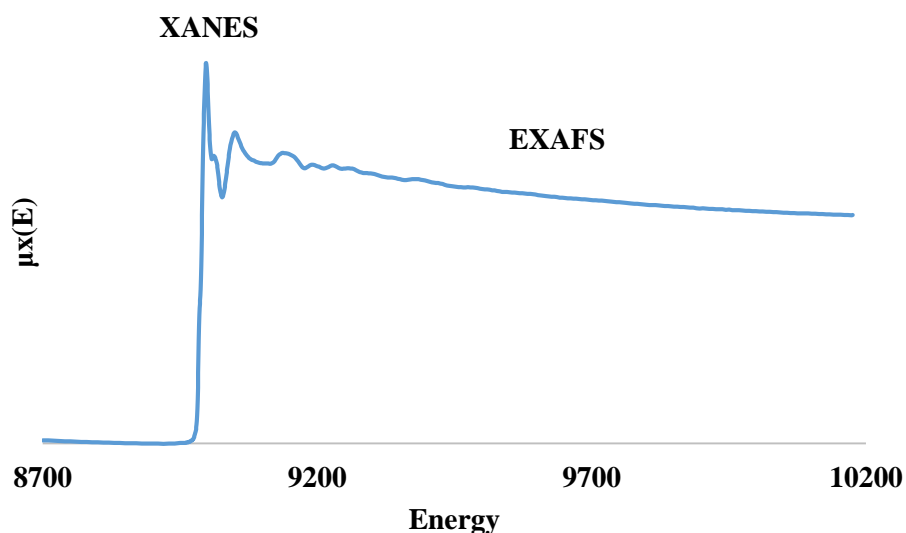


Figure 2.13: Illustration of a XAS spectrum and the element's hypothetical K-edge

The X-ray Absorption Near-edge Structure (XANES) region reaches from approximately 8 eV to around 40 eV after the edge⁵¹. Information from this region says something about the element's valence state, its coordination number and site symmetry. This can be obtained by comparing to known model compounds that contain the same elements as the one being analysed⁵².

The Extended X-ray Absorption Fine structure (EXAFS) region is the oscillating appearance of the absorption coefficient a few eV up to 1000 eV past the K-edge. The oscillating appearance is due to the interference between the ejection of photoelectron from the projected atom and the backscattering from the neighbouring atoms. Mathematically, this can be described by the following K-weighted EXAFS equation⁵¹:

$$\chi(k) = \sum_j \frac{N_j F_j(k) S_j(k) e^{-2k^2 \sigma_j^2} e^{-\frac{2R_j}{\lambda_j(k)}}}{k R_j^2} \sin[2kR_j + \Phi_{ij}(k)] \quad (15)$$

Where:

- i refers to the photo-absorbing element and j refers to the backscattering elements
- N_j is the coordination number of shell j
- $F_j(k)$ refers to the backscattering amplitude from one backscattering atom in shell j
- $S_j(k)$ is the amplitude reduction factor (AFAC)
- σ_j^2 is the Debye-Waller factor
- R_j is the interatomic distance from the photo-absorber to shell j
- λ is the mean free path of the photoelectron
- $\Phi_{ij}(k)$ refers to the total phase shift for the photoelectron

This equation is quite complicated and consequently, the analytical solution is impossible to obtain, but can be solved using *ab-initio* calculations.

In this thesis, XAS is used to determine differences concerning the copper(II)ions in hierarchical SAPO-34 pre and post HC-SCR. For determination of oxidation state and possible local environment of copper, two standards are used for comparison. These are copper(II)oxide and copper(I)oxide. Normalized XANES and normalized derivative XANES are shown below in figure 12. The orange curve represents Cu_2O , hence the blue curve represents CuO .

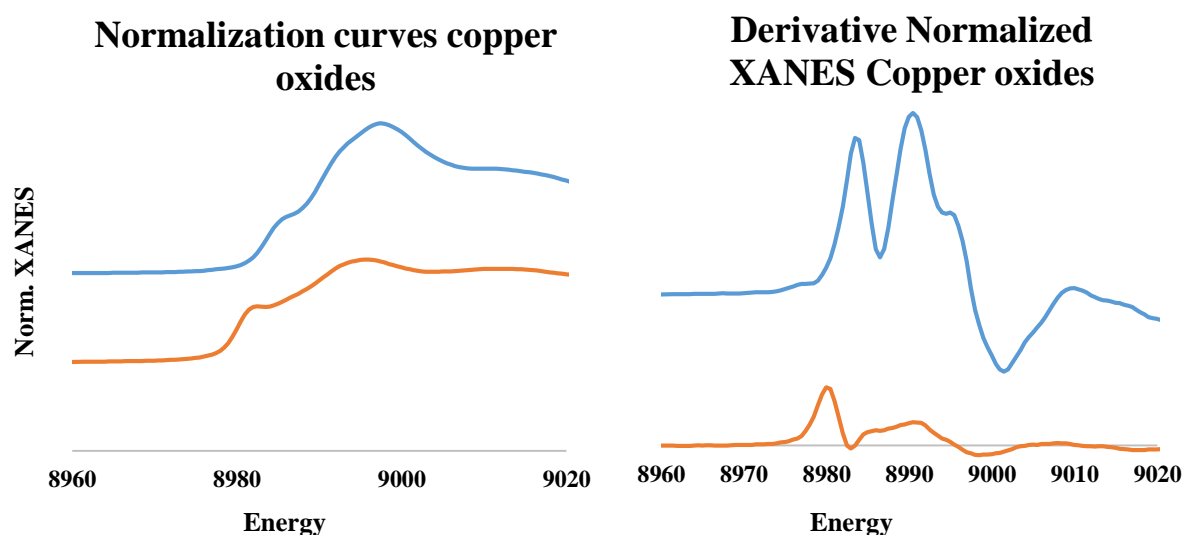


Figure 12: Normalized XANES for Cu_2O and CuO at the left and normalized derivative XANES for Cu_2O and CuO at the right.

3.0 Experimental

3.1 Synthesis

The main goal during this thesis is to obtain hierarchical SAPO-34 where copper is incorporated into the framework. This has never been performed before, hence it was necessary to make evaluations and developments during the project period. For comparison, a mesoporous SBA-15 was synthesised as well and conventional, microporous SAPO-34 was donated by Ph.D. Candidate Stian Forselv. All chemicals used are provided from Sigma Aldrich.

3.1.1 Hierarchical SAPO-34

To obtain the goal for this thesis, it was decided to base the work on two different synthesis routes. The first was synthesis of hierarchical SAPO-34 and try to incorporate copper(II) ions into the framework. Another synthesis route was to base the synthesis on a conventional SAPO-34 and differ the structure directing agents as well as try to incorporate copper(II) ions into the framework.

3.1.2.1 Turning hierarchical SAPO-34 into copper incorporated hierarchical SAPO-34

In the project group this work is centred from, earlier work has been done based on the work of Yang et al³⁹. Here, hierarchical SAPO-34 is synthesized by dry gel conversion of amorphous silicoaluminophosphate, where aluminium chloride hexahydrate ($\text{AlCl}_3 \cdot 6(\text{H}_2\text{O})$), tetramethoxysilane (TMOS) and diammonium hydrogen phosphate ($(\text{NH}_4)_2\text{HPO}_4$) are the sources of Al, Si and P respectively. However, halides interrupt the catalytic process of NO_x reduction with copper. The first modification was therefore to use aluminium isopropoxide ($\text{Al}[\text{OCH}(\text{CH}_3)_2]_3$) as aluminium source. TMOS (5g) was the source of Si for all experiments.

The theoretical gel composition is set to be:

$\text{Al} : \text{P} : 0.4\text{Si} : 31\text{H}_2\text{O} : 5\text{C}_2\text{H}_5\text{OH} : 6 \cdot 10^{-5} \text{PEO} : 3\text{PO}$.

In beaker number 1, all T-atoms are dissolved in half of deionized water together with eventual copper(II) additions. In the second beaker, polyethylene oxide (PEO, 0,5 g) was dissolved in ethanol ($\text{C}_2\text{H}_5\text{OH}$, ~ 96%, 20 g) and the rest of deionized water was added dropwise during stirring. The content of the second beaker was then added to the first under stirring. Final, propylene oxide (PO, 13 g) was added to the mixture.

The mixture was then sealed in a plastic container for gelation at 60 °C for 15 hours and then dried without lid at 60 °C for 48 hours. The dried gel was then mortared before calcination at 550 °C for 8 hours. Further, the calcined gel was transferred to an autoclave with Teflon liner and impregnated with tetraethylammonium hydroxide (TEAOH, ~40%). This was let to crystallize for 72 hours at 200 °C. The resultant samples were washed with deionized water and centrifuged before they were dried in a petri dish overnight at 70 °C. At last, they were calcined once more at 550 °C for 8 hours.

The amounts of T-atoms and water varied due to variations of sources, except of the silica source. In table 3.1, an overview of the different T-atoms is found together with the amount of the respective source. The amounts of ethanol, PEO and PO are fixed and did not vary of above.

Table 3.1: Variations of sources for the different T-atoms

Sample name	Source and amount of P (g)	Source and amount of Al (g)	Source of copper	Cu/A l ratio	Amount of water (g)
mon1	H ₃ PO ₄ 10.2	Pseudoboehmite 12.56	CuO	0.025	59.6
mon2	H ₃ PO ₄ 10.2	Pseudoboehmite 12.56	CuO	0.05	59.6
mon3	(NH ₄) ₂ HPO ₄ 11.65	AlCl ₃ •6(H ₂ O) 21.35	-		50
mon4	(NH ₄) ₂ HPO ₄ 11.65	Al[OCH(CH ₃) ₂] ₃ 18.06	-		59.6
mon5	(NH ₄) ₂ HPO ₄ 11.65	Al[OCH(CH ₃) ₂] ₃ 18.06	Cu(CH ₃ COO) ₂	0.05	59.6

During the first two syntheses, it was decided to use copper(II)oxide (CuO) as copper source, and due to low solubility, it was therefore decided to use concentrated phosphoric acid (H₃PO₄, 85%) as phosphorous source.

3.1.2.2 Ion exchange of structure directing agent

To obtain both the microporous and the mesoporous structure it is necessary to use appropriate structure directing agents. The synthesis was therefore based on the work of Najafi et al⁵³ and the mesoporous agent was decided to be the surfactant cetrimonium bromide (CTAB).

The mesoporous agent CTAB is a surfactant that may be suited for formation of mesopores. Unfortunately, the surfactant consists of the halide bromide (Br) and halides interrupt the catalytic process of NO_x reduction. In order to obtain the surfactant without bromide, an ion exchange had to be performed.

CTAB (20 g) was dissolved in deionized water (1 L). The following solution was sent through a resin column twice to obtain CTAOH and then tested with AgNO₃ in order to see if all bromide had ion exchanged. The solution was concentrated under reduced pressure.

3.1.2.3 Turning conventional SAPO-34 into hierarchical Cu-SAPO-34

Hierarchical SAPO-34 was synthesized by the hydrothermal method, where aluminium isopropoxide (Al[OCH(CH₃)₂]₃), phosphoric acid (85 wt%) and TEOS were sources of Al, P and Si, respectively. The source of copper(II)ions was copper(II)acetate. The molar ratio of the starting gel was 1.0 Al₂O₃: 1.0 P₂O₅: 0.6 SiO₂: 1.5 TEAOH: 70 H₂O: χ CTAOH: λ Cu. Values for χ and λ are given in table 3.2 and 3.3.

The first five syntheses were tried with solid CTAB in order to see if the synthesis would provide crystalline material and to have comparison to the ion exchanged CTAB. This can be seen in table 3.2 below. Here, the three first syntheses involved addition of CTAB firstly into the mixture. For the last two syntheses, CTAB was added in the end of synthesis.

Table 3.2: Synthesis of hierarchical SAPO-34 with CTAB as SDA. Different synthesis parameters as crystallization time and molar ratio of SDA/Al are listed here as well. Neither of these were added copper and had no aging time. Crystallization time was 200 °C for all syntheses.

Sample name	Molar ratio CTAB/Al	Crystallization time (h)
HSAPO_01	0,5	15
HSAPO_02	0,25	14,5
HSAPO_03	0,5	14,5
HSAPO_04	8,81E-04	15
HSAPO_05	5,58E-04	14

In a typical synthesis aluminium isopropoxide ($\text{Al}[\text{OCH}(\text{CH}_3)_2]_3$, 4 g) was dissolved in a beaker containing deionized water (17,5 g) and TEAOH (10,81 g), and stirred until a homogeneous solution was obtained. Then the source of silicon (TEOS, 2,45 g) was added dropwise under stirring. After that, the source of phosphorous (H_3PO_4 , 85 wt %, 2,26 g) was added dropwise as well and stirred 30 minutes. Finally, CTAOH was added and stirred another 30 minutes before the initial gel was set to aging for 24 hours. The initial gel was then sealed in a stainless steel autoclave and heated in an oven for 96 hours at 200 °C or 150 °C if the initial gel contained copper.

The resulting sample was then washed with deionized water and centrifuged before it was transferred to a petri dish and dried overnight at 70 °C. The dried powder was then mortared and calcined at 550 °C for 8 hours to remove the templates.

Table 3.3 below shows the synthesis parameters where CTAOH was used as mesoporous structure directing agent. Here, addition of copper is shown as well. For all samples, copper was added before addition of TEAOH. However, for sample HSAPO-34_16, HSAPO-34_19 and HSAPO-34_20, copper was dissolved first in another beaker. For the last two with copper addition, copper was added as copper(II)acetate salt.

Table 3.3: Synthesis of hierarchical SAPO-34 with CTAOH as structure directing agent. Different synthesis parameters are also listed here.

Sample name	Molar ratio Cu/Al	Molar ratio CTAOH/Al	Aging	Crystallization time (h)	Crystallization temperature (°C)
HSAPO_06	-	7.52E-04	-	14	200
HSAPO_07	-	1.01E-03	-	14	200
HSAPO_12	-	8.17E-04	24	24	200
HSAPO_13	-	8.17E-04	24	48	200
HSAPO_14	-	8.17E-04	24	72	200
HSAPO_15	-	8.17E-04	24	72	200
HSAPO_16	0.03	8.17E-04	24	72	150
HSAPO_17	-	8.17E-04	24	96	200
HSAPO_18	-	9.81E-04	24	117	200
HSAPO_19	0.025	9.81E-04	24	72	150
HSAPO_20	0.0125	9.81E-04	24	72	150
HSAPO_21	0.05	9.81E-04	19	120	150
HSAPO_22	0.025	9.81E-04	19	120	150
HSAPO_23	-	1.23E-03	19	120	200
HSAPO_24	-	2.61E-03	24	71	200
HSAPO_25	-	9.81E-04	70	71	200
HSAPO_26	-	9.81E-04	24	71	200

3.1.2 SBA-15

In order to compare effect of porosity of hierarchical SAPO-34 for the deNO_x process, it was necessary to synthesise a material consisting solely of mesopores as well as a microporous material. The mesoporous material was decided to be SBA-15 and here three different synthesis routes were chosen. The first was a conventional SBA-15, the second was a synthesis route with addition of CTAOH and the last route was an attempt of incorporating copper ions into the structure as synthesising. These three different synthesis routes will be explained in order here and the differences can be seen below in table 5.

Common for all syntheses, an acid is required for formation of silica. The most common for SBA-15 is hydrochloric acid (HCl). However, for deNO_x with copper, halides will interrupt so it was decided to use phosphoric acid. Concentrated phosphoric acid (26.52 g, 85 %) was diluted with deionized water until total volume reached 100 ml and the desired concentration of 2.3 M was reached. The common template for all syntheses is the triblock copolymer Pluronic 123 (EO₂₀PO₇₀EO₂₀), usually called P123 and tetraethyl orthosilicate (TEOS) is used as the silica source.

Conventional SBA-15:

The synthesis was inspired by the work of Iván Meléndez-Ortiz et al (2016)⁵⁴, and in a typical synthesis, P123 (1 g) was dissolved in ethanol (5 ml), deionized water (7.5 ml) and phosphoric acid (2.3 M, 15 ml). Then, TEOS (2.5 g) was added dropwise and the mixture was let to stir for 12 hours at 40 °C before it was set to age for 20 hours at 80 °C.

After aging the solid was filtrated using a G4 grit, first 2 times using ethanol, then 5 times with deionized water before once more with ethanol to speed up the drying process. The gel was transferred to a petri dish and let to dry overnight at room temperature. The dried material was then calcined at 550 °C for 12 hours.

SBA-15 with addition of CTAOH:

The synthesis was inspired by the work of as above. In a typical synthesis P123 (1 g) was dissolved in ethanol (5 ml), deionized water (5 ml) and phosphoric acid (2.3 M, 15 ml). Then, CTAOH was added (0.128 M, 2 ml) into the mixture while stirring before TEOS (2.5 g) was added dropwise. The mixture was stirred another 12 hours at 40 °C before aging at 80 °C the next 20 hours.

After aging the mixture was filtrated using a G4 grit, first 2 times using ethanol, then 5 times with deionized water before once more with ethanol to speed up the drying process. The gel was transferred to a petri dish and let to dry overnight at room temperature. The dried material was then calcined at 550 °C for 12 hours.

SBA-15 with incorporation with copper

This synthesis was inspired by the work of Wang et al (2005)⁵⁵. The original aluminium source was aluminium nitrate salt, and could not be used here due to HC-SCR experiments. Copper(II)acetate (Cu(CH₃COO)₂*H₂O) was dissolved in a beaker containing deionized water

(30 ml), concentrated phosphoric acid (H_3PO_4 , 85%, 6.75 g) and aluminium isopropoxide ($\text{Al}[\text{OCH}(\text{CH}_3)_2]_3$, 0.27 g) and left to stir for 3 hours. In the meantime, P123 (0.5 g) was dissolved in ethanol (9.48 g). This mixture was so added dropwise to the aqueous mixture above under vigorous stirring and left to stir 12 hours at 60 °C. Then TEOS (1.1 g) was added to the mixture and stirred at least another 20 hours at 60 °C. The mixture was so left to age for 48 hours at 90 °C.

The solid gel was filtrated using a G4 grit and washed with ethanol 2 times before 5 times with deionized water and a final time with ethanol to speed up the drying process. The gel was then transferred to a petri dish and let to dry at room temperature overnight. The solid powder was calcined at 550 °C for 6 hours. A list of all SBA-15 synthesized can be seen in table 3.4 below.

Table 3.4: Synthesized SBA-15

Sample name	Template	Co-template	Aging time (h)	Calcination temperature (°C) and time (h)	Cu/Si ratio incorporated
SBA-15_01	P123	CTAOH	20	550, 12	-
SBA-15_02	P123	-	20	550, 12	-
SBA-15_03	P123	-	48	550, 6	0.05
SBA-15_04	P123	CTAOH	20	550, 12	-
SBA-15_05	P123	-	20	550, 12	-
SBA-15_06	P123	-	48	550, 6	0.1
SBA-15_07	P123	CTAOH	20	550, 12	-
SBA-15_08	P123	-	20	550, 12	-

For characterization, small angle x-ray diffraction must be used due to the specific peaks around 1 degree 2θ . However, this type of instrument was not available. Hence, BET was decided to be sufficient as characterization method.

3.1.3 Ion exchange

For comparison, two conventional SAPO-34, two mesoporous SBA-15 and two hierarchical SAPO-34 was ion exchanged with both copper(II)nitrate solution (0.03 M) and copper(II)tetraamine solution (0.03 M). The two conventional SAPO-34 were provided by Ph.D. candidate Stian Forselv in the same research group. A total of 12 samples were ion exchanged. In order to make the two different solution of copper(II)nitrate and copper(II)tetraamine with desired concentration, copper(II)nitrate salt ($\text{Cu}(\text{NO}_3)_2 \cdot \text{H}_2\text{O}$, 1.812 g) was dissolved in deionized water (250 ml). Half of the solution was transferred to a beaker and let to stir. Concentrated ammonia was diluted with deionized water to a concentration of 5 M. Further, the diluted ammonia solution was then added carefully to the copper(II)nitrate solution until the solution had a dark, blue colour indicating formation of copper(II)tetraamine. For conformation, the pH was measured to be 8.5 and no more ammonia was added.

In a typical ion exchange, a sample was transferred to a beaker and a copper(II) solution (0.03 M) was added. This slurry was so let to stir at room temperature for 24 hours. Below is a table of samples and amount of copper(II) solution and amount of sample.

Table 3.5: List of all samples that were ion exchanged.

Sample name	Pore system	Amount of sample (g)	Copper(II)nitrate (0.03 M, ml)	Copper(II)tetraamine (0.03 M, ml)
SAPO-34_04	Microporous	0.5	15	15
SAPO-34_08	Microporous	0.5	15	15
SBA-15_07	Mesoporous	0.5	15	15
SBA-15_08	Mesoporous	0.5	15	15
HSAPO-34_14	Hierarchical	0.5	15	15
HSAPO-34_18	Hierarchical	0.25/0.5*	7.5	15

* Due to small amount of sample HSAPO-34_18, 0.25 grams were ion exchanged with 7.5 ml copper(II)nitrate and 0.5 grams were ion exchanged with 15 ml copper(II)tetraamine

After ion exchange, the samples were washed with deionised water and centrifuged 4-6 times, depending on how many times necessary for clear wash water. The samples were then transferred to a petri dish and let to dry overnight at 70 °C.

The samples ion exchanged with copper(II)nitrate solution are from here denoted Cu_1 , and the samples that were ion exchanged with copper(II)tetraamine solution are denoted Cu_2 .

3.2 Characterization

A various set of techniques were used in order to characterize the material and determine whether or not a hierarchical SAPO-34 with incorporated copper was obtained. In the following subchapter, the experimental parts of the characterization techniques will be described.

3.2.1 X-ray Diffraction (XRD)

For the XRD-analysis a Bruker D8 Advance DaVinci X-ray diffractometer is used. The sample is prepped in a sample holder and queued before analysis. Here, a Cu K α X-ray tube is used in combination with a lynxeyetm superspeed 1D detector. The divergence slit opens automatically such that the illuminated length on the sample is always 6 mm and the measurement parameters include angles from 5-75° 2 θ . The diffractograms were used to determine phase purity and degree of crystallinity in comparison to the chabazite (CHA) diffractogram.

3.2.2 BET

A micromeritics Tri Star 3000 Surface Area and Porosity Analyzer is used for BET analysis. The samples are weighed and set at degas at 250 °C for 20 hours before analysis. Then, the specific surface area is calculated from adsorption and desorption isotherm according to BET. The pore volume and pore size distribution is calculated according to BJH method. The results were used to determine the specific surface area, the porosity, and whether or not a sample is hierarchical.

3.2.3 Scanning Electron Microscopy (SEM)

A Hitachi S-3400N was applied for SEM analysis. This equipment can give resolution up to 4.0 nm in VP-mode and it is equipped with both a SE and a SBE detector. A carbon tape was mounted on a sample holder and small amounts of sample was scattered over the carbon tape. All excess grains were then removed by blowing air before the samples were carbon coated using low-vacuum sputtering. The sample holder with sample was then mounted into the Hitachi instrument and the chamber was vacuumed before analysis. Images were then taken at low magnification (400 eV), medium magnification (1.2k eV) and high magnification (~4k eV, depending on resolution).

3.2.4 Inductively Coupled Plasma- Mass Spectroscopy (ICP-MS)

ICP-MS elemental analysis were conducted by Syverin Lierhagen (IKJ) at NTNU using a High Resolution Inductively Coupled Plasma ELEMENT 2 connected to a mass spectrometer. The results were mainly used to determine copper content in different samples and also to see

whether or not the theoretical fractions of Al, Si and P were to be expected in the experimental samples.

The samples were weighed out (10-20 mg) in a Teflon tube (25 mL) and decomposed by adding concentrated nitric acid (HNO₃, 1.5 mL) and concentrated hydrofluoric acid (HF, 0.5 mL). The resultant solution was then transferred to a larger Teflon canister and diluted with deionized water until a total weight of 216.6 g was reached. A Teflon tube (16 mL) was then washed with deionized water and subsequently filled with the sample solution. Further, three blanks were made in order to eliminate background noise.

3.3 Experimental HC-SCR

The experimental rig used for catalytic testing is sketched in figure 3.1 below. Each gas bottle used for the experiment is coupled to a mass flow controller (MFC), controlled by the PC, in order to get the right mix of reaction gas into the furnace. The outlet is connected to a gas chromatograph mass spectrometer (GC-MS) for analyzation of outlet mixture. The sample is hold in place in the reaction tube within the furnace by quartz wool.

For these experiments, a mixture of helium (He, 5 ml flow), oxygen (O₂, 50 000 ppm), propene (C₃H₆, 1200 ppm) and nitrogen monoxide (NO, 1000 ppm) was used.

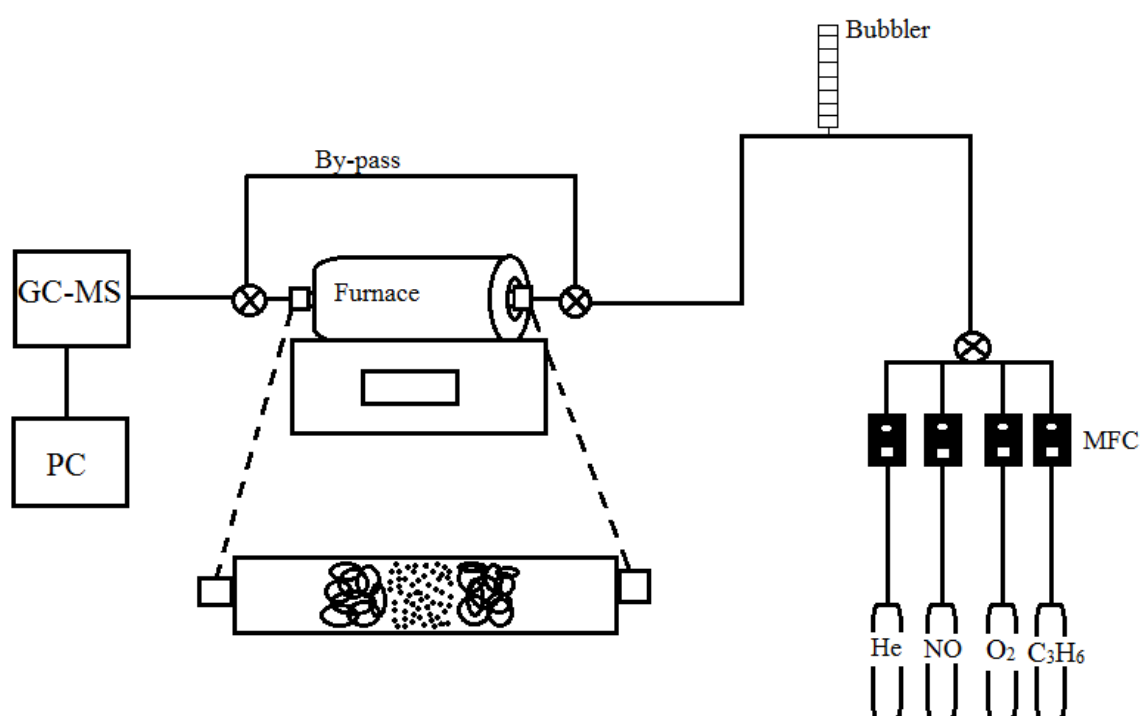


Figure 3.1: Catalytic microreactor used for measurements of NO_x conversion⁵⁶

Before each catalytic experiment the gas lines were flushed by reaction gas to make sure no air was in the lines. Afterwards, the sample was pressed to a pellet and then mortared lightly before it was sieved in order to get the correct particle size. The sample was weighed out (0.04 g) and put in the reaction tube between quartz wool. Next, the sample was calcined to 450 °C with a ramp rate of 10 °C/min and held at 450 °C for 30 minutes. After calcination, the reaction tube was then cooled to 250 °C and afterwards flushed by reaction gas for 30 minutes.

Then, the injection to GC-MS was applied using a program developed by Ph.D. Tina Kristiansen, where each analysis takes 5 minutes and 30 seconds. When finished with the first analysis, the temperature was increased another 50 °C with ramp rate of 10 °C and another

analysis was started. This was repeated until desired temperature was reached, depending on sample as shown in table 3.6 below. When finished, the furnace was cooled to room temperature and sample was kept in a sample glass. For two of the experiments the gas feed contained water by using a bubbler.

Table 3.6: Final temperature of catalytic experiments, noted dry or wet reaction feed

Experiment number	Sample	Final Temperature (°C)	Wet or Dry feed
1	HSAPO-34_18_Cu ₁	500	Dry
2	HSAPO-34_18_Cu ₂	500	Dry
3	HSAPO-34_14_Cu ₁	450	Dry
4	HSAPO-34_14_Cu ₂	450	Wet
5	HSAPO-34_14_Cu ₂	600	Wet
6	HSAPO-34_14_Cu ₂	500	Dry
7	HSAPO-34_14_Cu ₂	450	Dry
8	SAPO-34_04_Cu ₂	600	Dry
9	SBA-15_07_Cu ₂	600	Dry

Conversion of NO for the first 6 samples in table 3.6 is determined by following equation:

$$\% \text{ Conversion} = \frac{[NO]_{in} - [NO]_{reactor}}{[NO]_{in}} * 100\% \quad (14)$$

For experiment 7-9, conversion of NO was determined by equation 15 below. Here, the method is similar to above. Only difference is an extra injection over bypass at each temperature before the temperature was increased another 50 °C.

$$\% \text{ Conversion} = \frac{[NO]_{bypass} - [NO]_{reactor}}{[NO]_{bypass}} * 100\% \quad (15)$$

Originally, all of these three should be analysed up to 600 °C. However, during experiment number 7, the filaments in the GC-MS broke so the data was only collected up to 450 °C.

3.4 X-ray Absorption Spectroscopy (XAS)

XAS data was performed at the Swiss-Norwegian Beam Lines (SNBL) B-station at the European Synchrotron Radiation Facility (ESRF) in Grenoble, France. A schematic illustration of the sample setup is shown below in figure 3.2:

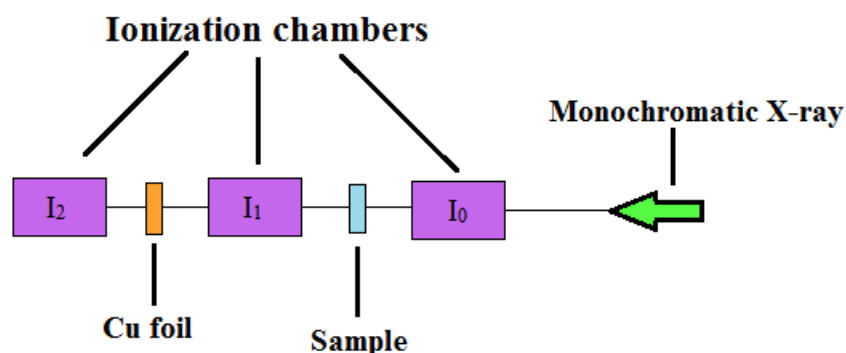


Figure 13: Illustration of the sample setup used for XAS data at SNBL

Samples were pressed into pellets and taped with Kapton® in order to make sure the pellet would hold. These were then attached to a sample wheel with 10 sample places. Model compound were measured with sample powder in aluminium sample holders with Kapton® tape in front and back in order to hold the powder in place. These were diluted with boron nitride.

Measurements on the copper k-edge (8979 eV) were performed in transmission mode in the scan range between 8700- 10 200 eV with a counting time of 0.8 s and a step length of 150 eV.

The Athena software from IFEFFIT package was used for data reduction, where the raw material was energy shifted in accordance with the copper foil and unnecessary noise were eliminated.⁵⁷ For XANES, a normalization range of 30-150 eV is used. For EXAFS a normalization range from 150 eV until end of data is used. These were then uploaded in the program DLV EXCURV. The program calculated the ab initio phaseshifts and backscattering amplitude by defining the atoms present in the sample. A k^3 - weighting was used for all samples. AFAC was not refined.

Following, table 3.7 lists the different samples that were performed measurements. The specifications of pre and post reaction are also found here.

Table 3.7: List of samples that were analysed at the SNBL with specifications concerning HC-SCR

Sample name	HC-SCR description	Pore distribution
HSAPO-34_14Cu ₁	Pre reaction	Hierarchical
HSAPO-34_14Cu ₁	Post dry feed 450 °C	Hierarchical
HSAPO-34_18Cu ₁	Pre reaction	Hierarchical
HSAPO-34_18Cu ₁	Post dry feed 500 °C	Hierarchical
HSAPO-34_14Cu ₂	Pre reaction	Hierarchical
HSAPO-34_14Cu ₂	Post dry feed 500 °C	Hierarchical
HSAPO-34_14Cu ₂	Post wet feed 450 °C	Hierarchical
HSAPO-34_14Cu ₂	Post wet feed 600 °C	Hierarchical
SAPO-34_04Cu ₁	Pre reaction	Microporous
SAPO-34_04Cu ₂	Pre reaction	Microporous
SAPO-34_08Cu ₁	Pre reaction	Microporous
SAPO-34_08Cu ₂	Pre reaction	Microporous
SBA-15_07Cu ₁	Pre reaction	Mesoporous
SBA-15_07Cu ₂	Pre reaction	Mesoporous
SBA-15_08Cu ₁	Pre reaction	Mesoporous
SBA-15_08Cu ₂	Pre reaction	Mesoporous

4.0 Results

4.1 Characterization

A different set of characterization techniques have been used and in this subchapter the results of characterization techniques will be presented.

4.1.1 X-ray Diffraction (XRD)

XRD is used for as a characterization technique to determine whether or not a sample obtains crystallinity. The results will be presented in order as of chapter 3.1

4.1.1.1 Turning hierarchical SAPO-34 into hierarchical Cu-SAPO-34

Of the five syntheses based on the synthesis of Yang et al. only 1 synthesis was completed. This is due to separation of two viscous phases in the gelation mixture of the other syntheses. The one completed is the one that is copied from Yang et al, and as table 4.1 below show, this is the only one synthesized with original aluminium source, marked in green. The other are tried synthesized with pseudoboehemite or aluminium isopropoxide due to chlorine content in the original aluminium source.

Table 4.1: Synthesis parameters of the five different syntheses based on the synthesis of Yang et. al.

Sample name	Source of P	Source of Al	Source of copper	Cu/Al ratio	Completed synthesis
mon1	H ₃ PO ₄	Pseudoboehemite	CuO	0.025	No
mon2	H ₃ PO ₄	Pseudoboehemite	CuO	0.05	No
mon3	(NH ₄) ₂ HPO ₄	AlCl ₃ •6(H ₂ O)	-		Yes
mon4	(NH ₄) ₂ HPO ₄	Al[OCH(CH ₃) ₂] ₃	-		No
mon5	(NH ₄) ₂ HPO ₄	Al[OCH(CH ₃) ₂] ₃	(Cu(CH ₃ COO) ₂) ₂	0.05	No

Due to the separation of the gelation mixture, the only XRD-result from this synthesis angle, is the one directly copied from Yang et al. This is shown in the diffractogram below, figure 4.1, where it is easy to see that the sample is phase pure and crystalline SAPO-34.

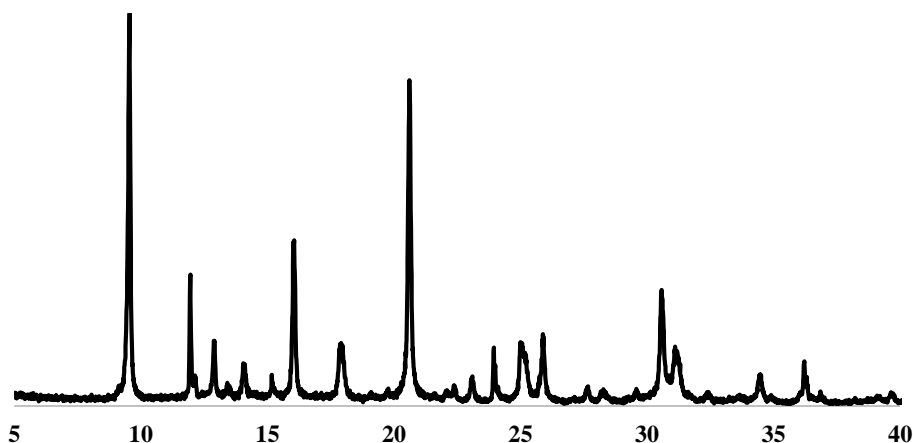


Figure 4.1: Diffractogram of hierarchical SAPO-34 based on the synthesis of Yang et al. This is the only sample where the synthesis was completed.

Common for syntheses of different aluminium source than the original, the synthesis mixture was quite white after addition of the aluminium source and did not become clearer. It is presumed that the aluminium not being able to dissolve enough might be the main reason for separation of the gelation mixture. Hence, a solvation project was initiated. Below is a table of the different efforts of dissolving both pseudoboehemite and aluminium isopropoxide with the same molar ratios of the original synthesis.

Table 4.2: Solvation project of different aluminium sources and combinations with reagents.

Aluminium source	Co reagents	Solvent	Result
$\text{Al}[\text{OCH}(\text{CH}_3)_2]_3$	TEAOH	H_2O	not dissolved
$\text{Al}[\text{OCH}(\text{CH}_3)_2]_3$	$(\text{NH}_4)_2\text{HPO}_4$	H_2O	not dissolved
$\text{Al}[\text{OCH}(\text{CH}_3)_2]_3$		EtOH	not dissolved
Pseudoboehemite		H_3PO_4	not dissolved
$\text{Al}[\text{OCH}(\text{CH}_3)_2]_3$		H_3PO_4	Not dissolved

As table 4.3 shows, neither of the tried combinations would provide dissolved aluminium. Hence, this route of obtaining hierarchical Cu-SAPO-34 was hold on pause.

4.1.1.2 Turning conventional SAPO-34 into hierarchical Cu-SAPO-34

The first goal along the way of obtaining hierarchical Cu-SAPO-34, was to first see whether or not this synthesis route would provide hierarchical SAPO-34. Hence, the first five syntheses were done with the salt CTAB as SDA, as seen in table 4.3 below. All of these syntheses were done with a crystallization time around 14 hours and a crystallization temperature of 200 °C. The main difference is hence the ratio of CTAB/Al, whereas the ratio of the first three are directly inspired by the original synthesis. After seeing that neither of these provided crystalline SAPO-34, as seen in figure 4.2, it was decided to decrease the concentration of CTAB below the critical micelle concentration (CMC).

Table 4.3: Synthesis of SAPO-34 with CTAB as mesoporous SDA. Different syntheses parameters that varied are shown here.

Sample name	Molar ratio CTAB/Al	Crystallization time (h)	XRD result
HSAPO_01	0.5	15	Amorphous
HSAPO_02	0.25	14.5	Amorphous
HSAPO_03	0.5	14.5	Amorphous
HSAPO_04	8.81E-04	15	Amorphous
HSAPO_05	5.58E-04	14	Amorphous

Following XRD-diffractogram show the corresponding XRD-results of the samples listed in the table above. Neither of the five samples are crystalline SAPO-34.

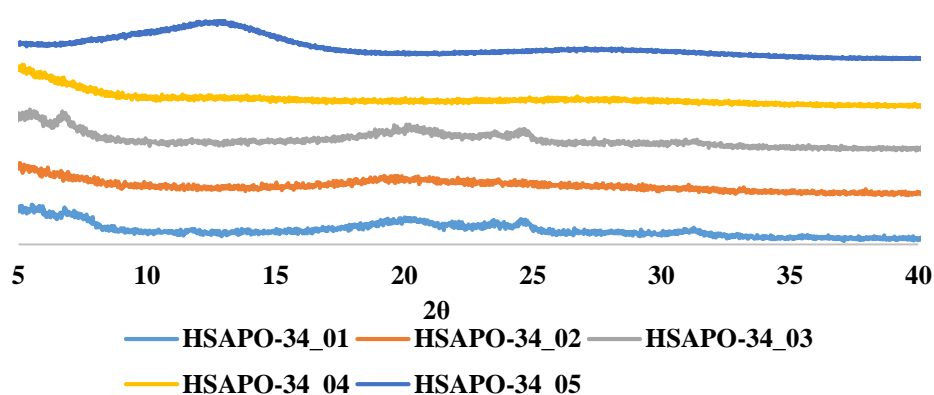


Figure 4.2: XRD-results of syntheses with CTAB as SDA

The mesoporous SDA was exchanged to CTAOH, in order to perhaps save some time to obtain parameters that would provide hierarchical SAPO-34. Table 4.4 below shows the different changes in the synthesis parameters, in particular aging time and crystallization time. The concentration of CTAOH was continued to be hold below CMC.

Table 4.4: The first five synthesis of hierarchical SAPO-34 with CTAOH as mesoporous SDA. Addition of aging time and longer crystallization time were two of the most important factors here. Crystallization temperature was 200 °C for all of these as well.

Sample name	Molar ratio CTAOH/Al	Aging time (h)	Crystallization time (h)	XRD result
HSAPO_06	7.52E-04	-	14	Amorphous
HSAPO_07	1.01E-03	-	14	Amorphous
HSAPO_12	8.17E-04	24	24	Amorphous
HSAPO_13	8.17E-04	24	48	Amorphous
HSAPO_14	8.17E-04	24	72	Crystalline
HSAPO_18	9.81E-04	24	117	Crystalline

The first four syntheses with CTAOH as mesoporous SDA provided non-crystalline SAPO-34. However, after addition of aging time and longer crystallization time, as for samples named HSAPO-34_12 and HSAPO-34_13, it is clear that something is happening. A peak around 10 and 20 is arising, indicating that something might be crystallizing.

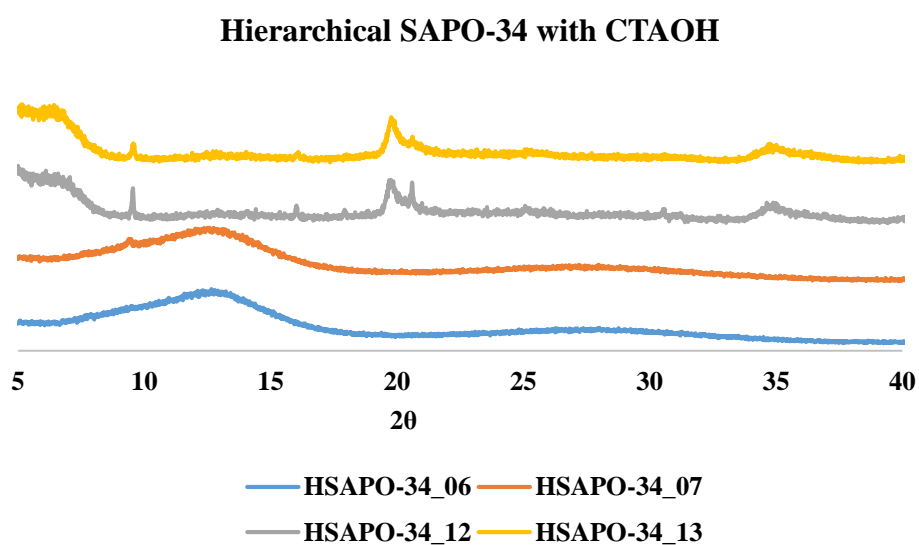


Figure 4.3: XRD-results of the first syntheses with CTAOH as SDA

The XRD-result of sample named HSAPO-34_14 is shown in figure 4.4 below together with the sample named HSAPO-34_18. These samples had crystallization time longer than 70 hours. Both samples are calcined and as the figure shows, they are both crystalline.

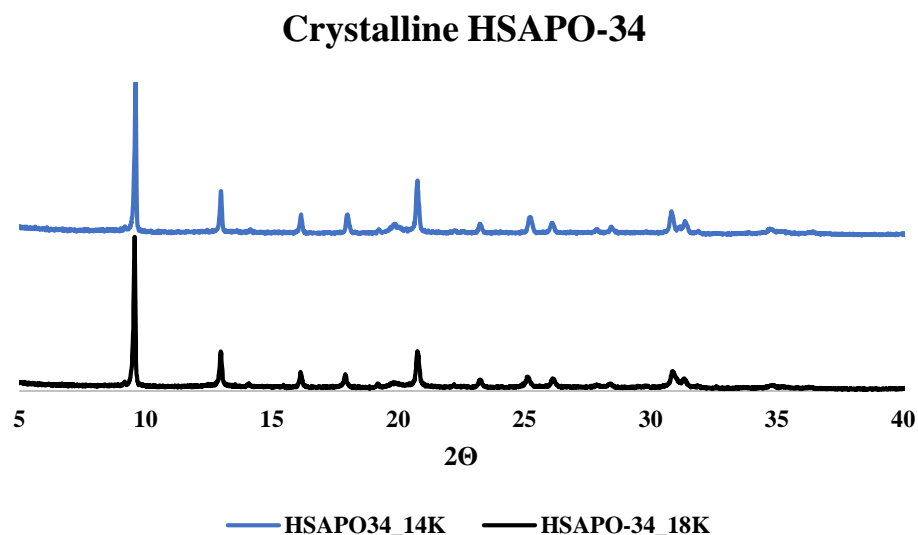


Figure 4.4: XRD-diffractograms of crystalline HSAPO-34_14 and HSAPO-34_18

The synthesis parameters that provided the crystalline SAPO-34 above were tried in combination with addition of copper(II)acetate into the mixture. A total of five syntheses were tried in order to incorporate the copper ions into the framework of hierarchical SAPO-34. The different combinations of copper-addition, aging time and crystallization time is shown in table 4.5 below. Crystallization temperature of these are 150 °C.

Table 4.5: Synthesis parameters of hierarchical SAPO-34 with incorporation of copper.

Sample name	Molar ratio Cu/Al	Molar ratio CTAOH/Al	Aging time (h)	Crystallization time (h)	XRD result
HSAPO_16	0.03	8.17E-04	24	72	Amorphous
HSAPO_19	0.025	9.81E-04	24	72	Amorphous
HSAPO_20	0.0125	9.81E-04	24	72	Amorphous
HSAPO_21	0.05	9.81E-04	19	120	Amorphous
HSAPO_22	0.025	9.81E-04	19	120	Amorphous

Figure 4.5 shows the XRD-diffractogram of the corresponding samples of table 4.5. These are tried synthesized as hierarchical SAPO-34 with incorporated copper(II)ions. As the figure shows, neither of the samples are crystalline

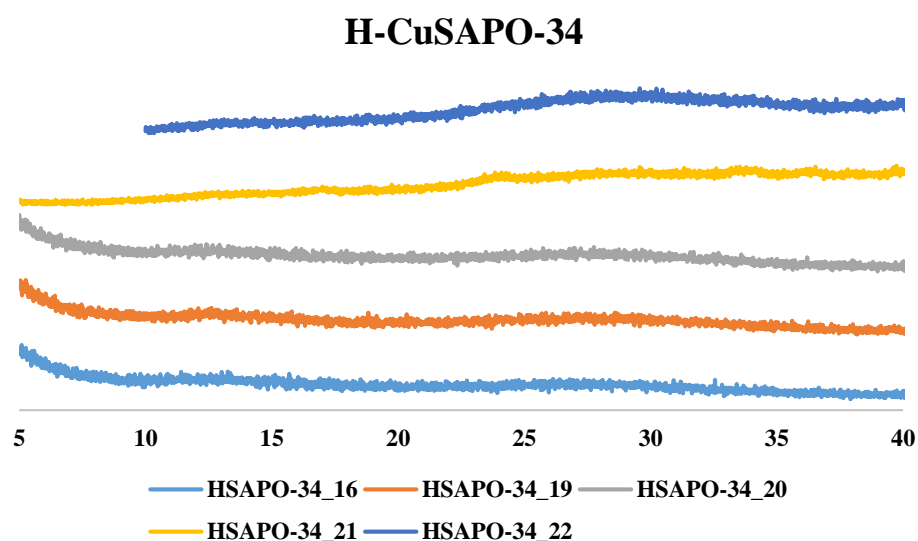


Figure 4.5: XRD- diffractograms of amorphous materials when copper(II)-ions were added to the gel mixture with the parameters that provided crystalline SAPO-34.

Due to not being able to synthesise crystalline hierarchical SAPO-34 with incorporated copper, it was decided to ion exchange the crystalline hierarchical SAPO-34 with a copper(II)solution. Hence, an effort of making even more crystalline SAPO-34 than the samples named HSAPO-34_14 and HSAPO-34_18 was initiated. Here, a bigger variation of aging time was done in order to see if this would make a difference. These differences in synthesis parameters are shown in table 4.6 below and the corresponding XRD-results are shown in figure 4.6 below.

Table 4.6: Synthesis parameters of the last synthesis of hierarchical SAPO-34. Crystallization time of these was 200 °C. C means crystalline and A means amorphous.

Sample name	Molar ratio CTAOH/Al	Aging time (h)	Crystallization time (h)	XRD results
HSAPO_15	8.17E-04	24	72	C + A
HSAPO_23	1.23E-03	19	120	C + A
HSAPO_24	2.61E-03	24	71	C + A
HSAPO_25	9.81E-04	70	71	C + A
HSAPO_26	9.81E-04	24	71	C + A

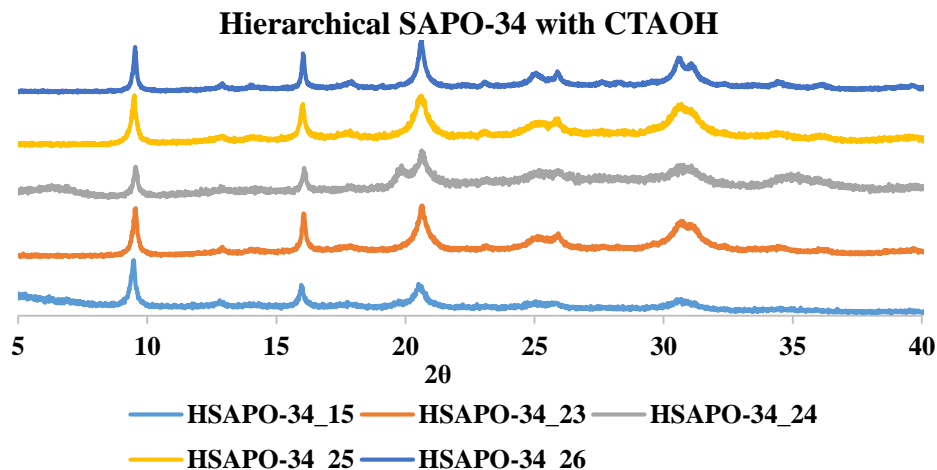


Figure 4.6: Synthesis of hierarchical SAPO-34. An effort of making even more crystalline sample than the ones named HSAPO-34_14 and HSAPO-34_18

As figure 4.6 shows, the samples have similarities of the diffractogram of chabazite, although the baselines have more noise and the intensity of the peaks is less than the diffractogram of HSAPO-34_14 and HSAPO-34_18. Hence, these samples are not more crystalline than HSAPO-34_14 and HSAPO-34_18.

The samples that were decided to be ion exchanged are consequently HSAPO-34_14 and HSAPO-34_18. Figure 4.7 and 4.8 show diffractograms of both fresh and calcined samples as comparison to the ion exchanged. The light blue diffractograms show crystallinity after ion exchange with a copper(II)nitrate solution and the purple diffractograms show crystallinity after ion exchange with copper(II)tetraamine solution.

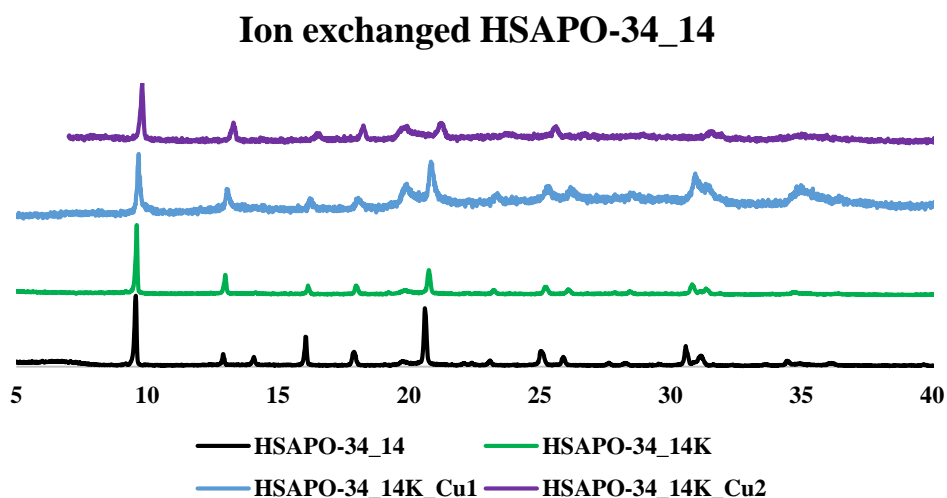


Figure 4.7: Diffractograms of HSAPO-34_14 before and after the two different ion exchanges

It is possible to see that sample HSAPO-34_14 have survived sufficiently after both ion exchanges. However, sample HSAPO-34_18 has collapsed during ion exchange with copper(II)tetraamine solution.

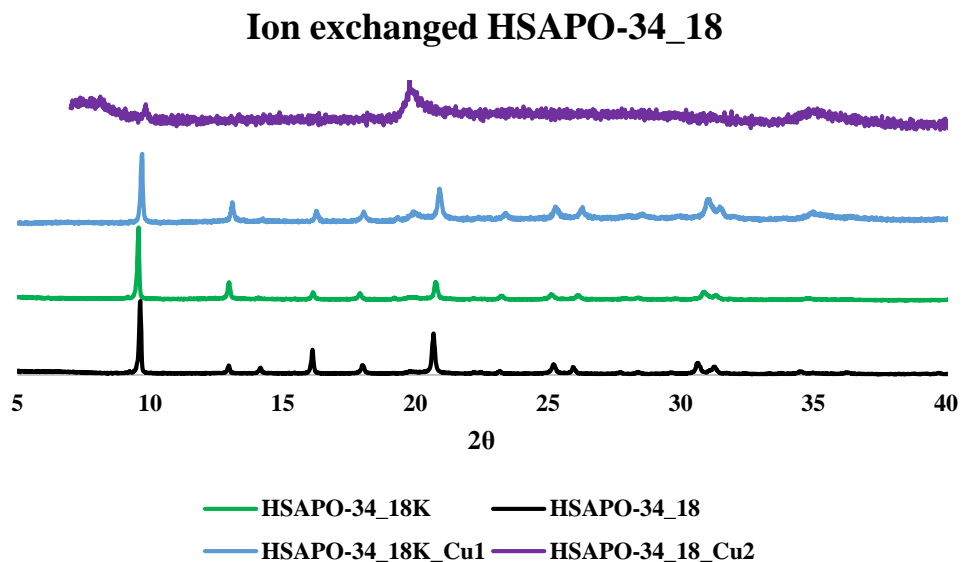


Figure 4.8: Diffractograms of HSAPO-34_18 before and after the two different ion exchanges. XRD was also taken for the two conventional SAPO-34 after ion exchange with copper(II)tetraamine. These were phase pure and crystalline after ion exchange, as seen in figure 4.9 below.

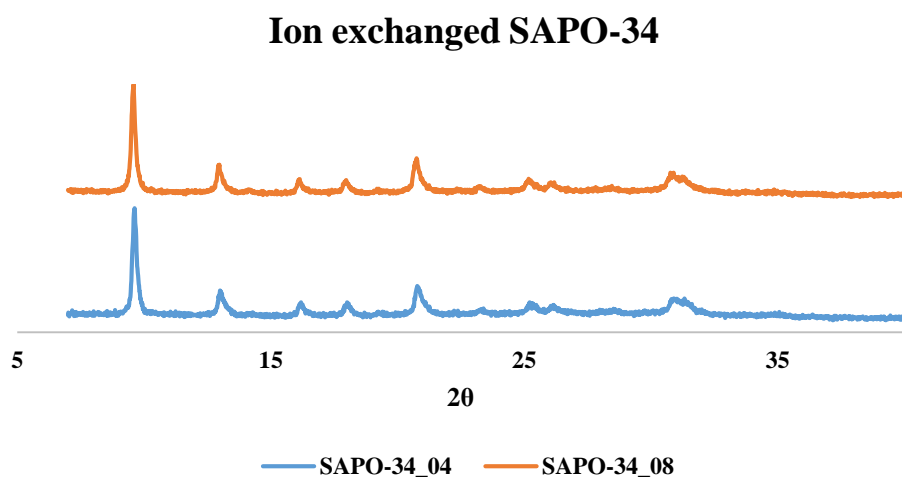


Figure 4.9: XRD diffractogram of the two conventional SAPO-34 after ion exchange with copper(II)tetraamine.

4.1.2 BET

BET is the main characterization method for determination of presence of mesopores. The specific surface area of the samples may also be obtained. For SBA-15, BET is also the only characterization method used in this thesis due to lack of small-angle XRD. BET analyses for the conventional SAPO-34 is shown in appendix B.

4.1.2.1 Hierarchical SAPO-34

BET analysis was taken in order to determine whether or not samples HSAPO-34_14 and HSAPO-34_18 were hierarchical. During BET analysis, the specific surface area and pore size may also be obtained, this is showed in table 4.7 below.

Table 4.7: BET results of samples HSAPO-34_14 and HSAPO-34_18

Sample	BET specific surface (m²/g)	Adsorption average pore width (Å)	V_{total} (cm³/g)	V_{micro} (cm³/g)	V_{meso} (cm³/g)
HSAPO-34_14	392.71	25.82	0.253	0.156	0.097
HSAPO-34_18	410.76	25.16	0.258	0.151	0.107

As table 4.7 shows, the specific surface area of the two samples HSAPO-34_14 and HSAPO-34_18. It is reported to be respectively 392,71 m²/g and 410,76 m²/g. Conventional SAPO-34 has a specific surface area of approximately 550 m²/g, hence the specific surface area of the two synthesized is a bit less than reported values of conventional SAPO-34. Further, other hierarchical SAPO-34 has been synthesised where the surface area was as high as 641 m²/g.³⁹

However, as figure 4.10 and 4.11 shows, both HSAPO-34_14 and HSAPO-34_18 has hysteresis. The hysteresis of HSAPO-34_14 is a combination of type H3 and H4 hysteresis. As a consequence, the mesopore structure is not well-defined. Hence, a well-defined pore width is difficult to obtain, as seen in figure 4.10. Here, an average of all sizes are reported and not a specific pore width can be interpreted. However, the total average is reported from BET to be 25.82 Å.

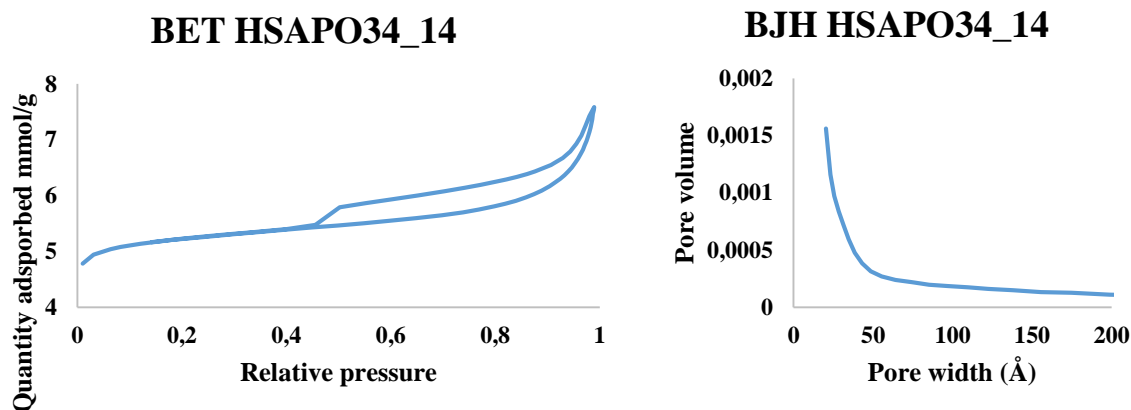


Figure 4.10: BET and BJH of sample HSAPO-34_14

The hysteresis of HSAPO-34_18, as seen in figure 4.11 below, is a combination of type H2 and H4 hysteresis. Hence, the mesopore structure is complex in which network effects are important. Neither here can a well-defined pore width be obtained due to the complexity of the mesopores.

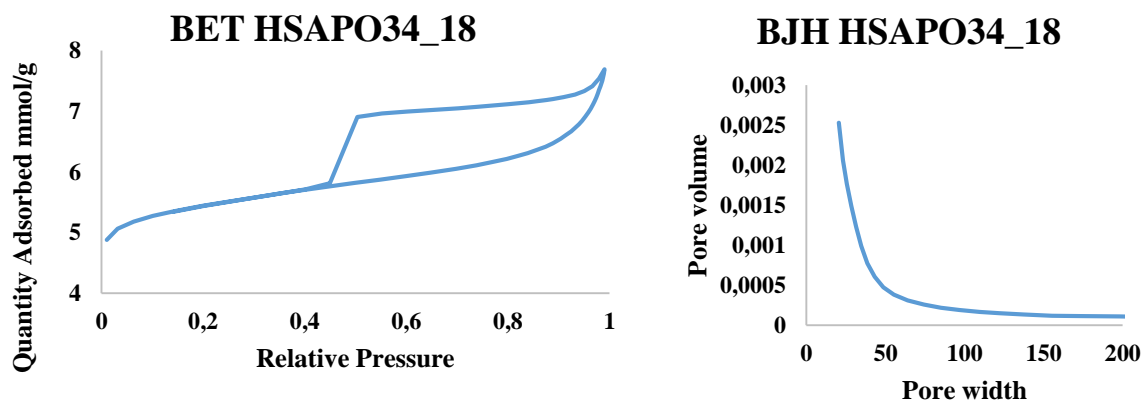


Figure 4.11: BET and BJH of sample HSAPO-34_18

Common for both HSAPO-34_14 and HSAPO-34_18 is that there are mesopores in the structure, but the structure of them is complex and not well-defined. They have, however, a mesopore volume of approximately $0.1 \text{ cm}^3/\text{g}$, whereas HSAPO-34_14 has a reported mesopore volume of $0.097 \text{ cm}^3/\text{g}$ and HSAPO-34_18 has $0.107 \text{ cm}^3/\text{g}$. Total, these results indicate that HSAPO-34_18 has some more mesoporosity compared to the other. This is somewhat less than what is previously reported, where mesopore volumes has been reported to be $0.13 \text{ cm}^3/\text{g}$.³⁷

4.1.2.2 SBA-15

The main characterization method for SBA-15 used for this thesis is BET due to no available small-angle XRD. BET results for SBA-15_01, SBA-15_02, SBA-15_04 and SBA-15_05 are shown in appendix B due to poor results and consequently new material had to be synthesized.

Table 4.8: List of different SBA-15 synthesized including specific surface area from BET and BJH pore width. The template P123 is used for all samples and are not included in this table.

Sample name	Co-template	Cu/Si ratio incorporated	BET specific surface area (m ² /g)	BJH pore width (Å)
SBA-15_01	CTAOH	-	196.39	49.70
SBA-15_02	-	-	328.97	47.54
SBA-15_03	-	0.05	731.53	60.08
SBA-15_04	CTAOH	-	586.39	28.14
SBA-15_05	-	-	836.51	36.28
SBA-15_06	-	0.1	842.92	71.11
SBA-15_07	CTAOH	-	852.63	30.95
SBA-15_07 amine	CTAOH	-	375.02	54.24
SBA-15_08	-	-	592.54	29.44
SBA-15_08 amine	-	-	291.58	59.54

Of the eight SBA-15 synthesized, two were tried incorporated with copper(II), as seen in table 4.8 above. These were the samples named SBA-15_03 and SBA-15_06, where SBA-15_06 had twice addition of copper(II)acetate compared to SBA-15_03. BET results of these are shown in figure 4.12 and 4.13. Here it is easy to see that these have hysteresis close of type H1, which means that the mesopores are ordered and approximately uniform. According to the BJH adsorption, the average pore widths are 60,08 Å and 7.11 Å for SBA-15_03 and SBA-15_06 respectively. This is as expected to the literature according to Wang et al.⁵⁵

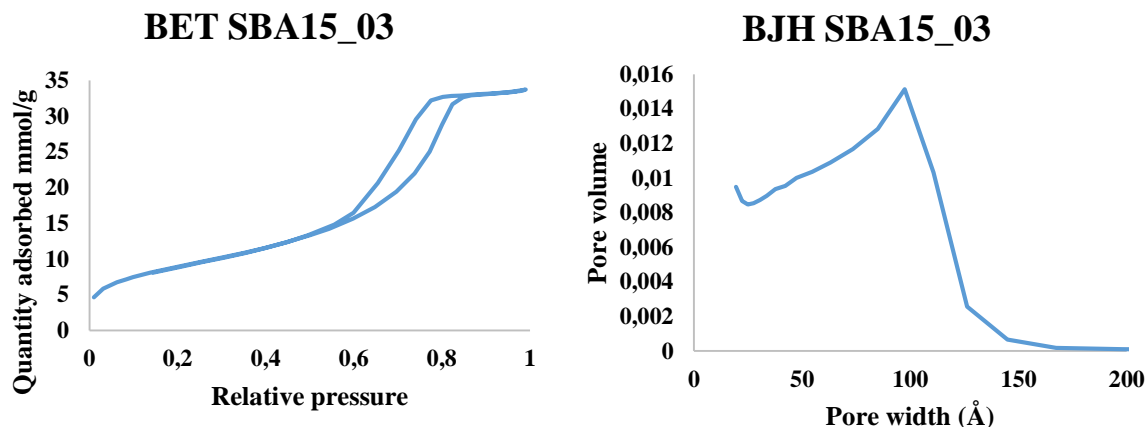


Figure 4.12: BET results of SBA-15_03, a SBA-15 with incorporated copper

Both SBA-15_03 and SBA-15_06 have quite large specific surface area, where the specific surface area of SBA-15_03 is reported to be 731.53 m²/g. The specific surface area of SBA-15_06 is a hint bigger and reported to be 842.92 m²/g.

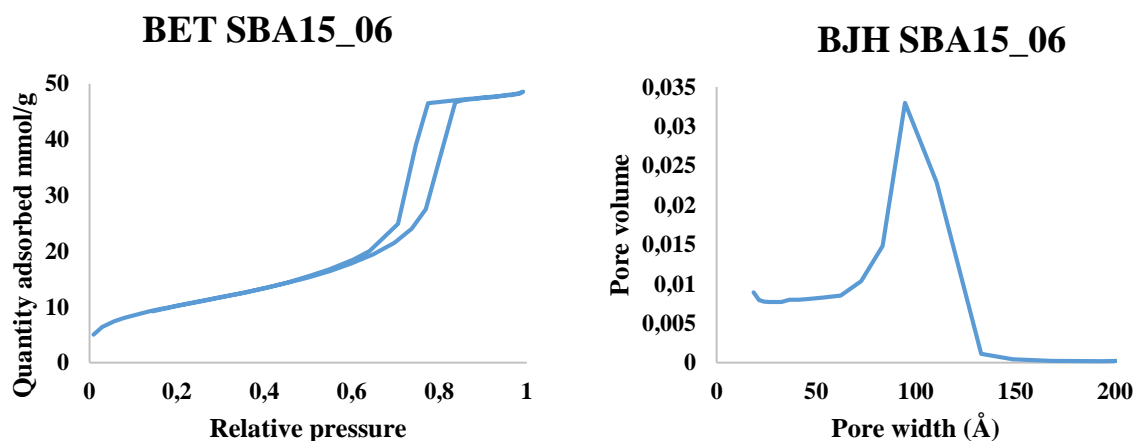


Figure 4.13: BET results of SBA-15_06, a SBA-15 with incorporated copper

Two SBA-15 were ion exchanged with both copper(II)nitrate and copper(II)tetraamine. These are the samples called SBA-15_07 and SBA-15_08, whereas SBA-15_07 was synthesized with P123 and the co-template CTAOH and SBA-15_08 was synthesized only with P123 as template.

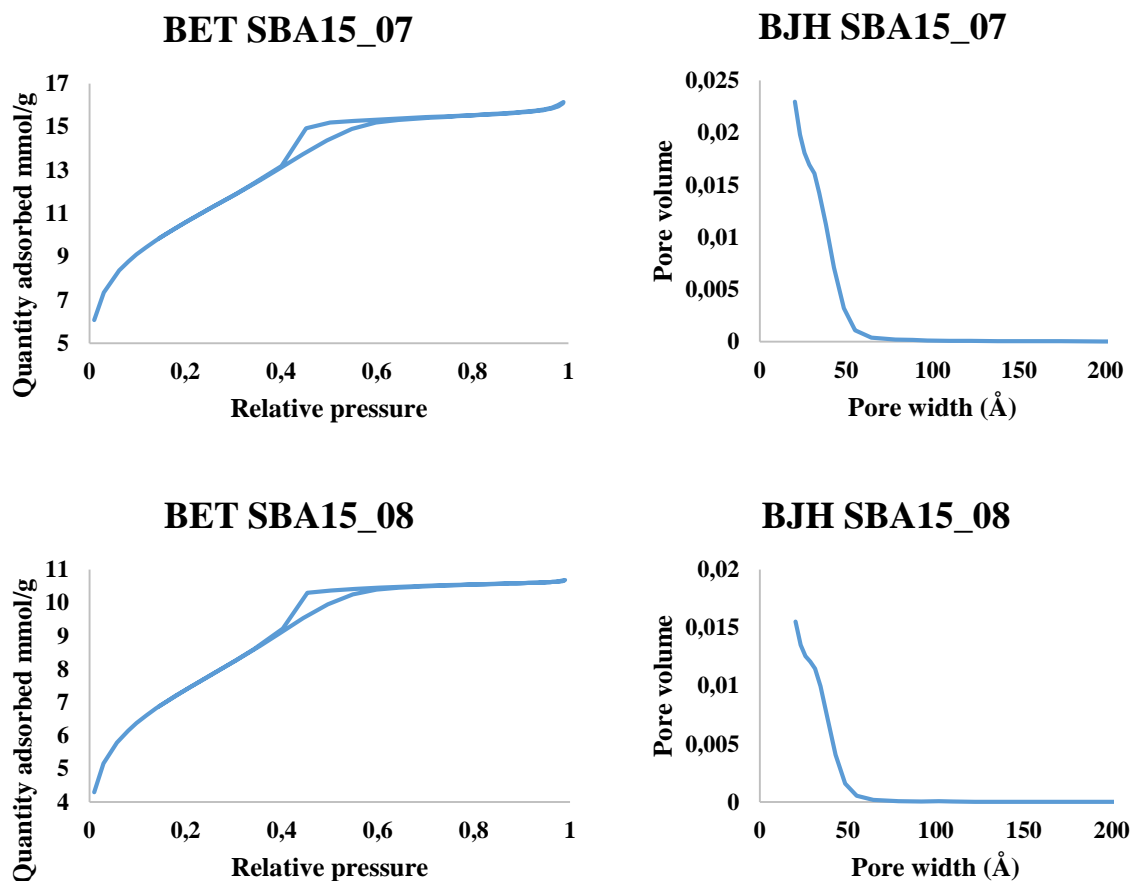


Figure 4.14: BET results of the two SBA-15 before ion exchange with copper(II)solutions. Shows BET and BJH of SBA-15_07 and SBA-15_08

Both hysteresis of SBA-15_07 and SBA-15_08 are quite similar, as seen in figure 4.14. The hystereses of these two SBA-15s might be a combination of type H1 and H4 hysteresis, which indicate that the mesopores might not have a uniform structure. They are quite similar to the hystereses as reported from Meléndez-Ortiz et al who report the shape due to the capillary condensation of nitrogen within the pores. However, SBA-15_07 is reported to have a specific surface area of $852.63 \text{ m}^2/\text{g}$. Compared to SBA-15_08, which has a reported specific surface area of $592.54 \text{ m}^2/\text{g}$, SBA-15_07 is definitely the better choice. These surface areas are also larger than the reported surface areas from Meléndez-Ortiz et al. Considering the average pore width reported from BJH adsorption, the pore width of SBA-15_07 is 30.95 \AA and 29.44 for SBA-15_08. As seen in the BJH plot, there are no narrow pore size distribution and this was not expected due to the uniformity in the literature⁵⁴.

After ion exchange with copper(II)tetraamine solution, the specific surface area of both SBA-15_07 and SBA-15_08 decreases and is reported to be 375.02 m²/g and 291.58 m²/g respectively. Hence, both SBA-15 collapses around 50 % during ion exchange based on the pre and post surface area.

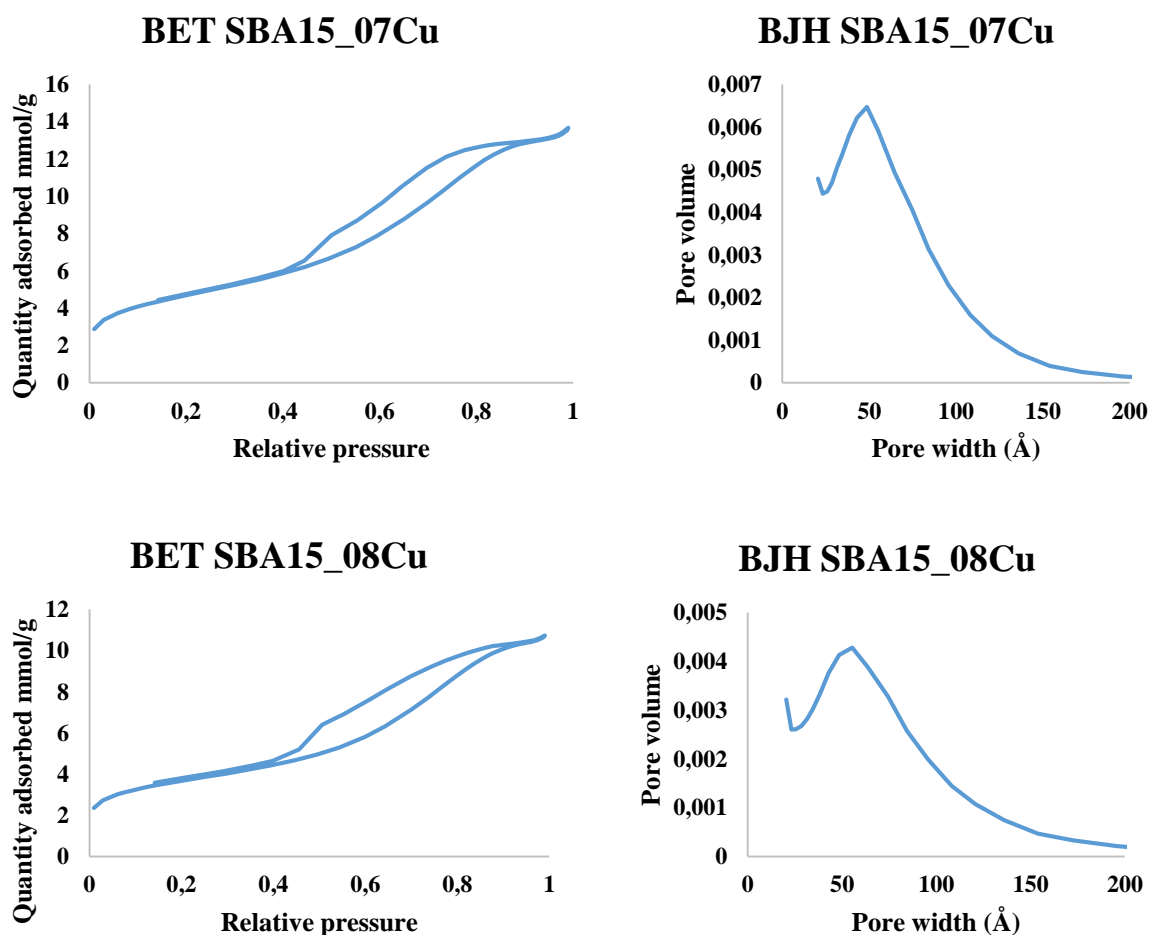


Figure 4.15: BET results of SBA-15_07 and SBA-15_08 after ion exchange with copper(II)tetraamine solution of 0,03 M.

As figure 4.15 shows, the BET results of both SBA-15_07 and SBA-15_08 have changed during ion exchange compared to figure 4.14 above. The hystereses are here much similar to the type H3 hysteresis, indicating a complex and un-defined mesopore structure. However, the reported BJH adsorption pore widths are set to be 54.24 Å and 59.54 Å, and according to the BJH plot, the pore size distribution is narrower than before treatment. The reported pore sizes are larger than compared to before treatment and this might be due to the structural collapse during treatment.

4.1.3 Scanning Electron Microscopy (SEM)

SEM were taken of the two samples named HSAPO-34_14 and HSAPO-34_18, especially for comparison to literature and for a better visualization. SEM were also taken of three first synthesised SBA-15, in order to tell if there would be a striking difference between the three different synthesis routes. Unfortunately, the quality of these was quite low and hence they can be seen in appendix C. Due to low experience with the apparatus, the photos are not of highest quality. The carbon coating of the SBA-15 and HSAPO-34_18 could also have been longer due to drifting of sample during the session. This is seen as small scratches in the photos.

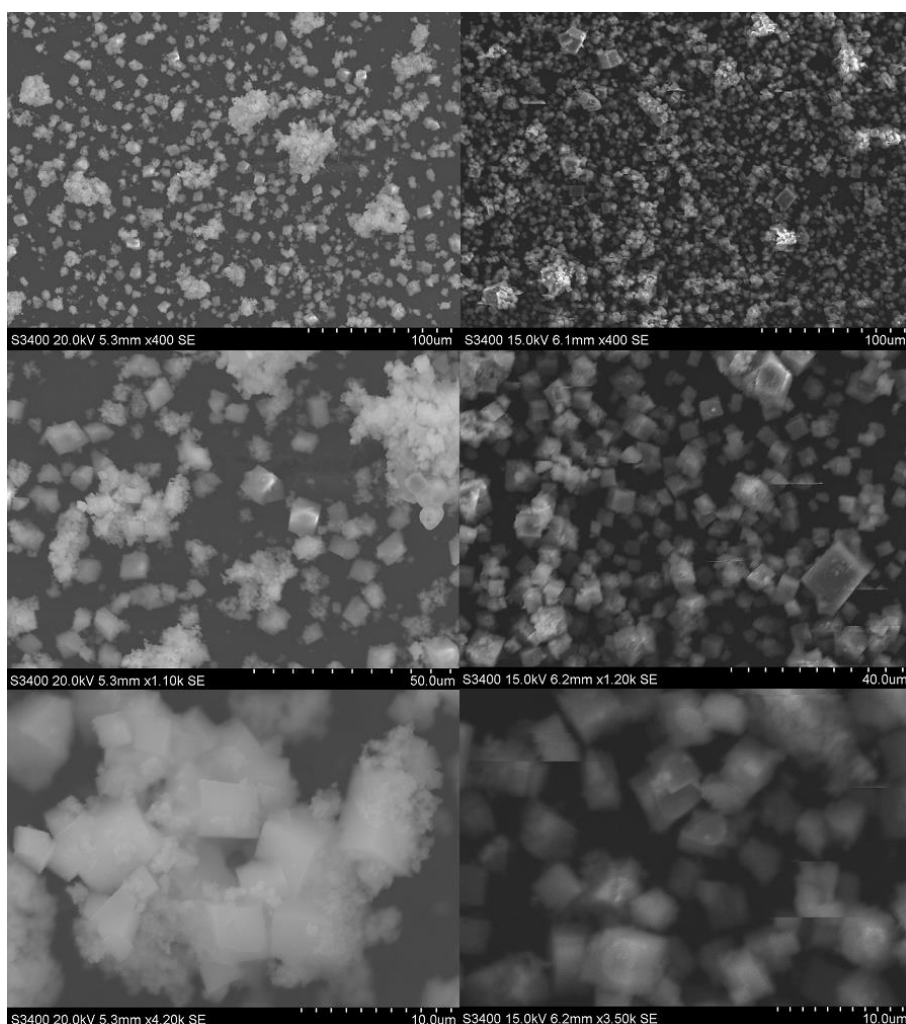


Figure 4.16: SEM results of HSAPO-34_14 (left) and HSAPO-34_18 (right). Magnification is increasing downwards, meaning that the SEM photos with highest magnifications are the ones at the bottom.

According to the XRD-results of HSAPO-34_14 and HSAPO-34_18, the intensity of the peaks in the diffractogram for HSAPO-34_18 are a bit higher than for HSAPO-34_14. This can be explained by less crystallinity in HSAPO-34_14, which is seen when comparing left and right

of figure 4.16. HSAPO-34_14 may be seen at the left and at the right HSAPO-34_18 is shown. When comparing left and right side at each magnification, it is clearly seen that HSAPO-34_14 (left) contains more amorphous phase compared to the right.

It is possible to see from figure 4.16 that the shape of both HSAPO-34_14 and HSAPO-34_18 is cubic, although in different sizes. This is especially seen when looking at the photos of HSAPO-34_18, where there is presence of less amorphous phase. However, the cubic shape is mostly reported considering conventional SAPO-34 and not so much considering hierarchical SAPO-34. There are some uncertainties in literature and the shape seems to vary in accordance with the synthesis method and templates used.^{39,62}

4.1.3 Inductively Coupled Plasma-MS (ICP-MS)

ICP-MS analysis was mainly performed in order to determine uptake of Cu^{2+} in the different samples that were either ion exchanged or incorporated. The notation Cu_1 is set to be ion exchanged with copper(II)nitrate solution (0,03 M) and ion exchanged with copper(II)tetraamine solution (0,03 M) has the notation Cu_2 . Due to low concentration of Cu^{2+} in the hierarchical SAPO-34 ion exchanged with copper(II)nitrate solution, it was decided to compare HC-SCR of the samples ion exchanged with copper(II)tetraamine. Hence, no ICP-MS results were taken for SBA-15 or conventional SAPO-34 which was ion exchanged with copper(II)nitrate solution.

Table 4.9 shows the ICP-MS results of the synthesized hierarchical SAPO-34. Theoretically the molar ratios between the T-atoms were: 1Al : 1P : 0.6 Si. The ICP-MS results report that the ratio of Si/Al has decreased with approximately 50 % compared to the theoretical value. For the ratio of P/Al, the ratio has decreased approximately 2/3 of the theoretical value. For Cu^{2+} addition, the uptake for samples ion exchanged with copper(II)nitrate is below 1 wt%, specifically 0.78 wt% for HSAPO-34_14 Cu_1 and 0.9 wt% for HSAPO-34_18 Cu_1 . However, the uptake of Cu^{2+} is quite higher for the samples ion exchanged with copper(II)tetraamine, as expected due to the basic environment.²⁵ Here, HSAPO-34_14 Cu_2 has copper concentration of 5.52 wt% and 5.30 wt% for HSAPO-34_18 Cu_2 .

Table 4.9: List of ICP-MS results of the hierarchical SAPO-34, ion exchanged with copper(II)nitrate and copper(II)tetraamine solution

Sample name	Si/Al	P/Al	Theoretical wt% Cu	wt% Cu
HSAPO-34_14Cu ₁	0.36	0.67	5.60	0.78
HSAPO-34_14Cu ₂	0.34	0.61	5.69	5.52
HSAPO-34_18Cu ₁	0.31	0.70	5.93	0.9
HSAPO-34_18Cu ₂	0.32	0.43	5.58	5.30

Two of the SBA-15 were tried incorporated with Cu²⁺, and as table 4.10 shows, the uptake for these were not successful. For SBA-15_03inc the concentration of copper is 0,01 wt% and 0,0009 wt% for SBA-15_06inc. This despite twice addition of copper in the initial gel mixture in SBA-15_06inc. The literature reported a Si/Cu ratio of 36⁵⁵. Wang et al also came to a conclusion that the aluminium salt was needed for Cu introduction. Here, the salt was changed and this might be the reason for the low uptake of copper.

Nevertheless, for the two ion exchanged with copper(II)tetraamine, the uptake of copper is quite more promising. Here, the concentration of copper resembles the concentration of the hierarchical SAPO-34. This applies for the samples named SBA-15_07_Cu₂ and SBA-15_08Cu₂, where the copper concentrations are 5,45 wt% and 5,58 wt% respectively. For SBA-15_08Cu₂, the reported copper content is higher than the theoretical value and this result cannot be explained.

Table 4.10: List of ICP-MS of SBA-15, incorporated and ion exchanged with copper(II)tetraamine solution

Sample name	Theoretical wt% Cu	wt% Cu	wt% Si
SBA-15_03inc	*	0.01	39.71
SBA-15_06inc	*	0.0009	76.50
SBA-15_07Cu ₂	5.62	5.45	32.06
SBA-15_08Cu ₂	5.52	5.58	34.57

* The theoretical wt% Cu cannot be given for the incorporated SBA-15 due to lack of sample weight as synthesised.

For the conventional SAPO-34 ion exchanged with copper(II)tetraamine, the uptake of Cu²⁺ is 5.22 wt% for SAPO-34_04Cu₂ and 4.72 wt% for SAPO-34_08Cu₂, as seen in table 4.11. This

resembles the uptake of the hierarchical HSAPO-34_14Cu₂. These copper contents are higher than the reported values from Jakobsen that were performed in similar way, where the copper content was below 4 wt%.²⁵

The molar ratio of P/Al is also quite similar to the theoretical value, which is set to 1. According to ICP-MS results, the ratio is above 0.9. However, the theoretical molar ratio of Si/Al for SAPO-34_04Cu₂ is 0.4, and according to ICP-MS the ratio is 0.27. Consequently, this has decreased compared to the theoretical value. More fascinating, the theoretical molar ratio Si/Al for SAPO-34_08Cu₂ is 0.8, but the experimental value is 0.26. This is quite similar to the sample that supposedly had half addition of silicon, and the result cannot be explained.

Table 4.11: List of ICP+-MS results of conventional SAPO-34 ion exchanged with copper(II)tetraamine solution

Sample name	Si/Al	P/Al	Theoretical wt% Cu	wt% Cu
SAPO-34_04Cu ₂	0.27	0.91	5.56	5.22
SAPO-34_08Cu ₂	0.26	0.93	5.70	4.72

4.2 HC-SCR

The first six reactions, as shown in table 4.12 below, were analysed as explained in chapter 3.3. Here the conversion of NO is measured with the assumption of constant NO concentration in the reaction flow into the furnace. Hence, NO conversion is defined as the difference between the theoretical NO concentration and the actual NO concentration at each injection. This can be explained mathematically by equation 12 below:

$$\% \text{ Conversion} = \frac{[NO]_{in} - [NO]_{reactor}}{[NO]_{in}} * 100\% \quad (14)$$

However, it turned out that these samples produced quite a bit N₂O and/or CO₂. Due to usage of GC-MS, the contribution of N₂O onto NO is significant, and some conversion results at some temperatures are negative. In addition, the theoretical NO concentration may vary compared to the actual value. Hence, the specific percentage value of each conversion result cannot be trusted 100% percent. There was performed a calibration addressed to N₂O in order to adjust for the abovementioned errors. Unfortunately, opposite trends were discovered when compared to the experiments. Hence, no adjustment could be made.

The results of table 4.12 will be elaborated below, and as the table shows, the sample names are from here changed to names that include the copper content in wt% and the copper precursor.

Table 4.12: The first six experiments were performed in such a way that NO conversion was measured by equation 14. The last three was measured conversion by equation 15 and will be elaborated below.

Sample	Final Temperature (°C)	Wet or Dry feed	wt% Cu	New sample name*
HSAPO-34_18Cu ₁	500	Dry	0.9	H-0.9nitrate
HSAPO-34_18Cu ₂	500	Dry	5.3	-
HSAPO-34_14Cu ₁	450	Dry	0.78	H-0.78nitrate
HSAPO-34_14Cu ₂	450	Wet	5.52	H-5.52amine
HSAPO-34_14Cu ₂	600	Wet	5.52	H-5.52amine
HSAPO-34_14Cu ₂	500	Dry	5.52	H-5.52amine
HSAPO-34_14Cu ₂	600	Dry	5.52	H-5.52amine
SAPO-34_04Cu ₂	600	Dry	5.22	Con-5.22amine
SBA-15_07Cu ₂	600	Dry	5.45	SBA-5.45amine

* H =hierarchical SAPO-34, Con = conventional SAPO-34, SBA = SBA-15.

Note specially, that an experiment with dry feed was taken with sample HSAPO-34_18_Cu₂. Unfortunately, this sample had died during ion exchange and results will not be shown. The experiment was run due to queue at the XRD-instrument and crystallinity could not be determined before the experiment.

First, in figure 4.17, conversion of NO is reported for H-0.9nitrate and H-0.78nitrate. As the figure shows, the conversion of H-0.78nitrate is quite low at 250 °C, but increases for higher temperatures. The conversion reaches a maximum of approximately 20% at 400 °C. H-0.9nitrate, the trend is quite the same, but the conversion is much higher for all temperatures. For temperatures from 300 °C to 400 °C the conversion is above 60%. The conversion at 500 °C, however, is negative. Here, the contribution of N₂O at NO is significant and hence it is difficult to say whether or not the catalyst is still alive.

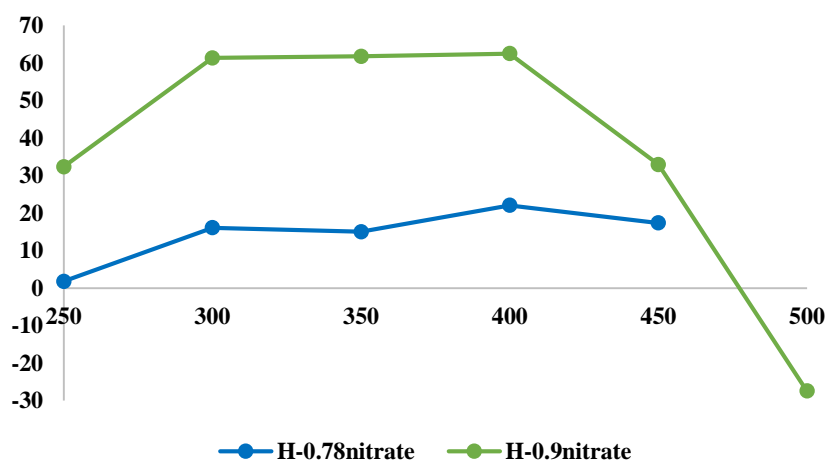


Figure 4.17: Conversion of NO of both H-0.9nitrate and H-0.78nitrate.

The negative conversion was also reported for the three experiments performed on sample H-5.52amine. Hence, these results may be seen in appendix D.

An assessment was made due to the negative conversion, and it was decided to measure the conversion of NO over the bypass. At each temperature there was an injection where the reaction feed was sent in over the sample and another injection over the bypass. Hence, the conversion of NO may be defined as the concentration difference between these two injections. This can be described mathematically by equation 13 below:

$$\% \text{ Conversion} = \frac{[NO]_{bypass} - [NO]_{reactor}}{[NO]_{bypass}} * 100\% \quad (15)$$

This would eliminate the contribution of N₂O and the assumption of constant NO concentration on the reaction flow.

For sample H-5.52amine, the result can be seen in figure 4.18 below. This was supposed to be performed up to 600 °C. Unfortunately, due to technical issues with the GC-MS, the experiment was cancelled at 450 °C. This sample, showed maximum conversion at 400 °C with a percentage of approximately 32 % conversion. Otherwise, it shows the same main trend as the other experiment performed on this sample. However, the exact conversion is more trustworthy here compared to the ones showed in appendix D, although the trends are the same.

Furthermore, for comparison, two additional experiments were performed with mesoporous SBA-5.45amine and con-5.22amine. These experiments were performed according to equation 13 in order to exclude N₂O contribution and were both done up to 600 °C. They are shown below in figure 4.19 together with the result of H-5.52amine where the experiment was performed identically. These give quite interesting results, where both SBA-5.45amine and H-5.52amine have more or less the same maximum conversion. However, for SBA-5.45amine, the maximum conversion appears at 350 °C, and for H-5.52amine it appears at 400 °C and both have conversion of approximately 32 %. Sample con-5.22amine has maximum conversion at 400 °C as well, with a conversion percentage of almost 92 %.

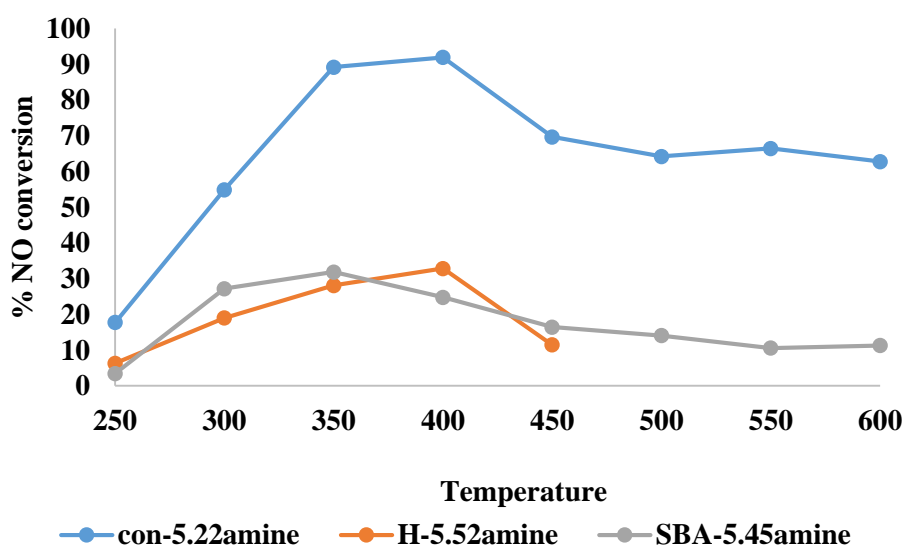


Figure 4.18: Conversion of NO for samples con-5.22amine, H-5.52amine and SBA-5.45amine. The conversion was measured over bypass for each injection in order to eliminate contribution of N₂O.

As figure 4.18 shows, there is quite a big difference between the conversion of NO of the con-5.22amine and the other two samples. After 400 °C, the conversion of the con-5.22amine is

decreasing, but seems to be stabilizing right above 60 % until the end of the experiment. The same trend might be seen for SBA-5.45amine, although the conversion is down to approximately 10 % until the end. For the H-5.22amine, it is difficult to say what is happening after the decrease at 450 °C due to the technical issues causing the end of the experiment, although the trends above indicate collapse of the catalyst. These results indicate that all of the samples are active for HC-SCR, however the con-5.22amine had best conversion of NO.

Compared to the results of Jakobsen, the trends here are opposite compared to his results.²⁵ The hierarchical SAPO-34 showed far better catalytic activity compared to the conventional and seemed to exhibit better catalytic activity in wet feed. Furthermore, at higher temperatures the NO conversion increased as reported from Jakobsen. This trend was not detected here, as the NO conversion decreased at higher temperatures.

4.3 X-ray Absorption Spectroscopy (XAS)

Copper containing SAPO-34, conventional and hierarchical, and SBA-15 were analysed Ex Situ. The main focus was to tell if there were any differences for the local environment of copper sites before and after HC-SCR. Hence, the most important samples were the ones where reaction had been performed. This concerns the samples marked in green in table 4.13 below. Of all samples that were analysed at the SNBL, results were obtained only seven of the 16 samples analysed.

Table 4.13: List over samples analysed Ex Situ XAS and results obtained

Sample name	HC-SCR description	Pore distribution	Results obtained
H-0.78nitrate	Pre reaction	Hierarchical	Y
H-0.78nitrate	Post dry feed 450 °C	Hierarchical	N
H-0.9nitrate	Pre reaction	Hierarchical	N
H-0.9nitrate	Post dry feed 500 °C	Hierarchical	N
H-5.52amine	Pre reaction	Hierarchical	N
H-5.52amine	Post dry feed 500 °C	Hierarchical	N
H-5.52amine	Post wet feed 450 °C	Hierarchical	Y
H-5.52amine	Post wet feed 600 °C	Hierarchical	Y
SAPO-34_04Cu ₁	Pre reaction	Microporous	N
Con-5.22amine	Pre reaction	Microporous	Y
SAPO-34_08Cu ₁	Pre reaction	Microporous	N
Con-4.72amine	Pre reaction	Microporous	Y
SBA-15_07Cu ₁	Pre reaction	Mesoporous	N
SBA-5.45amine	Pre reaction	Mesoporous	Y
SBA-15_08Cu ₁	Pre reaction	Mesoporous	N
SBA-5.58amine	Pre reaction	Mesoporous	Y

Due to small amounts of the hierarchical samples and hence low concentration of copper, only one pre result was obtained; sample H-0.78nitrate. Furthermore, only two post results; H-5.52amine in wet feed run to 450 and 600. Consequently, it is impossible to tell if there has been a direct difference in the local environment before and after reaction for the three different samples. It is possible, however, to compare the results against model compounds and tell something about oxidation state and multiplicity of copper. For both the conventional SAPO-

34 and mesoporous SBA-15 results were obtained for the samples that were ion exchanged with copper(II)tetraamine. This is due to poor copper loading during ion exchange with copper(II)nitrate.

4.3.1 XANES

In this subchapter, most focus will be on the hierarchical SAPO-34 pre and post reaction. The results for con-5.22amine and SBA-5.45amine are shown here as well, but the other results can be found in Appendix E.

Figure 4.19 shows the linear relation of absorption energy and oxidation state of copper. All samples that were analysed for XAS appear right around oxidation state 2+, ergo Cu^{2+} . The two H-5.52amine which is run in wet feed appear somewhat to the left. The two SBA-15 ion exchanged with copper(II)tetraamine appear somewhat to the right of oxidation state 2. Anyhow, they are all close enough to oxidation state 2+ in order to presume that the oxidation state of copper in the samples are mainly 2+.

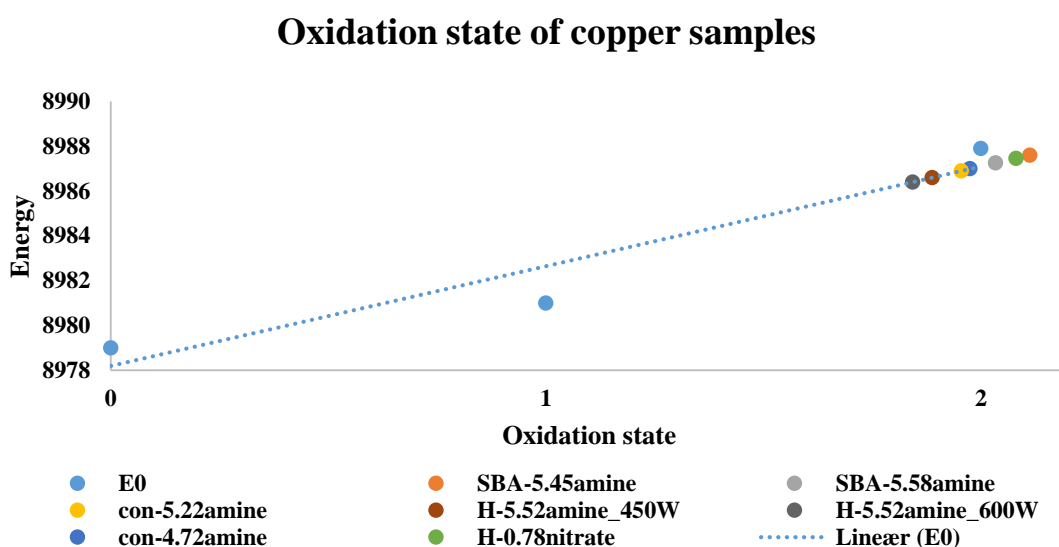


Figure 4.19: Linear trend of absorption energy vs oxidation state of copper

Figure 4.20 shows the normalized XANES in the region 8970-9015 eV for the results of the hierarchical SAPO. The blue curve shows results for H-0.78nitrate. The other two curves show results for the same sample ion exchanged in copper(II)tetraamine after reaction, up to 450 °C and 600 °C in wet feed.

Typical for all copper-containing XANES is a pre-edge at 8979 eV.⁵⁷ For copper(II)oxide and copper tutton this pre-edge is of low intensity due to the La Porte selection rule. Pre-edge is

here determined by the 1s-3d transition and this is forbidden in centrosymmetric sites. For the monovalent copper(I) the pre-edge arises from the 1s-4p transition and have consequently higher intensity.

Furthermore, for copper(II) compounds, there is a characteristic shoulder around 8985-8986 eV. This applies for both copper(II)oxide and copper tutton. However, the intensity is higher for copper(II)oxide due to varying degree of axial distortion. Meaning, tetragonal distorted octahedral environment due to Jahn-Teller effect.⁵⁸

As seen in figure 4.20, for sample H-0.78nitrate, there is a pre-edge around 8979 eV with very low intensity, indicating copper(II) compound with an octahedral or tetrahedral environment. However, the remaining XANES does not resemble any of the two model compounds that were analysed. Comparing to other literature and research, it is found that the model compound copper tutton resembles the XANES of this sample.⁵⁸ Furthermore, a shoulder of low intensity is also seen at 8986-8987 eV indicating an octahedral environment tetragonally distorted.

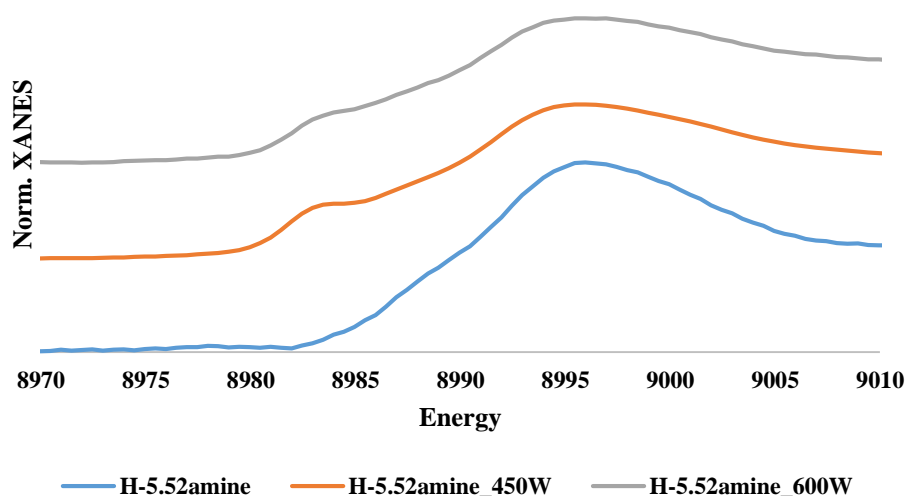


Figure 4.20: Normalized XANES for HSAPO-34_14 around the absorption edge

For H-5.52amine_450W and H-5.52amine_600W there is a shoulder at 8983 eV and 8984 eV respectively. For copper(II) compounds this is expected to be at a higher energy, as mentioned above. Hence, it might be that these two samples contain both monovalent copper(I) and divalent copper(II), making the characteristic shoulder from copper(II) energy shift due to the characteristic pre-edge of copper(I) caused by the 1s-4p transition. However, the remaining XANES is more similar to the one of copper(II)oxide, especially for H-5.52amine_600W. The content of copper(I) is probably a minority compared to the copper(II) content in these samples,

and due to the similarity between the XANES of copper(II)oxide and H-5.52amine_600W it is reason to believe that copper(II)oxide is formed at high temperature.

Figure 4.21 shows the corresponding first derivative of the normalized XANES in figure 31. As seen, the data for both H-0.78nitrate and H-5.52amine_600W are quite poor and may lead to misconceptions. However, when comparing the first derivative of H-0.78nitrate to the research done by Tina Kristiansen, one might say that this resembles the first derivative XANES of copper tutton, as seen in the normalized XANES above. The same applies for H-5.52amine_450W and H-5.52amine_600W in the region 8984-8910 eV. However, the first peak in the region between 8978-8984 eV does not appear for copper tutton. Comparing to the model compounds copper(I)oxide and copper(II)oxide, where a peak of this resemblance appear at 8980 eV and 8984 eV respectively, there is reason to believe that the samples contain monovalent copper(I) due to the lower energy where the peak arises.

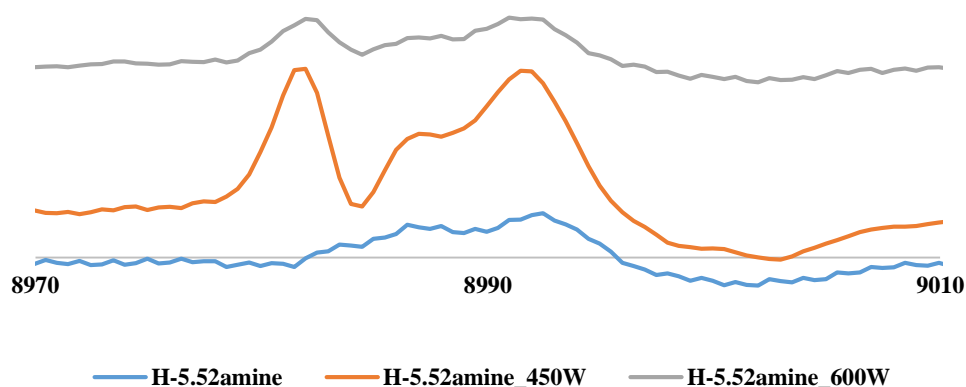


Figure 4.21: Derivative normalized XANES for the corresponding normalized XANES in figure 31.

Altogether, these results indicate that sample HSAPO-34_14Cu₁ contain copper in the form of copper tutton, and that samples H-5.52amine_450W and H-5.52amine_600W contain copper as both monovalent copper(I) and copper(II) in the form of both copper tutton and copper(II)oxide.

Following are the XANES and the first derivative XANES of samples con-5.22amine and SBA-5.45 amine. Here it is possible to see a shoulder at approximately 8987 eV, and a similar shape of copper(II)oxide. However, the shoulder appears at higher energy than for copper(II) compounds. This indicate a difference in the copper species compared to the hierarchical SAPO-34s as shown above.

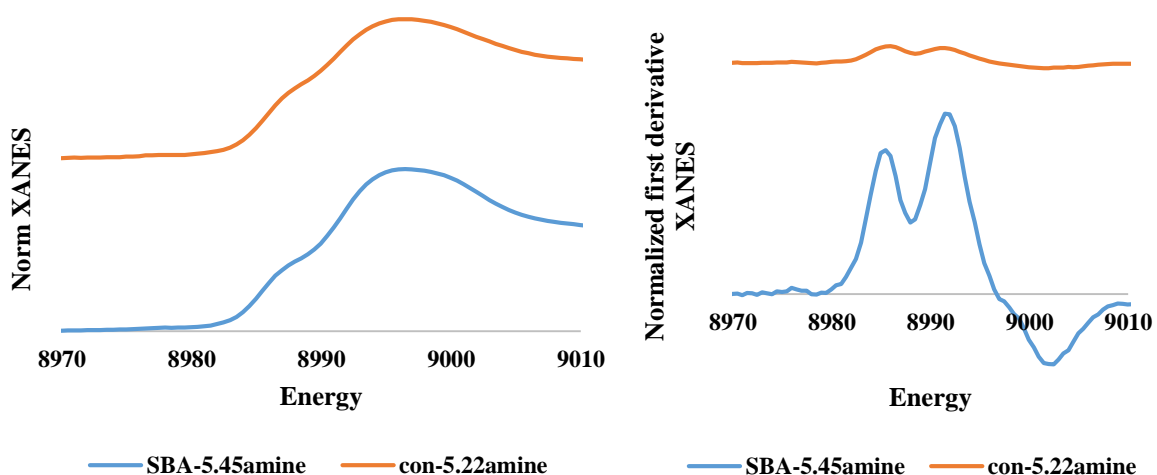


Figure 4.22: Normalized XANES of samples con-5.22amine and SBA-5.45amine (left) and its respective first derivatives (right)

For sample SBA-5.45 the XANES results have similarities to the XANES of $\text{Cu}(\text{OH})_2$, as reported by T.Jakobsen²⁵ in addition to copper tutton due to the shape of the normalized XANES. However, the experimental data for sample con-5.22amine were quite poor and definite references are difficult to obtain. It seems as if the copper species are of a copper(II) compound with similarities of both copper tutton and copper(II)oxide due to the appearance of the shoulder and the shape of the normalized XANES. The first derivative is of so low intensity that references are difficult to obtain.

4.3.2 EXAFS

In this subchapter, most focus will be on the hierarchical SAPO-34 post reaction. Hence, the EXAFS of the other samples are shown in Appendix F.

Through the analyzation and refinements using DLV EXCURV, results are refined by the experimental data, and the first interesting to present here is a list of what type of shells were found, at what distances and their multiplicity. This is shown in table 4.14 below.

Table 4.14: Results after refining the EXAFS data in DLV EXCURV. Here, a list of type of shell, multiplicity and distance is shown.

Sample	Shell	EF (eV)	$2\sigma^2$ (Å ²)	N	r (Å)	R%
H-0.78nitrate Pre reaction	Cu-O	1(2)	0.005(3)	4.1(5)	1.98(2)	54.03
	Cu...Si		0.04(13)	2(2)	2.8(1)	
	Cu...Al		0.04(5)	2(2)	3.01(9)	
H-5.52amine Post 450 °C wet feed	Cu-O	-3(1)	0.003(1)	2.0(2)	1.962(9)	47.36
	Cu...Al		0.005(5)	1.0(4)	3.20(3)	
H-5.52amine Post 600 °C wet feed	Cu-O	-4(2)	0.018(9)	2.7(7)	1.98(2)	57.6
	Cu...Cu		0.01(1)	0.9(5)	2.48(4)	
	Cu...Si		0.02(2)	0.9(8)	2.74(7)	
Con-5.22amine Pre reaction	Cu-O	-4(1)	0.015(5)	2.8(4)	2.00(2)	56.98
	Cu...Cu		0.02(2)	0.9(8)	2.75(5)	
	Cu...Si		0.004(13)	0.8(6)	3.2(1)	
SBA-5.45amine Pre reaction	Cu-O	-2,6(6)	0.009(1)	3.1(2)	1.965(6)	28.04
	Cu...Cu		0.04(13)	2(2)	2.8(1)	
	Cu...Si		0.04(5)	2(2)	3.01(9)	

The first one should notice is that a Cu...Cu shell cannot be found for samples H-0.78nitrate pre reaction and H-5.52amine_450W. However, this can be found for sample H-5.52amine_600W. This implies formation of copper oxide at high temperatures in wet feed. As table 4.14 also shows, the R-factors are quite high and the reason may be seen below in the figures 4.24-4.29. Here it is possible to see that the experimental data are very noisy and due to this, excellent adaptations through refinements cannot be obtained.

This phenomenon also applies for the certainty for each value in the table above. The Debye-Waller factor ($2\sigma^2$) should be in between 0,008-0,03 in order to be sure the peak is significant. This does not concern the Cu...Si and Cu...Al shell for sample H-0.78nitrate, especially not for Cu...Si where the uncertainty is bigger than the given value. For the other values of the Debye-Waller factor where it is in between the significant interval, it is possible to observe that the uncertainty of the multiplicity and radial distance is hence decreased compared to the abovementioned shell.

Further details concerning the results of sample H-0.78nitrate are shown below in figure 4.23 and 4.24. In figure 4.23, the normalized and Fourier Transformed EXAFS are shown for H-0.78nitrate. It can be seen that the adaption of the calculated data is not excellent, hence the R-factor of 54,03 %. After $K(\text{\AA}^{-1})$ value of approximately 5, the experimental data is very noisy, seen at the normalized EXAFS, which also affects the adaption before the noise appears.

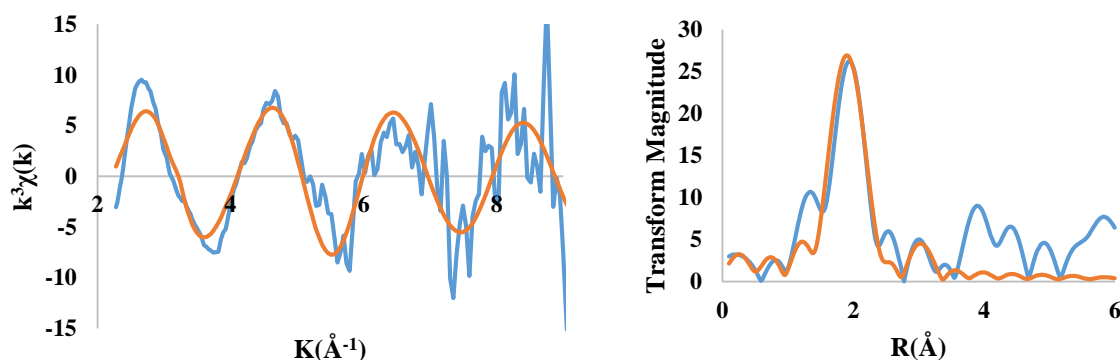


Figure 4.23: Normalized EXAFS for H-0.78nitrate pre reaction at the left. On the right, the Fourier Transformation of normalized EXAFS can be seen. The blue curves represent the experimental data, and the orange curves represents the calculated data

However, the adaption of the Fourier Transformed EXAFS seems to be better adapted, concerning shell at radius 2 and 3. The first shell was found to be oxygen, with multiplicity of approximately 4, as seen in figure 4.24. The next shell was found to be a combination of Si and

Al with the same multiplicity of approximately 1. When refinements with copper in this shell were performed, it provided negative values of the Debye-Waller factor. Hence, copper could not be found.

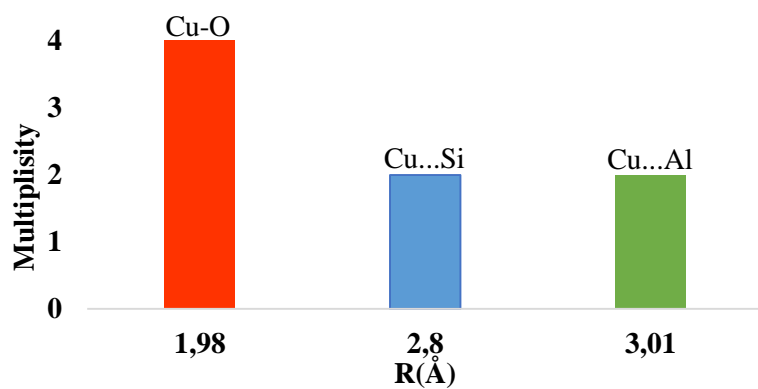


Figure 4.24: View of bonding multiplicity at calculated distances of sample H-0.78nitrate

EXAFS result for H-5.52amine_450W and H-5.52amine_600W are shown together in figure 4.45 below. The lowest fitting of the experimental data concerns sample H-5.52amine_600W, given R factor of 57,60 %. However, the Debye-Waller factors for both shells are well within the significant interval, indicating significant peaks. The low fitting can be explained by the tremendous amount of noise in figure 4.25 below when looking at the normalized EXAFS. After a $K(\text{\AA}^{-1})$ value of 5 the experimental data is more noise than useful signal, making a calculated adaption difficult. For sample H-5.52amine_450W the experimental data is quite noisy as well, however, not completely chaos before after $K(\text{\AA}^{-1})$ of approximately 7. The R-factor here is 47,36 % and hence a bit lower compared to H-5.52amine_600W4

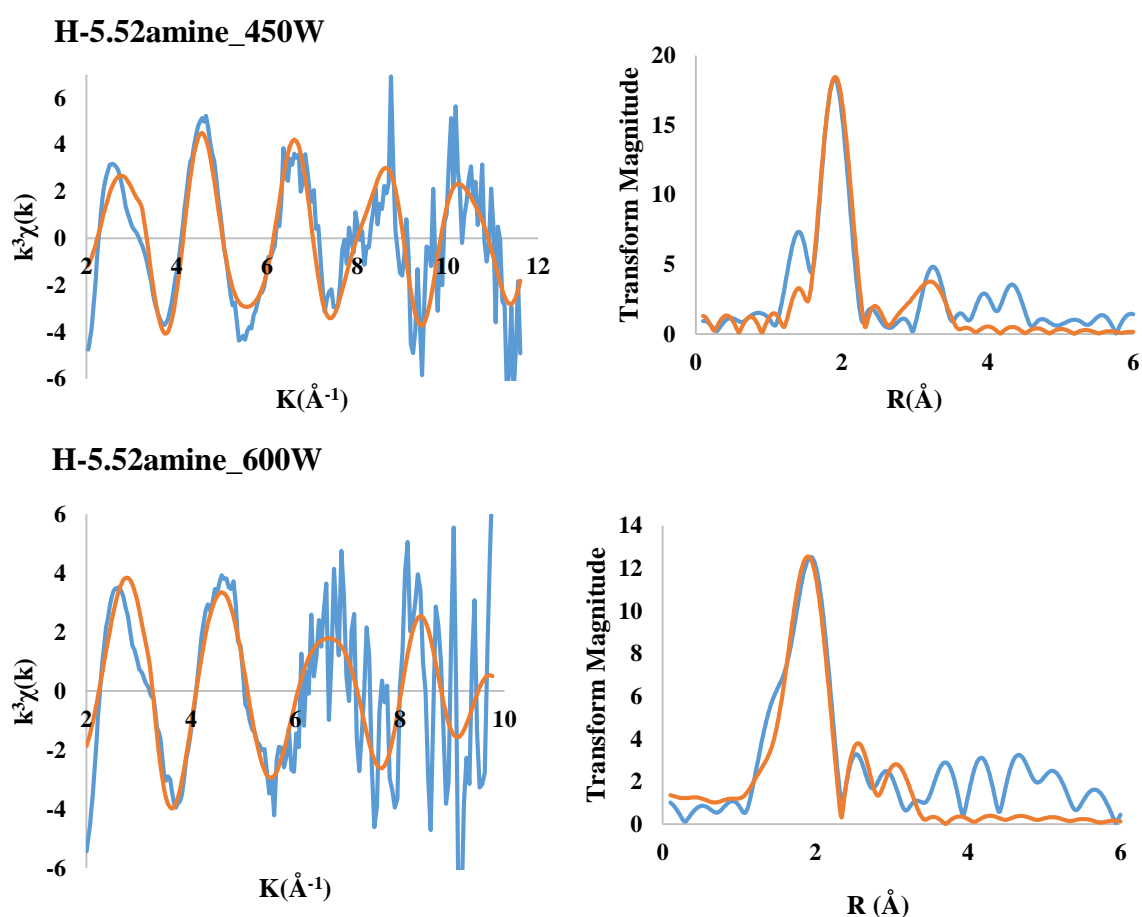


Figure 4.25: Normalized EXAFS (left) and FT normalized EXAFS (right) for H-5.52amine_450W (top) and H-5.52amine_600W (bottom). The blue curves represent the experimental data, and the orange curves represents the calculated data

The fitting of the experimental data is done for the first and second shell. When comparing the results of H-5.52amine-sample, the main difference is reported copper in the second shell for H-5.52amine_600W and not for H-5.52amine_450W. Further, oxygen is bound in the first shell with a multiplicity of 3 and 2 respectively. When refining with addition of copper in the second shell for H-5.52amine_450W, the Debye-Waller factor and the multiplicity becomes negative. Given this, the experimental data cannot provide information on copper oxide formation at this temperature. In addition, the second shell for sample H-5.52amie_600W is found a bit closer compared to the other sample. This implies formation of copper oxide when the sample is exposed to wet feed up to 600 °C.

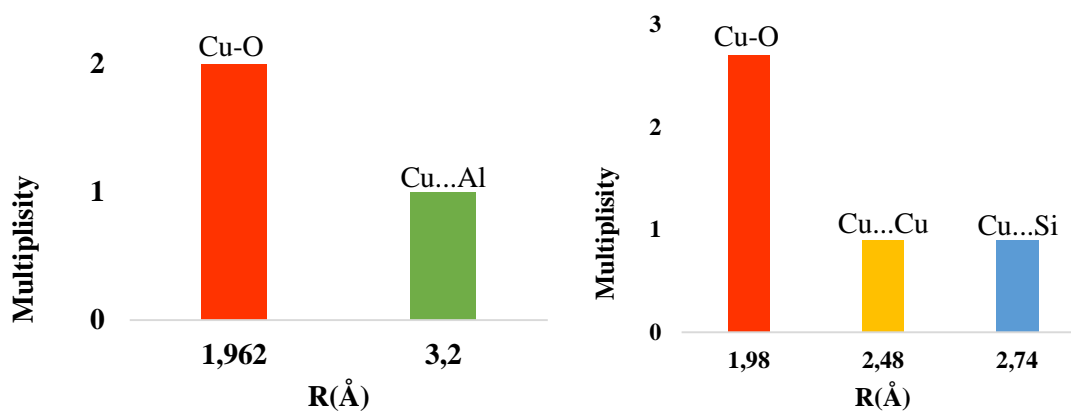


Figure 4.26: View of the bonding multiplicities of defined calculated for sample H-5.52amine_450W (left) and H-5.52amine_600W (right)

The EXAFS results of sample con-5.22amine and SBA-5.45amine are shown together in figure 4.27. For con-5.22amine, the experimental data is quite noisy as well which explains the R-factor of 56.98%. Sample SBA-5.45amine was by far the sample that involved least noise in the experimental data, as seen in figure 4.31, and this explains the R-factor of 28.04 %. As for the other samples, the refinements and fittings were also here addressed to the first and second shell.

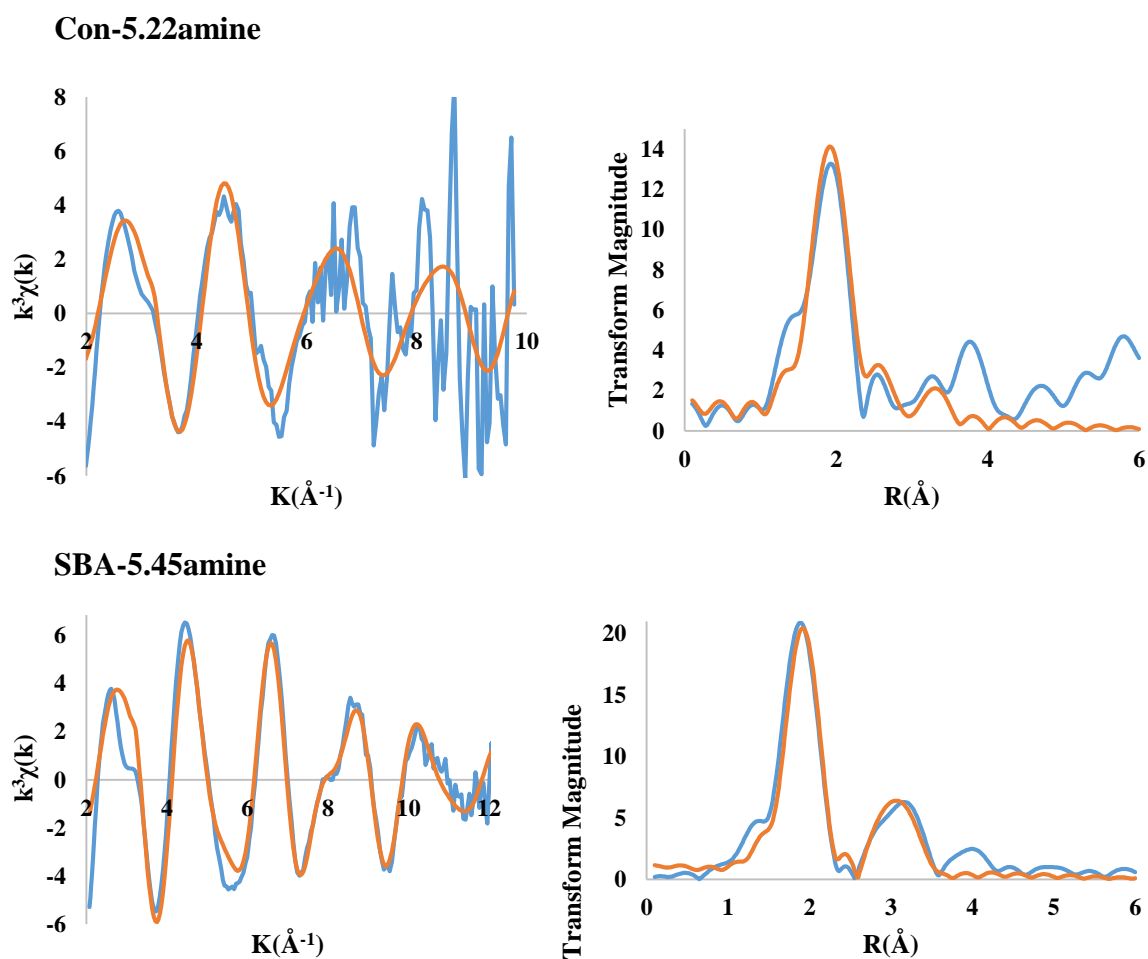


Figure 4.27: Normalized EXAFS (left) and FT normalized EXAFS (right) for con-5.22amine (top) and SBA-5.45amine (bottom)

The refinements showed that oxygen is bound in the first shell for con-5.22amine with a multiplicity of approximately 3. In the second shell, there is a combination of Cu and Si with multiplicities of 0.9 and 0.8 respectively, as seen in figure 4.29 below. For SBA-5.45amine, the first shell was also found to be oxygen with a multiplicity of 3. However, the second shell is found to be a combination of Cu and Si with multiplicities of 2 of both, as seen below.

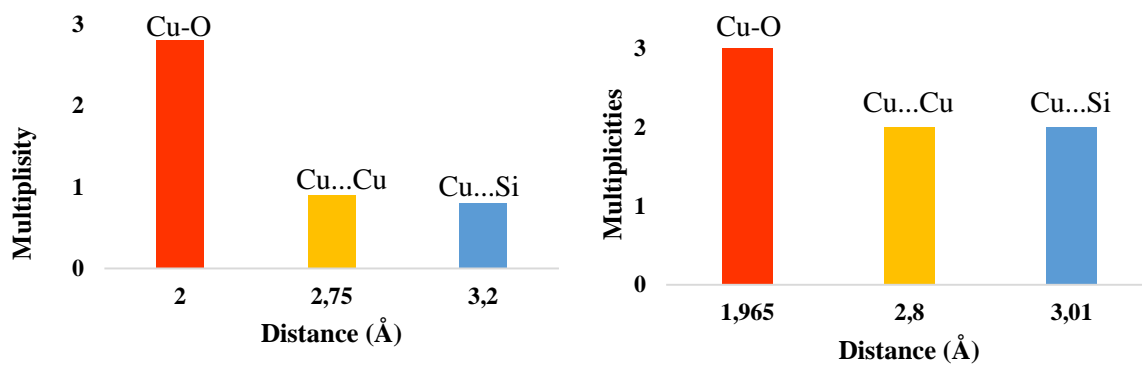


Figure 4.29: Given multiplicities for sample con-5.22amine (left) and SBA-5.45amine (right)

The conventional SAPO-34 and the SBA-15 here have different copper species compared to the hierarchical SAPO-34. Here, SBA-5.45amine has the highest multiplicity of copper in the second shell, indicating increased formation of copper(II)oxides in this sample during ion exchange.

5.0 Discussion

5.1 Synthesis

The main goal for this thesis was to incorporate copper(II) ions into the framework of hierarchical SAPO-34. As for the results above, different routes were tried, but neither of them provided the desired catalyst material. Synthesising hierarchical Cu-SAPO-34 based on the work of Yang et al, seemed to be declined by the low solubility of wanted aluminium source. Due to the chlorine content of the original aluminium source, this had to be solved somehow and was only tried with change of aluminium source. Another solution might have been to wash out the chlorine after the first calcination and then add copper(II) ions into the mixture before the crystallization.

The other direction, based on the work of Najafi et al did not provide wanted catalyst material either. Due to time limitations and difficulty in developing a synthesis route for hierarchical SAPO-34 with CTAOH as mesoporous agent, there wasn't enough time finding a solution with the addition of copper in this synthesis. With the same synthesis parameters that provided crystalline SAPO-34, a crystalline Cu-SAPO-34 was not obtained. The solution might have been as simple as adjusting the addition of reactants, and it could have been as difficult as changing all synthesis parameters and/or reactants.

However, this direction did provide crystalline SAPO-34 and according to the BET, these samples did contain mesopores; samples HSAPO-34_14 and HSAPO-34_18. Unfortunately, the mesopores were not ordered and uniform, but the samples may be said to be hierarchical due to the presence of both micropores and mesopores. This is especially confirmed when seeing that the mesopore volume of these samples were approximately $0.1 \text{ cm}^3/\text{g}$. When the XRD results of these are compared to the chabazite diffractogram, it is possible to observe that the intensity of the peaks is not as high as for the chabazite diffractogram. This means that the samples are not as crystalline as they potentially could have been, although sample HSAPO-34_18 seems to be a bit more crystalline than the other. This is also observable when looking at the SEM photographs of these samples. Here, some amorphous phase is seen at the pictures of HSAPO-34_14 compared to HSAPO-34_18.

Consequently, these observations points into the direction that the synthesis parameters should have been varied even more. This concerns addition of CTAOH, both in amount and order of addition to see whether or not the uniformity might could have been achieved. For the

crystallinity, the crystallization time should have been tried increased even more the 120 hours in order to see whether or not the sample could have had better crystallinity. In addition, a variation in crystallization temperature should have been performed in order to see how this affect the final product.

However, it does not seem as if the synthesis is so reproducible, considering table 4.6 and corresponding figure 4.6. Here, longer crystallization times and/or aging times were tried in order to make a more crystalline hierarchical SAPO-34, according to the other synthesis parameters that provided HSAPO-34_14 and HSAPO-34_18. Neither of these syntheses provided a fully crystalline HSAPO-34. Kong et al⁵⁵ have synthesised hierarchical SAPO-34 using CTAB as a mesoporous template in addition with TEOH and TEA as microporous templates. Here they also used phosphoric acid and pseudoboehmite as respective P and Al sources, and they also used longer stirring time during the synthesis. In addition, they aged the samples at ambient temperatures 24 hours before crystallization at 180 °C for 72 hours. Hence, there are some similarities although it might be that the differences are the border line between a fully crystalline hierarchical SAPO-34.

Considering SBA-15, some parameters had to be changed during the period where the eight different samples were synthesized. For the three first samples, only SBA-15_03 was stirred at higher temperatures than ambient temperature. In addition, all three were aged in a stainless steel autoclave and washed only with water afterwards. According to the BET, SBA-15_01 and SBA-15_02 had low specific surface areas, below 350 m²/g and SBA-15_03 had a specific surface area of over 700 m²/g. This implied that an increase of stirring temperature for the conventional and CTAOH-based synthesis of SBA-15 was necessary, as reported from Zhao et al⁴⁰. Here, it is reported that SBA-15 has been successfully synthesised in the temperature range from 35- 80 °C.

According to Thielemann et al⁵⁹ as well, increased surface area would be obtained by aging in a sealed plastic container in combination with a washing routine that involved mixing water and ethanol. By changing these parameters, SBA-15 was obtained with high specific surface areas.

5.2 Effect of porosity

As elaborated in chapter 4.2 there were quite a few differences concerning the NO conversion of the different samples. Sample con-5.22amine was by far the most efficient concerning this purpose and here an effort of explaining this phenomenon will be enhanced. Activity for NO conversion depends on many factors, amongst other the availability for active sites, copper loading, copper species, surface area and the particle size of the catalyst. The samples of interest here are mainly SBA-5.45amine, con-5.22amine and H-5.52amine. However, sample H-0.9nitrate is quite interesting due to the low copper content and the high NO conversion.

Table 5.1: List of different BET results, Si-content and maximum conversion for the samples of interest concerning HC-SCR

Sample	Maximum NO conversion (%)	wt% Cu	Si/(Al+P) ratio	S _{BET} (m ² /g)	S _{EXT} (m ² /g)	V _{meso} (cm ³ /g)
SBA-5.45amine	32	5.45	-	375.02	304.63	0.438
Con-5.22amine	92	5.22	0.14	295.48	44.45	0.089
H-5.52amine	33	5.52	0.21	392.7*	56.9*	0.097
H-0.9nitrate	62	0.9	0.18	410.8*	84.5*	0.107

* BET results taken **before** ion exchange due to lack of enough sample after

Zuo et al²¹ report that different preparation methods of the catalyst affect the activity for HC-SCR, especially considering pore structure and anti-aging abilities. Amongst other, they report that increased surface areas favour catalytic reactions. For samples H-5.52amine and H-0.9nitrate, BET results could not be obtained after ion exchange and hence there are some uncertainties considering the actual surface areas. However, for H-0.9nitrate, the XRD shows little change from before the ion exchange, hence there is reason to believe that the sample remains a good part of its reported surface area, as seen in table 5.1. For sample H-5.52amine the XRD shows less crystallinity compared to before treatment. Consequently, there is reason to believe that the somewhat amorphous sample has become even more amorphous after ion exchange. Hence, the surface area of these samples have probably decreased some, but somewhat more for H-5.52amine.

For both samples, SBA-5.45amine and Con-5.22amine, BET was taken after ion exchange with copper(II)tetraamine. The reported surface areas are 375.02 and 295.48 m²/g respectively. As shown in chapter 4.1.2.2, the SBA-15 collapsed approximately 50 % during the ion exchange. For the conventional SAPO-34 the surface area before ion exchange was 539.75 m²/g as seen

in appendix B, and the structure has collapsed approximately 44 %. Given this, it is reason to believe that the hierarchical SAPO-34 collapsed more or less the same, due to the noisier XRD-results. This provides that all samples analysed had low surface areas compared to optimal conditions.

Zheng et al⁶⁰ report the similarity between external surface area and particle sizes. For larger external surface areas, the particles tend to be smaller and vice versa. Comparing the two hierarchical samples as listed in the table above, it is possible to see that sample H-0.9nitrate possesses larger external surface area than H-5.52amine. Consequently, there is reason to believe that the particle size of H-0.9nitrate might be a hint smaller than compared to the above. For con-5.22amine the external surface area is reported to be 44.45 m²/g, implying larger particles. Furthermore, SBA-5.45amine the one with the largest external surface area of these samples, with a reported value of 304.63 m²/g. When comparing these, it is reason the believe that the SBA-5.45amine is the sample with the smallest particle size.

Shen et al⁶¹ report that Si content in SAPO-34 has little effect on the Brönsted acid strength, however it does affect the acid concentration. Here, Si content is determined by the ratio Si/(Al+P), and as the Si content is higher, the higher acid concentration is present in the zeotype as vice versa. High content of Si is here defined as 0.23 and low content is defined as 0.09. Compared to the SAPO-34s in table 5.1 above, one can see that neither of the samples have low Si content. However, sample con-5.22amine has a Si content of 0.14 which is the lowest value of these samples. The highest Si content is obtained in sample H-5.52amine, where it is 0.21. Hence, it is reason to believe that there are more Si islands formed in the framework of H-5.52amine compared to the other, as reported in Shen et al.

The higher Si content of the sample, may also be the reason for the amorphous result after ion exchange. As Gao et al reported⁴⁰, the higher acid concentration, the more likely it is for irreversible hydrolysis to appear during ion exchange. For sample H-0.9nitrate, the Si content can be seen as a medium content as one should expect some collapsing of the framework here as well. According to the XRD, this has not occurred in such a high degree, which implies that the starting crystallinity and stability of the sample before ion exchange will affect the result after treatment.

Considering copper loading, there are clearly no obvious correlation between catalytic activity and copper content in the samples, as seen in table 5.1. The two samples with least copper content, con-5.22amine and H-0.9nitrate has the greatest activity concerning HC-SCR. The

copper content is tried hold constant, especially for the samples that were ion exchanged with copper(II)tetraamine where an assessment was made considering the ICP-MS results before HC-SCR experiments. However, the NO conversion of sample H-0.9nitrate is almost double compared to H-5.52amine and SBA-5.45amine despite 1/6th copper content.

For HC-SCR the active sites, in this case copper, must be available for reaction. Here, it is worth suspicion that the copper in both H-5.52amine and SBA-5.22amine was not as available as compared to the other two samples. From the XAS data it might seem that the copper in H-5.52amine migrate to copper(II)oxide in high temperatures and during high temperatures in wet feed, the sample seems to collapse. This may imply that the stability of this type of hierarchical SAPO-34 was not as great as expected.

Unfortunately, there are no post reaction data for con-5.22amine and SBA-5.45amine, but the XAS data report that there are some other copper species in the pre reaction samples compared to the hierarchical SAPO-34. Especially for SBA-5.45amine, where copper has multiplicity of 2 in the second shell as reported from the EXAFS. The exact differences require further analysis and XAS data before and after reaction for all samples. This may imply that the copper species in con-5.22amine were more favourable considering HC-SCR compared to the other samples together with the stability of the framework as discussed above.

Based on the topics discussed above, it is difficult to see a clear trend that could explain why the conventional SAPO-34 had best NO conversion and to get a final answer, further analysis is required.

6.0 Conclusion

Hierarchical SAPO-34 with incorporated copper was not successfully synthesised. However, hierarchical SAPO-34 was successfully synthesised and these were ion exchanged with copper(II)nitrate and copper(II)tetraamine. The degree of mesoporosity of these might be discussed, but they both show clear hystereses from BET and they have both a mesopore volume of approximately $0.1 \text{ cm}^3/\text{g}$. The uniformity of the mesopores are not present, but there are mesopores and micropores present in the catalyst material.

The ion exchanged hierarchical SAPO-34 that survived treatment, were also active considering NO conversion in HC-SCR. However, the ion exchanged conventional SAPO-34 showed far better catalytic activity and there are no clear trends that could explain this. Unfortunately, it was not possible to analyse BET on the hierarchical SAPO-34s after ion exchange, although this would have given many answers considering porosity of these. Even so, the degree of survival of treatments seems to have great impact on the catalytic activity when considering the XRD- results of the different samples in addition to other copper species in con-5.22amine. It seems as if the stability of the framework and consequently the availability of active copper sites are the main factors for high catalytic activity concerning HC-SCR.

The synthesis and treatment of this kind of hierarchical CuSAPO-34 did not improve the hydrothermal stability for the HC-SCR compared to the conventional SAPO-34.

7.0 Further work

As reported from Shen et al, the acid concentration varies with Si content. FTIR could have given answers to whether or not there was a clear trend for the acid concentrations in the different samples, especially if this could have been analysed before and after ion exchange. This could have helped in answering why the conventional SAPO-34 had better catalytic activity than the others.

Considering the porosity, BET should be analysed before and after ion exchange in order to have a better view of how this treatment affects the catalyst material.

Furthermore, due to the fact that this type of hierarchical SAPO-34 seemed to either not survive ion exchange or high temperatures in wet feed, it might indicate that this synthesis route might not provide a hydrothermal CuSAPO-34. Templates have great impact on stabilizing the framework of a zeotype as it is being synthesised, so it might be that another mesoporous template could have been better.

In addition, the difficulties concerning incorporation of copper into the framework of hierarchical SAPO-34 must also be analysed further. Alternation of the different synthesis parameters, addition sequence of reactants and changing different reactants may provide a copper incorporated hierarchical SAPO-34.

8.0 References

1. Miljøstatus.no [Internet] Norway: environment Agency; 2015 [sourced 4.02.2016]. Available at: <http://www.miljostatus.no/Tema/Luftforurensning/Sur-nedbor/Nitrogenoksid-NOx/>
2. Kjøretøysforskriften. 1994. Forskrift om tekniske krav og godkjenning av kjøretøy, deler og utstyr, Kap 25, § 25-4. 22.09.2008 nr: 1038
3. R. Hagman, A.H. Amundsen, Transportøkonomisk Institutt (TØI). In *Utslipp fra kjøretøy med Euro 6/VI teknologi* [Electronic Report] 2013 nr 1259. [Sourced 15.02.2016]. Available at: <https://www.toi.no/getfile.php?Mmfileid=32415>
4. R. Hotten. Volkswagen: The Scandal Explained [Internet]. UK: BBC News 2015; [Sourced 10.03.2016]. Available at: <http://www.bbc.com/news/business-34324772>
5. S. Manahan in *Environmental Chemistry*. 9th edition. Boca Raton, USA: CRC Press Taylor & Francis Group; 2010. Pp. 292-294
6. S. Manahan in *Environmental Chemistry*. 9th edition. Boca Raton, USA: CRC Press Taylor & Francis Group; 2010. Pp. 296 & 349-351
7. S. Manahan in *Environmental Chemistry*. 9th edition. Boca Raton, USA: CRC Press Taylor & Francis Group; 2010. Pp. 294-296
8. Faiz, Weaver, Walsh. Air Pollution From Motor Vehicles. Washington (1996); 66-70
9. S. Manahan in *Environmental Chemistry*. 9th edition. Boca Raton, USA: CRC Press Taylor & Francis Group; 2010. P. 336
10. How A Car Works[internet] 2016 [sourced: 19.05.2016] available from: www.howacarworks.com/technology/lean-burn-engines
11. Jäaskeläinen, H., Khair, M.K. Common Rail System [Internet] Canada: Diesel Net; 2015 [Sourced 02.03.2016]. Available at: https://www.dieselnets.com/tech/diesel_fi_common-rail.php
12. Jäaskeläinen, H., Khair, M.K. Exhaust Gas Recirculation [Internet] Canada: Diesel Net; 2014 [Sourced 02.03.2016]. Available at: https://www.dieselnets.com/tech/engine_egr.php
13. Majewski, W.A. Lean NOx Catalyst [Internet] Canada: Diesel Net; 2004 [Sourced 02.03.2016]. Available at: https://www.dieselnets.com/tech/cat_lean-NOx.php
14. Hepburn, J.S, Google Patents, 1998

15. Torre, U., Pereda-Ayo, B., González-Velasco, J. Cu-zeolite NH₃-SCR catalysts for NO_x removal in the combined NSR-SCR technology. *Chemical Engineering Journal* 2012, 207-208; 10-17
16. J.H Kwak, D. Tran, S. Burton, J. Szanyi, J.H. Lee, C. Peden. Effects of hydrothermal aging on NH₃-SCR reaction over Cu/zeolites. *Journ. Of Catal.* 2012, 287; 203-209
17. D. Wang, L. Zhang, J. Li, K. Kamasamudram, W. Epling. NH₃-SCR over Cu/SAPO-34 – Zeolite acidity and Cu structure changes as a function of Cu loading. *Catal. Today* 2014, 231; 64-74
18. U. Deka, I. Lezcano-Gonzalez, B. Weckhuysen, A. Beale. Local Environment and Nature of Cu Active Sites in Zeolite-Based Catalysts for the Selective Catalytic Reduction of NO_x . *ACS Catal.* 2013, 3; 413-427
19. H. Yahiro, M. Iwamoto. Copper ion-exchanged zeolite catalysts in deNO_x reaction. *Applied Catalysis A: General* 2001, 22 (1-2); 163-181
20. H. Nishiguchi, S. Kimura, T. Ishihara and Y. Takita. Selective reduction of NO_x with C₃H₆ over Cu incorporated into silicoaluminophosphate (SAPO). *Research on Chemical Intermediates* 1998, 24; 391-399
21. Y. Zuo, L. Han, W. Bao, L. Chang, J. Wang. Effect of CuSAPO-34 catalyst preparation method on NO_x removal from diesel vehicle exhaust. *Chinese Journal of Catal.* 2013, 34; 1112-1122
22. P. Granger and V. I. Parvulescu, *Chemical Reviews*, 2011, 111, 3155-3207
23. Li, Guan. Hc-SCR reaction pathways on ion exchanged ZSM-5 catalysts. *Microporous and Mesoporous Materials.* 2009, 117 (1-2); 450-457
24. M. Iwamoto, H. Yahiro, S. Shundo, Y. Yu-u, N. Mizuno. Influence of sulfur dioxide on catalytic removal of nitric oxide over copper ion-exchanged ZSM-5 zeolite. *Appl. Catal.* 1991, 69 (1); L15-L19
25. T. Jakobsen. Investigation of hierarchical pore characteristics and interactions with copper for catalytic applications [Master thesis]. Trondheim: NTNU. 2014
26. M. Hartmann and L. Kevan, *Chemical reviews*, 1999, 99, 635-664
27. C. Baerlocher, L. B. Mccusker, D. Olson and W. M. Meier, *Atlas of zeolite framework types*, Published on behalf of the Structure Commission of the International Zeolite Association by Elsevier, Amsterdam, 2007
28. Wilson, S., Barger, P. The characteristics of SAPO-34 which influence the conversion of methanol to light olefins. *Microporous and Mesoporous Materials* 1999, 29; 117-126

29. Schmidt, F. Paasch, S., Brunner E., Kaskel, Carbon templated SAPO-34 with improved adsorption kinetics and catalytic performance in the MTO-reaction. *Microporous and Mesoporous Materials*, 2012, 164; 214-221
30. K. Momma and F. Izumi, "VESTA 3 for three-dimensional visualization of crystal, volumetric and morphology data," *J. Appl. Crystallogr.*, **44**, 2011; 1272-1276
31. Atkins, Overton, Rourke, Weller, Armstrong in *Inorganic Chemistry*. 5th edition. Oxford: Oxford University Press; 2010. P 353-354
32. J. Li, Y. Wei, G. Liu, Y. Qi, P. Tian, B. Li et al. Comparative study of MTO conversion over SAPO-34, H-ZSM-5 and H-ZSM-22: Correlating catalytic performance and reaction mechanism to zeolite topology. *Catal.Today* 2011, 171 (1); 221-228.
33. I. Chorkendorff and J.W Niemannsverdriet in *Concepts of Modern Catalysis and Kinetics*. 2nd edition. Weinheim: Wiley-VHC Verlag gmbh & Co. Kga;2007;207-214
34. Singh, K. S. W., Rouquerol, J., Bergeret, G., Gallezot, P., Vaarkamp, M., Koningsberger, D. C., Datye, A. K., Niemannsverdriet, J. W., Butz, T., Engelhardt, G., Mestl, G., Knözinger, H. And Jobic, H. (1997) Characterization of Solid Catalysts: Sections 3.1.1 – 3.1.3, in *Handbook of Heterogeneous Catalysis* (eds G. Ertl, H. Knözinger and J. Weitkamp), Wiley-VCH Verlag gmbh, Weinheim, Germany. Doi: 10.1002/9783527619474.ch3a
35. S. J. Gregg and K. S. W. Sing, *Adsorption, surface area and porosity*, Academic Press, London, 1982.
36. Pérez-Ramírez et al. Hierarchical zeolites: enhanced utilisation of microporous crystals in catalysis by advances in materials design. *Chem. Soc. Rev.* 2008, 37; 2530-2542. DOI: 10.1039/B809030K
37. D. Ali. *Pore Characteristics and Acid Properties of Hierarchical SAPO-34* [Master thesis]. Trondheim: NTNU. 2015
38. Yang et al. Synthesis of hierarchical ALPO-*n* molecular sieves templated by saccharides. *Microporous and Mesoporous Materials*. 2011, 144 (1-3); 176-182
39. Yang et al. Synthesis and catalytic performances of hierarchical SAPO-34 monolith. *Journ. of Mat. Chem.* 2010, 20 (16); 3227-3231
40. Zhao et al. Triblock Copolymer Syntheses of Mesoporous Silicca with Periodic 50 to 300 Angstrom Pores. DOI: DOI: 10.1126/science.279.5350.548
41. R. Martínez-Franco, M. Moliner, C. Franch, A. Kustov and A. Corma, *Applied Catalysis B: Environmental*, 2012, 127, 273-280M.

42. Zamadics, X. Chen and L. Kevan, *The Journal of Physical Chemistry*, 1992, 96, 2652-2657
43. Gao, Walter, Washton, Szanyi, Peden. Synthesis and evaluation of Cu-SAPO-34 catalysts for Ammonia Selective Catalytic Reduction. 1. Aqueous solution Ion Exchange. *ACS Catal.* 2013, 3(9); 2083-2093
44. Xiang, Yang, Gao, Qiao, Tian, Xu, Liu. Direct Cu²⁺ ion-exchanges into as-synthesized SAPO-34 and its catalytic application in the selective catalytic reduction of NO with NH₃. *RSC Adv.* 2016, 6; 12544-12552
45. I. Chorkendorff and J.W Niemannsverdriet in *Concepts of Modern Catalysis and Kinetics*. 2nd edition. Weinheim: Wiley-VHC Verlag gmbh & Co. Kga; 2007. Pp. 131-134
46. I. Chorkendorff and J.W Niemannsverdriet in *Concepts of Modern Catalysis and Kinetics*. 2nd edition. Weinheim: Wiley-VHC Verlag gmbh & Co. Kga; 2007. Pp. 185-190
47. Y. Wang, V. Penova. Scanning electron microscopy. G. W. Padua, Q. Wang, ed. *Nanotechnology Research Methods for Foods and Bioproducts*. 1st edition. Hoboken, USA: Wiley-Blackwell; 2012. Pp: 103-127.
48. Howard Taylor in *Inductively Coupled Plasma-Mass Spectrometry*. California: Academic press; 2001.
49. European Synchrotron Radiation Facility [Internet]. [Sourced 19.05.16] available from: <http://www.esrf.eu/about/synchrotron-science>
50. van Dorssen, Koningsberger, Mojet, Ramaker. Xafs spectroscopy; fundamental principles and data analysis. *Topics in Catal.*
51. Fay, Proctor, Hoffman, Hercules. *Anal. Chem.* 1988, 60, 1225
52. Koningsberger and Prins (1988)
53. Najafi, Askari, Halladj. Hydrothermal synthesis of nanosized SAPO-34 molecular sieves by different combinations of multi templates. *Powder technology.* 2014, 254; 324-330
54. Iván Meléndez-Ortiz, Puente-Urbina, Castruita-de Leon, Manuel Mata-Padilla, García-Uriostegui. Synthesis of spherical SBA-15 mesoporous silica. Influence of reaction conditions in the structural order and stability. *Ceramics International.* 2016, 42 (6); 7564-7570

55. Wang, Kong, Chen, Ding, Shan, He. Direct synthesis, characterization of Cu-SBA-15 and its high catalytic activity in hydroxylation of phenol by H₂O₂. *Journ. of Molecular catal.* 2005 (230); 143-150
56. Karina Mathisen. X-ray absorption spectroscopic studies on active metal sites in zeotypes during the selective catalytic reduction of NO_x with propene in an oxygen rich atmosphere. [Doctoral thesis] Trondheim: NTNU; 2005. 130
57. Exafs Materials: Reference X-ray Spectra of Metal Foils. USA: Danville
58. T.Kristiansen. Growth Limitations of Copper Nanoparticles in Silica Aerogels: An In Situ XAS Study. [Master thesis]. Trondheim: NTNU. 2009
59. Thielemann, Girgsdies, Schlögl, Hess. Pore structure and surface area of silica SBA-15: Influence of washing and scale-up. *Beilstein J. Nanotechnol.* 2011, 2; 110-118
60. Zheng et al. Unraveling the non-classic crystallization of SAPO-34 in a dry gel system towards controlling meso-structure with the assistance of growth inhibitor: Growth mechanism, hierarchical structure control and catalytic properties. *Microporous and Mesoporous.* 2016, 225; 74-87
61. Shen et al. A study of the acidity of SAPO-34 by solid-state NMR spectroscopy. *Microporous and Mesoporous.* 2012, 158; 19-25

9.0 Appendices

Appendix A: Risk evaluation

Appendix B: Additional BET

Appendix C: Additional SEM

Appendix D: Additional HC-SCR results

Appendix E: Additional XANES

Appendix F: Additional EXAFS

NTNU	Kartlegging av risikofylt aktivitet	Utarbeidet av	Nummer	Dato	
		HMS-avd.	HMSRV2601	22.03.2011	
HMS		Godkjent av		Erstatter	
		Rektor		01.12.2006	

Appendix A: Risk evaluation

Enhet: **Institutt for kjemi**

Dato: **10.september 2015**

Linjeleder: **Marie-Laure Olivier**

Deltakere ved kartleggingen (m/ funksjon): **Guro Sørli (masterstudent), Karina Mathisen (ansvarlig veileder/romansvarlig), Karsten Kirste (medveileder)**

(Ansv. veileder, student, evt. medveiledere, evt. andre m. kompetanse)

Kort beskrivelse av hovedaktivitet/hovedprosess: Masteroppgave student **Guro Sørli**. Tittel på oppgaven: "Effect of porosity on the hydrothermal stability of CuSAPO-34 for the deNOx process"

Er oppgaven rent teoretisk? (JA/NEI): **NEI** «JA» betyr at veileder inntår for at oppgaven ikke inneholder noen aktiviteter som krever risikovurdering. Dersom «JA»: Beskriv kort aktiviteten i kartleggingskjemaet under. Risikovurdering trenger ikke å fylles ut.

Signaturer: Ansvarlig veileder:

Student:

ID nr.	Aktivitet/prosess	Ansvarlig	Eksisterende dokumentasjon	Eksisterende sikringstiltak	Lov, forskrift o.l.	Kommentar
E2-117 - 1	Uorganisk syntese	Karina Mathisen	Kjemikalieforskriften, AML, Merkeforskriften	NTNU's Lab- og verkstedhåndbok, EcoOnline Stoffkartotek		Egen SJA for hver syntese med risikovurdering kjemikalier

NTNU	Kartlegging av risikofylt aktivitet	Utarbeidet av	Nummer	Dato	
		HMS-avd.	HMSRV2601	22.03.2011	
HMS		Godkjent av		Erstatter	
		Rektor		01.12.2006	


E2-117 - 3	Bruk av høytemperaturovn (inntil 1200 grader)	Karina Mathisen	AML	NTNU's Lab- og verkstedhåndbok, Apparatorkort		
E2-117 - 4	Vask med Kongevann	Karina Mathisen	Kjemikalieforskriften, AML, Merkeforskriften	NTNU's Lab- og verkstedhåndbok, EcoOnline Stoffkartotek		
E2-117 - 5	IR- instrument analyser	Karina Mathisen		NTNU's Lab- og verkstedhåndbok, Apparatorkort	Opplæring blir gitt ved bruk av instrumentet.	Egen risikovurdering i driftsinstruks
E2-117 - 6	GC/MS instrument analyser	Karina Mathisen		NTNU's Lab- og verkstedhåndbok, Apparatorkort	Opplæring blir gitt ved bruk av instrumentet.	Egen risikovurdering i driftsinstruks
E2-117 - 7	UV/VIS instrument analyser	Karina Mathisen		NTNU's Lab- og verkstedhåndbok, Apparatorkort	Opplæring blir gitt ved bruk av instrumentet.	Egen risikovurdering i driftsinstruks
E2-117 - 8	Bruk av varmeskap	Karina Mathisen		NTNU's Lab- og verkstedhåndbok, Apparatorkort		Varmeskapet brukes kun til tørking – ingen farer.
E2-117 - 9	Bruk av sentrifuge	Karina Mathisen				Sentrifugen er i et lukket system – ingen farer.

NTNU	Kartlegging av risikofylt aktivitet	Utarbeidet av	Nummer	Dato	
		HMS-avd.	HMSRV2601	22.03.2011	
HMS		Godkjent av		Erstatter	
		Rektor		01.12.2006	

E2-117 - 11	lonebyttingsprosedyrer	Karina Mathisen	Kjemikalieforskriften, AML, Merkeforskriften	NTNU's Lab- og verkstedhåndbok, EcoOnline Stoffkartotek		
E2-117 - 12	Bruk av vekter	Karina Mathisen				Grovvekt står i avtrekkskap - ingen farer for damp ved veiing.
E2-117 - 13	Bruk av PC	Karina Mathisen				PC brukes kun til noen spesielle dataprogrammer - ingen farer.
E2-117 - 16	Arbeid med flytende nitrogen	Karina Mathisen	Kjemikalieforskriften, AML, merkeforskriften	NTNU's Lab- og verkstedhåndbok, EcoOnline Stoffkartotek		
E2-117 - 18	Arbeid med forskjellige typer gass	Karina Mathisen	Kjemikalieforskriften, AML, Merkeforskriften			
E2-117 - 19	Arbeid med syrer og baser	Karina Mathisen	Kjemikalieforskriften, AML, Merkeforskriften	NTNU's Lab- og verkstedhåndbok, EcoOnline Stoffkartotek		
E2-117-21	Katalysemålinger i in situ celle	Karina Mathisen		Apparaturkort	Opplæring blir gitt ved bruk av instrumentet.	
E2-117-22	Katalysemålinger i tubeovn	Karina Mathisen		Apparaturkort	Opplæring blir gitt ved bruk av instrumentet.	

NTNU	Kartlegging av risikofylt aktivitet	Utarbeidet av	Nummer	Dato	
		HMS-avd.	HMSRV2601	22.03.2011	
HMS		Godkjent av		Erstatter	
		Rektor		01.12.2006	

E2-117-23	Håndtering av produkt, zeolitt, AIPO-n, SAPO-n, MOF, aerogel	Karina Mathisen	Kjemikalieforskriften, AML, Merkeforskriften			
E2-117-25	Bruk av vakuulinje ifm IR målinger	Karina Mathisen		Apparaturkort	Opplæring blir gitt ved bruk av instrumentet.	
GS-1	ICP-MS analyser	Syverin Lierhagen	Kjemikalieforskriften, AML, Merkeforskriften		Utføres av operatør	
GS-2	BET målinger	BET ansvarlig IMT		Apparaturkort	Opplæring blir gitt ved bruk av instrumentet.	
GS-3	TGA målinger	TGA ansvarlig IKP		Apparaturkort	Opplæring blir gitt ved bruk av instrumentet.	
GS-4	XRD-målinger	XRD ansvarlig IMT		Apparaturkort	Opplæring blir gitt ved bruk av instrumentet.	

NTNU	Risikovurdering	Utarbeidet av	Nummer	Dato	
		HMS-avd.	HMSRV2601	22.03.2011	
HMS		Godkjent av		Erstatter	
		Rektor		01.12.2006	

Enhet: Institutt for kjemi

Dato: 10.september 2015


Linjeleder: Marie-Laure Olivier

Deltakere ved kartleggingen (m/ funksjon): **Guro Sørli (masterstudent), Karina Mathisen (ansvarlig veileder/romansvarlig), Karsten Kirste (medveileder)**



(Ansv. veileder, student, evt. medveiledere, evt. andre m. kompetanse)

Kort beskrivelse av hovedaktivitet/hovedprosess: Masteroppgave student **Guro Sørli**. Tittel på oppgaven: "Effect of porosity on the hydrothermal stability of CuSAPO-34 for the deNO_x process"



ID nr	Aktivitet kartleggings-skjemaet fra	Mulig uønsket hendelse/belastning	Vurdering av sannsynlighet (1-5)	Vurdering av konsekvens:				Risiko-Verdi (menneske)	Kommentarer/status Forslag til tiltak
				Menneske (A-E)	Ytre miljø (A-E)	Øk/materiell (A-E)	Om-dømme (A-E)		
E2-117-1	Uorganisk syntese	Inhalering/søl/spill av organisk amin på hud evt øyner	2	A	A	A	A	2A	Hansker, briller, avtrekk
		Søl/spill av syre/base på hud evt øyner	4	A	A	A	A	4A	Hansker og briller. Kun fortynnede syrer.
		Inhalering fint silikapulver	2	A	A	A	A	2A	

NTNU	<h1>Risikovurdering</h1>	Utarbeidet av	Nummer	Dato	
		HMS-avd.	HMSRV2601	22.03.2011	
HMS		Godkjent av		Erstatter	
		Rektor		01.12.2006	

		Overtrykk høytrykksautoklav kan gi eksplosjon	2	B	A	A	A	2B	Ikke vurdert helsefarlig i små mengder v/ sjelden eksponering. Ansiktsmasker? Opplæring gis. Sikkerhetsventil installert på alle autoklaver.
E2-117-3	Bruk av høytemperaturovn (inntil 1200 grader)	Forbrenningsskader, aminavgasser, mulig produksjon av CO ved kalsinering	2	A	A	A	A	2A	Thermoresistente hansker, opplæring kreves. Ovn plassert i avtrekk.
E2-117-4	Vask med Kongevann	Søl/spill på hud evt øyner. Utvikling av gass.	2	A	A	A	A	2A	Hansker, briller og avtrekk. Vaskeprosedyre gitt i tilfelle søl. Krever følgeperson.
E2-117-11	lonebyttingsprosedyrer	Søl/spill av syre eller baser på hud evt øyner	4	A	A	A	A	4A	Hansker og briller. Fortynnede syrer og baser.
E2-117-16	Arbeid med flytende nitrogen	Forfrysningsskader	2	A	A	A	A	2A	Ansiktskjerm og hansker

NTNU	<h1>Risikovurdering</h1>	Utarbeidet av	Nummer	Dato	
		HMS-avd.	HMSRV2601	22.03.2011	
HMS		Godkjent av		Erstatter	
		Rektor		01.12.2006	


E2-117-18	Arbeid med forskjellige typer gass	Gasslekkasje. Eksplosjonsfare. Kvelning CO (rent?) NO (0-1% i He) Propene (0-10%) N ₂ O (<1%) NO ₂ (<1%) Acrolein (<2%)	3	C	A	C	C	3C	Gassdetektor/sniffer benyttes. Bruk av CO etter varsling av annen ansatt og bruk kun små lukkede volum. <u>Ved graviditet fjernes flasken og systemet flushes grundig.</u> Gassflasker ikke over 10 liter, festet på vegg etter forskrifter. Krever opplæring. Benytter kun godkjente regulatorer. Lekkasetesting utføres. Laben utstyrt med kortlås.
E2-117-19	Arbeid med syrer og baser	Søl/spill av syre på hud evt øyner.	4	A	A	A	A	4A	Hansker og briller. Kun bruk av fortynnede syrer og baser. Vasking.
E2-117-22	Bruk av tubereaktor for katalysemålinger	Fare for gasslekkasje	2	A	A	A	A	2A	Kun lav flow av gass benyttes. Lekkasetesting før bruk.

NTNU	Risikovurdering	Utarbeidet av	Nummer	Dato	
		HMS-avd.	HMSRV2601	22.03.2011	
HMS		Godkjent av		Erstatter	
		Rektor		01.12.2006	

E2-117-23	Håndtering av produkt, zeolitt, AIPO-n, SAPO-n, MOF, aerogel	Innhalering av fint pulver	2	A	A	A	A	2A	Små mengder produseres (under 5 g). Ansiktsmaske tilgjengelig ved håndtering av finkornet materiale. Se produktdatablad.
E2-117-25	Bruk av vakuulinja ifm med IR målinger	Implosjon, gasslekkasje, kuttskader	2	C	A	A	A	2C	Krever opplæring. Trykkmålere innstallert. Fylling av ballong i avtrekksskap.
GS-1	ICP-MS analyser	Bruk av kongevann eller HF til oppløsning	2	B				2B	Oppløsning lages med måleflaske. Små mengder.
GS-2	BET målinger		1	A				1A	
GS-3	TGA målinger	Gasslekkasje	2	A					Detektor installert
GS-4	XRD målinger	Strålefare	1	A				1A	Lukket kilde

Sannsynlighet vurderes etter følgende kriterier:

Svært liten	Liten	Middels	Stor	Svært stor
1	2	3	4	5
1 gang pr 50 år eller sjeldnere	1 gang pr 10 år eller sjeldnere	1 gang pr år eller sjeldnere	1 gang pr måned eller sjeldnere	Skjer ukentlig


NTNU	Risikovurdering	Utarbeidet av	Nummer	Dato	
		HMS-avd.	HMSRV2601	22.03.2011	
HMS		Godkjent av		Erstatter	
		Rektor		01.12.2006	

Konsekvens vurderes etter følgende kriterier:

Gradering	Menneske	Ytre miljø Vann, jord og luft	Øk/materiell	Omdømme
E Svært Alvorlig	Død	Svært langvarig og ikke reversibel skade	Drifts- eller aktivitetsstans >1 år.	Troverdighet og respekt betydelig og varig svekket
D Alvorlig	Alvorlig personskade. Mulig uførhet.	Langvarig skade. Lang restitusjonstid	Driftsstans > ½ år Aktivitetsstans i opp til 1 år	Troverdighet og respekt betydelig svekket
C Moderat	Alvorlig personskade.	Mindre skade og lang restitusjonstid	Drifts- eller aktivitetsstans < 1 mnd	Troverdighet og respekt svekket
B Liten	Skade som krever medisinsk behandling	Mindre skade og kort restitusjonstid	Drifts- eller aktivitetsstans < 1uke	Negativ påvirkning på troverdighet og respekt
A Svært liten	Skade som krever førstehjelp	Ubetydelig skade og kort restitusjonstid	Drifts- eller aktivitetsstans < 1dag	Liten påvirkning på troverdighet og respekt



Risikoverdi = Sannsynlighet x Konsekvens

Beregn risikoverdi for Menneske. Enheten vurderer selv om de i tillegg vil beregne risikoverdi for Ytre miljø, Økonomi/materiell og Omdømme. I så fall beregnes disse hver for seg.

NTNU	Risikovurdering	Utarbeidet av	Nummer	Dato	
		HMS-avd.	HMSRV2601	22.03.2011	
HMS		Godkjent av		Erstatter	
		Rektor		01.12.2006	

Til kolonnen "Kommentarer/status, forslag til forebyggende og korrigerende tiltak":

Tiltak kan påvirke både sannsynlighet og konsekvens. Prioriter tiltak som kan forhindre at hendelsen inntreffer, dvs. sannsynlighetsreduserende tiltak foran skjerpet beredskap, dvs. konsekvensreduserende tiltak.

NTNU	Risikovurdering	Utarbeidet av	Nummer	Dato	
		HMS-avd.	HMSRV 2601	22.03.2011	
HMS		Godkjent av		Erstatte r	
		Rektor		01.12.2006	

MATRISE FOR RISIKOVURDERINGER ved NTNU

KONSEKVENSENS	Svært alvorlig	E1	E2	E3	E4	E5
	Alvorlig	D1	D2	D3	D4	D5
	Moderat	C1	C2	C3	C4	C5
	Liten	B1	B2	B3	B4	B5
	Svært liten	A1	A2	A3	A4	A5
		Svært liten	Liten	Middels	Stor	Svært stor
		SANNSYNLIGHET				

Prinsipp over akseptkriterium. Forklaring av fargene som er brukt i risikomatriksen.

Farge	Beskrivelse
Rød	Uakseptabel risiko. Tiltak skal gjennomføres for å redusere risikoen.
Gul	Vurderingsområde. Tiltak skal vurderes.
Grønn	Akseptabel risiko. Tiltak kan vurderes ut fra andre hensyn.

Appendix B: Additional BET

Table B.1: List of the specific surface area, calculated from BET, and pore width calculated from BJH for the four remaining SBA-15.

Sample name	BET specific surface area (m ² /g)	BJH pore width (Å)
SBA-15_01	196.39	49.70
SBA-15_02	328.97	47.54
SBA-15_04	586.39	28.14
SBA-15_05	836.51	36.28
SAPO-34_04	593.75	Not reported
SAPO-34_04Cu ₂	295.48	Not reported

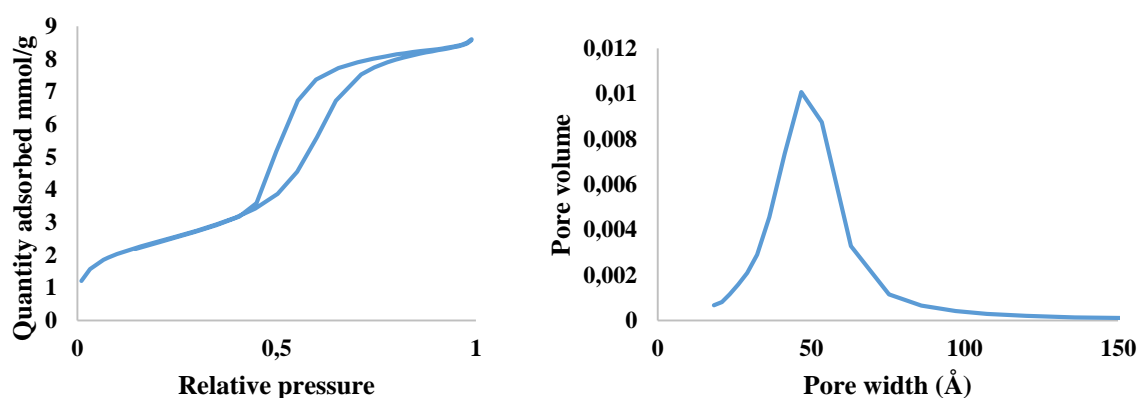


Figure B.1: BET and BJH for sample SBA-15_01. BET is shown at the left and BJH at the right. The hysteresis is similar of a H1 hysteresis, indicating somewhat uniformity of the mesopores.

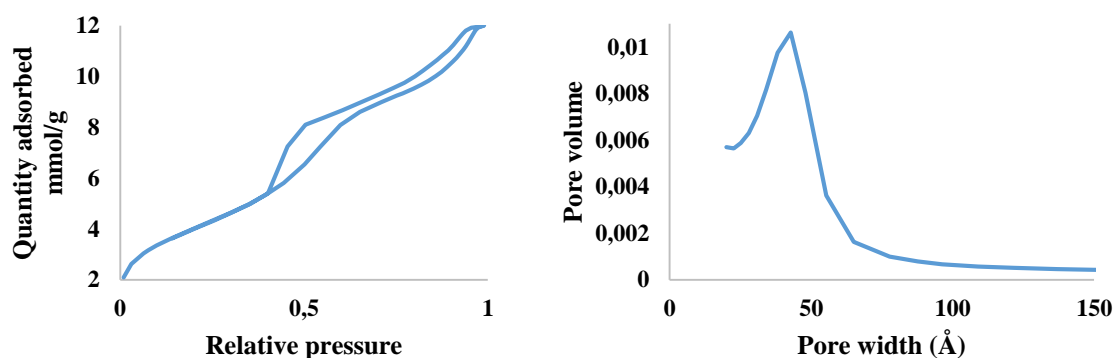


Figure B.2: BET and BJH for sample SBA-15_02, whereas the BET is shown at the left and BJH at the right. The hysteresis can be seen as a mixture of H1 and H4, implying both uniform mesopores and undefined mesopores.

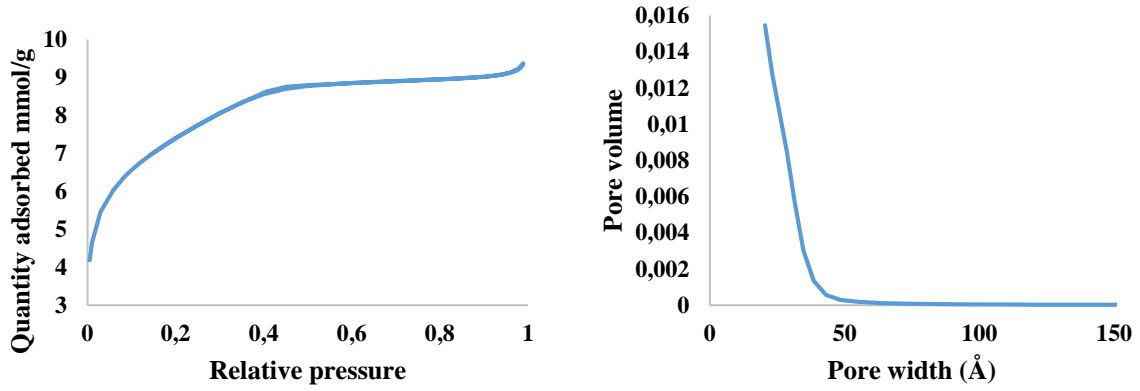


Figure B.3: BET and BJH for sample SBA-15_04. The BET at the left shows practically no hysteresis, implying mostly a microporous material. The BJH at the right confirms this by not having a defined pore width.

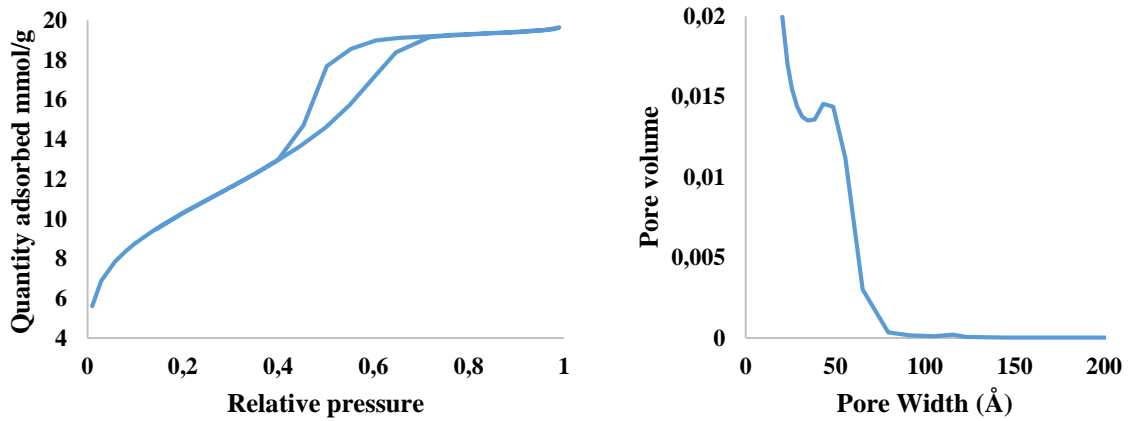


Figure B.4: BET and BJH for sample SBA-15_05. BET (left) shows a hysteresis combined by H2 and H4 hysteresis, implying a complex mesopore structure. BJH (right) shows however a bump, implying that several pores have the pore width of 49 Å.

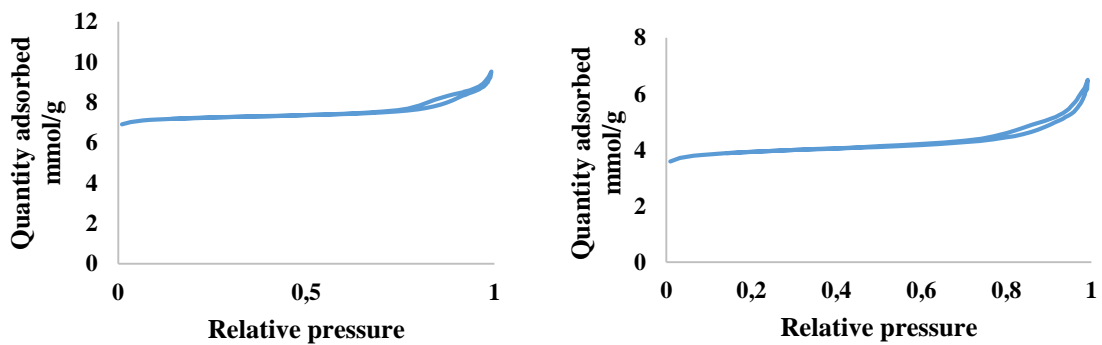


Figure B.5: BET of SAPO-34_04 before (left) and after (right) ion exchange

Appendix C: Additional SEM

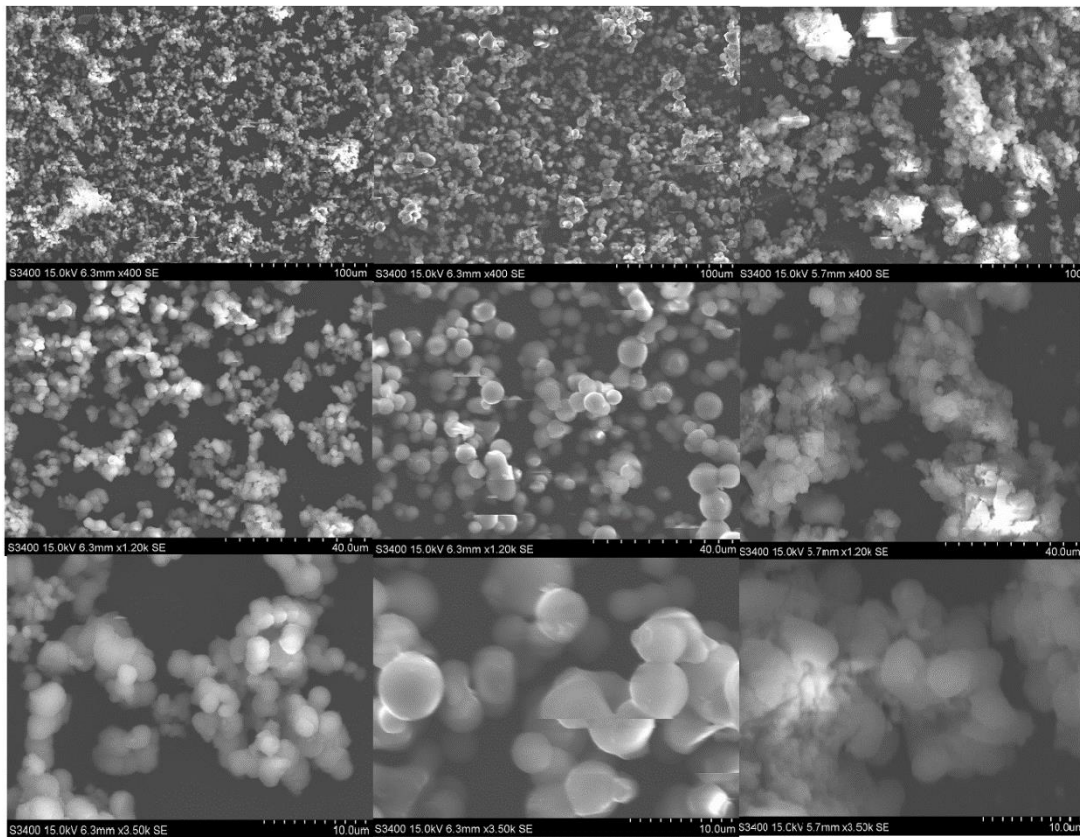


Figure C.1: SEM of sample SBA-14_01 (left), SBA-15_02 (middle) and SBA-15_03 (right). Top photos taken at 400 eV, middle photos at 1,20k eV and the bottom photos taken at 3.50k eV. There are bigger particles for SBA-15_03 compared to the others, especially SBA-15_02.

Appendix D: Additional HC-SCR results

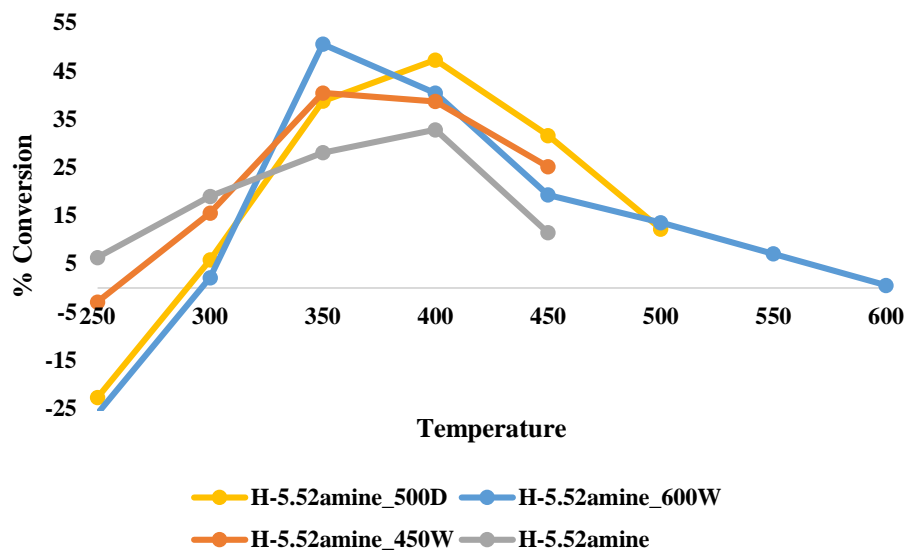


Figure D.1: Conversion results of all experiments performed on sample H-5.52amine. Both the yellow and the grey curve are performed in dry feed and the other two are performed in wet feed. The grey curve shows the conversion over bypass.

Appendix E: Additional XANES

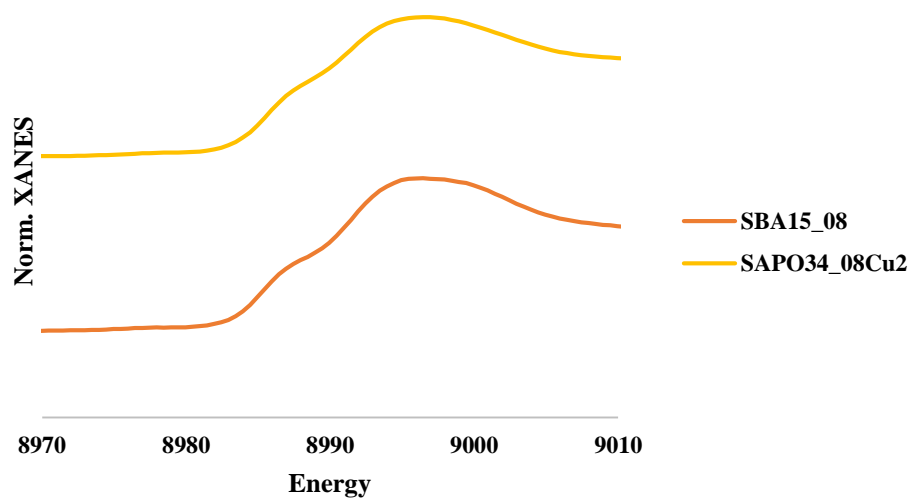


Figure E.1: Normalized XANES of the conventional, microporous SAPO-34 and mesoporous SBA-15. All of these are pre HC-SCR.

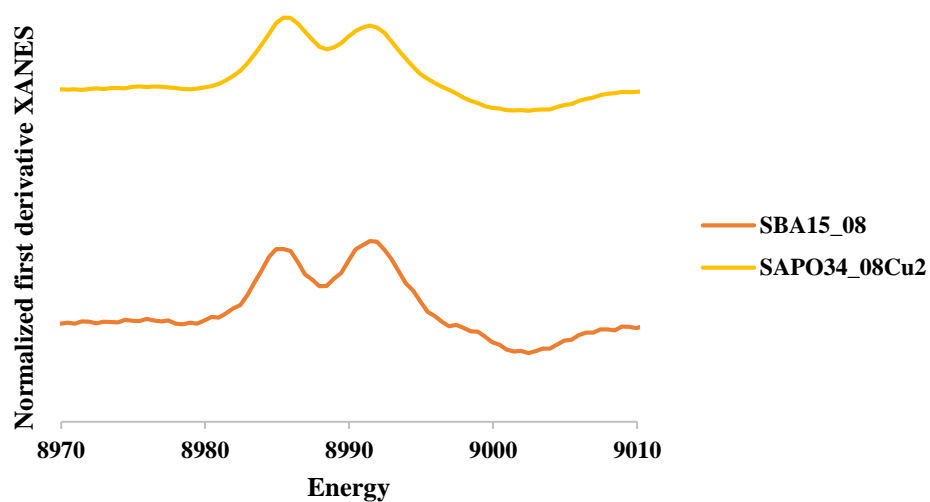


Figure E.2: First derivative normalized XANES of the conventional, microporous SAPO-34 and the mesoporous SBA-15

Appendix F: Additional EXAFS

Table F.1: Results after refinements in DLV EXCURV. Debye-Waller factor, multiplicity and distance are the main factors that were refined.

Sample	Shell	EF (eV)	$2\sigma^2$ (\AA^2)	N	r (\AA)	R%
SBA-15_08Cu ₂	Cu-O	-3(1)	0.007(2)	2.8(2)	1.970(8)	40.66
	Cu...Cu		0.006(2)	0.9(2)	2.94(1)	
	Cu...Si		0.06(7)	2(2)	3.2(2)	
SAPO-34_08Cu ₂	Cu-O	-3(1)	0.001(1)	2.1(2)	1.974(8)	39.95
	Cu...Cu		0.04(2)	1(1)	2.69(6)	
	Cu...P		0.001(3)	0.8(3)	3.1(1)	

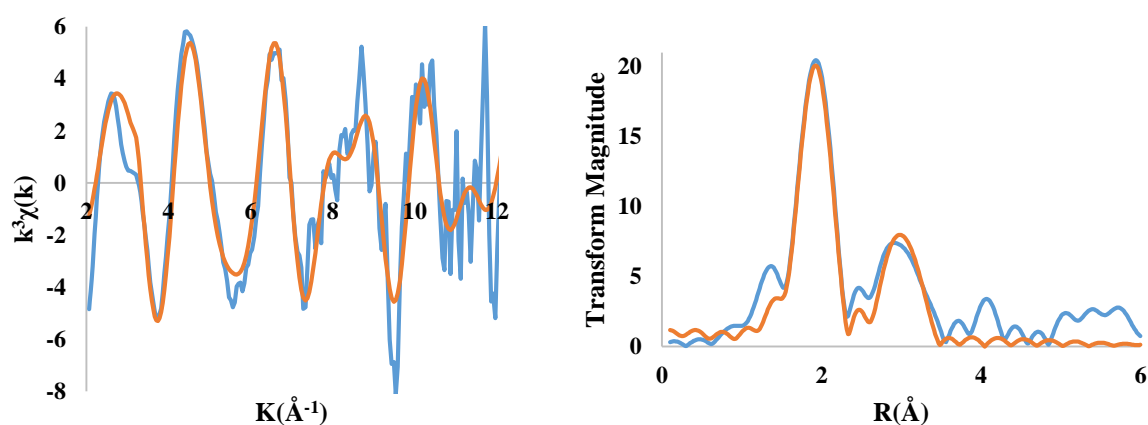


Figure F.1: Normalized EXAFS (left) and FT normalized EXAFS (right) for SBA-15_08Cu₂

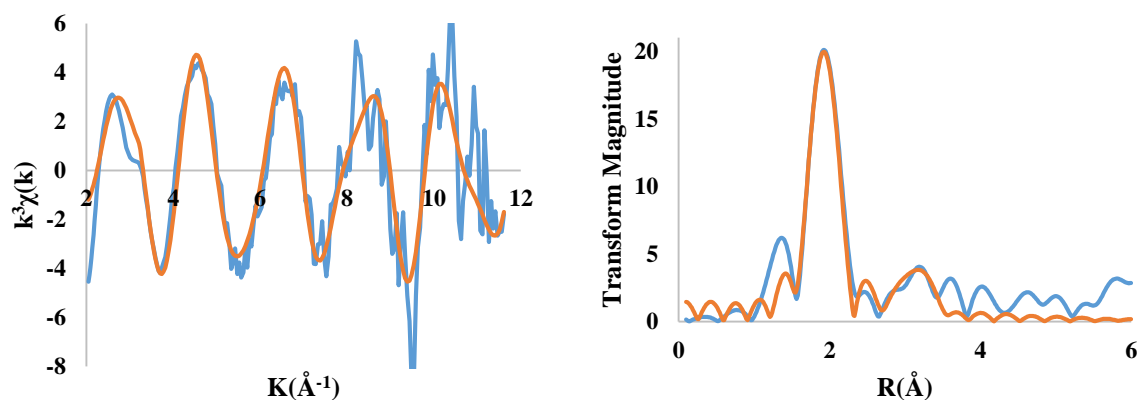


Figure F.2: Normalized EXAFS (left) and FT normalized EXAFS (right) for SAPO-34_08Cu₂